DISS. ETH NO. 23282

Mitochondria trafficking in dividing cells: the role of Cenp-F

A thesis submitted to attain the degree of
DOCTOR OF SCIENCES of ETH ZURICH
(Dr. sc. ETH Zurich)

presented by

GIL KANFER

Master of Science in Medical Sciences
University of Tel-Aviv, Israel

born on 15.09.1980 citizen of Israel

accepted on the recommendation of
Prof. Benoît Kornmann
Prof. Paola Picotti
Prof. Patrick Meraldi
Prof. Anne Spang

Zurich, 2016

Abstract

During cell-cycle, organelles undergo massive reorganization and deformation. Mitochondria, in particular, are very dynamic organelles, which constantly divide, fuse and are transported, in order to achieve specific architecture, and to ensure accurate distribution of the metabolism (e.g. ATP synthesis), Ca2+ buffering, and for ensuring inheritance of functional organelles. In the course of cell division cycle, mitochondria undergo dramatic alteration in distribution. In the current study, the key players participating in mitochondria spreading following mitosis were identified. In particular, the cell-cycle-dependent microtubule-associated protein Centromeric protein F (Cenp-F), was found to be recruited to the mitochondria by the mitochondrial Rho-GTPase Miro. Cenp-F-Miro interaction promotes mitochondria transport and re-distribution following cell-division by attaching the mitochondria to growing microtubules.

Zusammenfassung

Im Laufe des Zellzyklus werden Organellen umfassend verformt und reorganisiert. Mitochondrien sind besonders dynamische Organellen, welche sich kontinuierlich teilen, fusionieren, und transportiert werden. Der regulierte Aufbau des mitochondrialen Netzwerkes stellt sicher, dass Metabolismus (z.B. ATP Synthese), Ca2+ Pufferung, und Vererbung gesunder/funktionaler Organellen problemlos ablaufen. Während des Zellzyklus wird die subzelluläre Verteilung von Mitochondrien dramatischen Veränderungen unterworfen. In dieser Studie wurden Schlüsselspieler für die Verteilung von Mitochondrien nach Abschluss der Mitose identifiziert. Desweiteren konnte gezeigt werden, dass das cycle-dependent microtubule-associated protein Centromeric protein F (Cenp-F) von der mitochondrialen Rho-GTPase Miro zu Mitochondrien rekrutiert wird. Die Interaktion zwischen Cenp-F und Miro vermittelt dann den Transport und die Reorganisation von Mitochondrien durch die Befestigung von Mitochondrien an expandierende Mikrotubuli.

Statement of contribution

The first result chapter in the present work is the published manuscript “Mitotic redistribution of the mitochondrial network by Miro and Cenp-F” (Kanfer et al., 2015b). The abstract, introduction and discussion are partly based on the submitted review “Dynamics of the mitochondrial network during mitosis” (Kanfer and Kornmann, submitted).

In the second result section, I performed all the microscopy acquisition and image analysis presented in this work. The protein purification and microtubule dynamics assay were generated together with Martin Peterka and Vladimir Volkov.

Prof. Benoît Kornmann supervised the project and made significant contributions to the writing of the published manuscripts.

Table of Content

1. Introduction

Eukaryotic cell division has been studied since the mid-nineteenth century. The focus was laid on deciphering how the accurate and time-efficient process of chromosome segregation is achieved. Specifically, the detailed molecular mechanisms and the cellular signaling, which ensure the accurate segregation of replicated chromosomes to daughter cells have been under extensive exploration.

The building blocks that the cells are made of are not just genomic material wrapped in membranes, the cells are also composed of organelles such as the endoplasmic reticulum, the Golgi apparatus, peroxisomes, mitochondria etc. The inheritance, biogenesis and spatiotemporal organization of these organelles are crucial for the determination of cell fate (Fagarasanu et al., 2010; Jongsma et al., 2014; Ouellet and Barral, 2012).

During progression in cell division, organelles undergo dynamic spatiotemporal reorganization that facilitates their accurate inheritance to the daughter cells and the progression of mitosis.

For example, in interphase cells, the structure of the Endoplasmic Reticulum (ER) is composed of sheets, which are located at the perinuclear region, and tubules that are found at the cell periphery.

Several studies indicate, that during mitosis, the ER undergoes sheets to tubule transformation, which allows space for mitotic spindle generation (Schlaitz et al., 2013; Smyth et al., 2012). The rate of this sheet-to-tubule transformation seems to vary and depends on the cell line used (Lu et al., 2009; Puhka et al., 2007) .

Like the ER, the mammalian Golgi network is composed of connected membranes. The Golgi is located close to the nucleus and the microtubule-organizing center (MTOC). During cell division, the ribbon structure of the Golgi undergoes massive architecture alteration. In interphase, the Golgi consists of stacked cisternae, some of which are connected by tubules. At the onset of mitosis, the tubule structures begin to disassemble. Then, during metaphase, the small cisternae further fragment and disperse throughout the cytosol. Next, at the beginning of anaphase, the fragmented Golgi particles start to aggregate with the ER. Finally, at cytokinesis, the Golgi is transported adjacent to the MTOC and reassembled to the cisternae stack configuration, which is typical for interphase cells (Acharya et al., 1998; Hidalgo Carcedo et al., 2004; Sütterlin et al., 2001).

In addition to the ER and Golgi, the mitochondrial network morphology is also affected by cell cycle progression. In interphase cells, the mitochondria network is composed of interconnected tubular structures that undergo fusion, fission and transport. The balance

between these processes determines appropriate spreading of the mitochondrial network. Defects in mitochondrial fission can hinder cell cycle progression, and even result in cell senescence (Mishra and Chan, 2014).

This introduction focuses on the processes that govern mitochondria network organization. Specifically, it emphasizes the various means by which mitochondria trafficking is achieved during cell cycle in symmetrically duplicating cells.

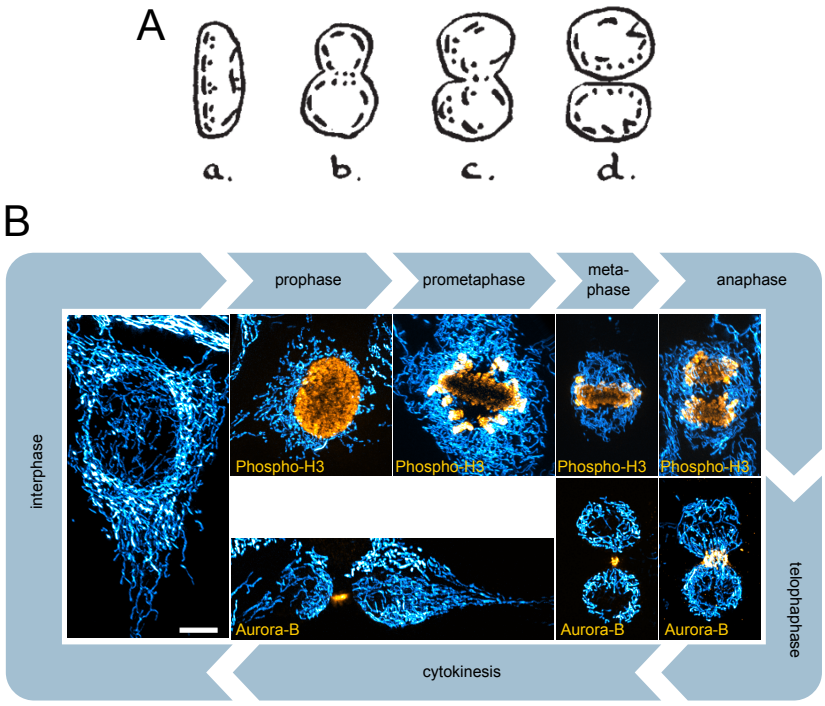

Introduction Figure 1: Behavior of the mitochondrial network during mitosis. (**A**) Drawing of mitochondria in mitotic cells from (Christiansen EG., 1949). (**B**) Images of the mitochondrial network (cyan) in cells in different phases of mitosis. When indicated, a mitotic marker (either phosphorylated Histone H3, phospho-H3, which stains mitotic chromatin, or Aurora-B, which stains the midbody) is shown (orange).

1.1. The mitochondrial network during cell cycle

Mitochondria are semi-autonomous multifunctional organelles that play critical roles in many cellular processes, including energy production, metabolism, apoptosis, and senescence. Although, most of the mitochondrial proteins are encoded in the nucleus and are transported post-translationally to the mitochondria, the mitochondrial genome also encodes critical proteins required for cellular respiration.

In cells, mitochondria form a highly dynamic network, the distribution of which depends on a balance between three integrated processes: a) fission, the ability of mitochondria to divide, b) fusion, the merging of separate mitochondria and c) motility, the active transfer of mitochondria along the cytoskeleton.

Back in the fifties, a study published by E.G. Christiansen described alteration in mitochondrial network during cell cycle progression (Christiansen EG., 1949). In interphase cells, the mitochondria are arranged in elongated tubules, whereas in mitosis, the network is fragmented. At the exit of mitosis and initiation of cytokinesis, the mitochondria tubules merge again to form an interconnected network.

The process of mitochondrial division is mediated by the highly conserved GTPase named Dynamin related protein (Drp1). Drp1 adaptors reside on the outer mitochondria membrane (OMM) and recruit Drp1 to the mitochondria at specific constriction sites. At this location, Drp1 forms a homo-oligomeric ring, which wraps the membrane and performs mitochondrial cleavage upon GTP hydrolysis.

Upon mitotic entry, Drp1 is activated by phosphorylation. The activation is mediated by two mitotic kinases: Aurora A and cyclin B–CDK1. Besides activation by phosphorylation, Drp1 activation can be driven by another type of post-translational modification; at G2/mitosis transition, the mitochondrial SUMO ligase called MAPL (designated for Mitochondrial-anchored protein ligase) targets Drp1 to stimulate mitochondrial fission (Braschi et al., 2009). The mitochondrial network fission rates are enhanced during mitosis, which is enabled by the deSUMOylation of DRP1 (Zunino et al., 2009). While SUMOylation of Drp1 leads to its membrane recruitment, deSUMOylation is linked to membrane release. Later, in G1, the fission machinery is inhibited to allow mitochondrial network reformation. For example, Drp1 is ubiquitylated by the APC/CCdh1 and afterwards submitted to proteasomal degradation (Horn et al., 2011).

The balance between fusion and fission determines the overall changes in mitochondria network formation. The cell-cycle dependent regulation of mitochondria fusion machinery is not well studied. However, one study shows that in mitosis, the mitochondrial fusion proteins Mfn1/2 (fzo1 in budding yeast) are undergoing ubiquitin-dependent proteasomal degradation (Park and Cho, 2012). Thus, mammalian cells possess a large repertoire of different regulatory factors to modulate mitochondrial dynamics in response to various signals during cell division.

1.2. Mitochondria and mitosis - Mechanism and function

Until now, the molecular mechanisms governing mitochondrial morphology during cell cycle have been described. However, now the focus will be on the functional and physiological aspects of mitochondrial dynamics during cell development and asymmetric cell division.

Mitochondrial network scattering is important for supplying the metabolism and energy required in different subcellular locations (Schwarz, 2013). For instance, in neuronal cells, the mitochondria are actively transported along the axons towards the synapses, which are energy-demanding sites responsible for releasing neurotransmitters, building action potential, restoring ion gradient, axonal transport etc. Therefore, neurons are a classical model system for deciphering the specific function of mitochondrial positioning (Schwarz, 2013). Yet, since neurons are fully specialized differentiated cells they are not suitable for investigating organelle dynamics during cell division.

However, a recent study in adult stem cells illustrates the importance of mitochondria network repositioning and organization during symmetric and asymmetric cell division (Katajisto, 2015). Progenitor stem cells asymmetric division gives rise to one specialized differentiated adult cell of the tissue and one identical progenitor stem cell, while the symmetric division generates two identical stem cells for maintaining the renewing capacity of the tissue. In these cells, mitochondria containing newly synthesized proteins (“young mitochondria”) or mitochondria consisting of proteins which were synthesized prior to cell division (“old mitochondria”) are sorted by unknown mechanism. The researchers observed that, the proportion of “old mitochondria” adjacent to the nuclear envelope is higher in progenitors stem cells prior to asymmetric cell division. However, in progenitor stem cells undergoing symmetric cell division the “young and old mitochondria” are distributed evenly in the cytoplasm (Katajisto, 2015). Additionally, the selective sorting of mitochondria according to the nature of the protein composition can be abrogated by altering mitochondrial distribution (Katajisto, 2015). This was achieved

by silencing fission factors. This caused defects in the stemness maintenance of the tissue. This case emphasizes the importance of mitochondrial distribution for the fate of the cell (Katajisto, 2015).

The spatiotemporal organization of the mitochondrial network influences a variety of cellular processes, such as buffering calcium, supplying energy in axons, renewal ability of adult stem cell, control of the movement and direction of motile cells etc (Friedman and Nunnari, 2014; Mishra and Chan, 2014). Besides the ability of the mitochondria to rapidly divide and fuse, the active organization of the mitochondrial network is also dependent on motility. These activities govern the overall connectedness, shape and location of mitochondria within cells, and thus influence both organelle and cellular function.

1.3. The mitochondrial transport machinery

In proliferating higher eukaryotic cells, the mechanisms governing mitochondrial trafficking are not completely understood. Symmetrically dividing cells are not the optimal system to study mitochondria active transport, since differences in mitochondria inheritance are hard to observe and might lead to misleading conclusions. On the contrary, polarized cells, such as the budding yeast *Saccharomyces cerevisiae,* are attractive model systems to study the mechanisms involved in mitochondria distribution and segregation. In budding yeast, cell division occurs by the formation of a daughter bud, which appears at a distinct site on the mother cell surface. The inheritance of mitochondrial content to the bud is a very regulated and monitored procedure, since during bud growth, there is a perfect linear link between bud size and the amount of mitochondria transported to the bud (Rafelski et al., 2012). In yeast, active mitochondrial transport is associated with actin cytoskeleton. The first actin-related factor, which was recognized to be associated with the mitochondria was the central regulator of actin dynamics, Arp2/3. Arp2/3 is localized at the mitochondria (Boldogh et al., 2001; Senning and Marcus, 2010).

Given its localization and the ability to induce actin polymerization, Arp2/3 is considered to be a master regulator of mitochondria transport in yeast. In addition, an actin motor protein Myo2 was shown to transport mitochondria along actin filaments (Altmann et al., 2008). Myo2 binds mitochondria via the adapter proteins Mmr1 and Ypt11, the deletion of which leads to impaired mitochondrial inheritance (Chernyakov et al., 2013). Thus, proper mitochondria inheritance in yeast relies on actin motor proteins and their adaptors.

Compared to budding yeast, in higher eukaryotic cells the molecular machinery that drives mitochondrial motility is less understood. The preferred model for

mitochondria motility research is neurons. Neurons are polarized cells. Mitochondria move along the polarized axons and dendrites. The microtubules (MTs) are organized such that the MT plus ends are closer to the cell tips and the MT minus ends are pointed to the cell body. Hence, the directionality of mitochondrial movement is determined by tracking mitochondria movement relatively to the MTs. In addition, live-cell imaging of single mitochondrion is easier since the mitochondria are fragmented and travel for long distance in axons (Macaskill et al., 2009).

Both in budding yeast and mammalian cells, mitochondria move along the cytoskeleton. However, in budding yeast, the actin cytoskeleton serves as the main platform for mitochondria trafficking, while in higher eukaryotes, mitochondria motility is mainly associated with MTs. This motility relies on motor proteins, where the mitochondria anterograde movement (transport towards the MT plus-end) is governed by Kinesins, while the retrograde mitochondria movement (transport towards the MT minus-end) is driven by Dyneins (Nangaku et al., 1994; Varadi et al., 2004). The MT plus end-directed protein Kinesin is localized at the mitochondria. The transport of mitochondria on microtubules was reconstituted *in vitro* by adding recombinantly purified Kif5B (a member of Kinesin-1 superfamily) to purified mitochondria and microtubules. Mitochondria underwent deformation and formed tubules as they travelled towards the MT plus end. The active deformation and direction-driven alteration indicates that kinesin can generate the force required for active pulling of mitochondrial membrane (Wang et al., 2015).

Although the central players of organelle transport are motor proteins, their recruitment to specific organelles is mediated by distinct adaptors. Indeed, the discovery of specific mitochondrial adaptor proteins, which link the organelle to the microtubules was an enormous step towards understanding the mechanism and function of mitochondrial motility in higher eukaryotes. The initial breakthrough came from a *Drosophila* mutant screen for blind flies. This screen identified a mutation in a gene named Milton. A closer look on the cellular phenotype of milton mutants showed axons lacking mitochondria. Milton was found to co-precipitate with mitochondria and kinesin. Therefore, it was suggested to be involved in mitochondria trafficking in neurons (Stowers et al., 2002). In later studies, additional components of the mitochondria transport machinery were identified. The mitochondria transport complex is composed of at least three proteins: the motor protein kinesin (or dynein) which directly interacts with Trak1/2 (Milton's mammalian orthologs designated as Trafficking Kinesis-Binding Protein) and an outer mitochondrial, Rho-like GTPase, called Miro. Miro regulates mitochondria movement by

recruiting Trak1/2 to the mitochondria and promotes motor protein-dependent movement along microtubules (Glater et al., 2006). In mammals, the link between mitochondria and MT motors is mediated by two Miro proteins, Miro1 and Miro2.

1.1. The Miro GTPases: Mechanism and function

The Miro proteins, localized at the mitochondrial outer membrane, are highly conserved throughout eukaryotes. The proteins interact with the outer mitochondrial membrane via their C-terminal trans-membrane domains while the N-terminus is exposed to the cytosol (Fransson et al., 2003; Frederick et al., 2004; Reis et al., 2009). Miro consists of two GTPase domains flanking two EF hands (Introduction Figure 2). The C-terminal GTPase domain of Miro homolog in fruit fly displays high structural similarity to the Rheb GTPase, a subfamily of RAS. Miro's N-terminal GTPase domain is of unknown structure with no similarity to any other GTPases.

The structural model of the EF hands revealed that the Ca^{2+} binding sites are accompanied by non-canonical "hidden" EF hands (hEF 1 and 2) followed by single helices (LM helices 1 and 2) (Klosowiak et al., 2013).

Yeast Miro has weak GTPase activity (Koshiba et al., 2011). Interestingly, the human Miro GTPase activity was found to increase upon interaction with a novel Miro interactor guanine activating protein (GAP) VopE. This GAP is a Vibrio cholerae Type 3 secretion system effector (Suzuki et al., 2014). This result implies that Miro1 GTPase activation might rely on a specific effector protein, but the endogenous GAP(s) is/are unknown.

As mentioned above, in metazoans, Miro is a component of the protein complex that regulates mitochondrial transport. The importance of Miro in mitochondria distribution was first revealed in overexpression studies in mammalian cells, where the mitochondria network was mislocalized upon ectopic expression of Miro (Fransson et al., 2003). The machinery involved in transport in somatic cells is identical as in neurons (Macaskill et al., 2009; van Spronsen et al., 2013; Wang and Schwarz, 2009). In proliferating cells, the motility and dynamics of mitochondria are highly regulated in a cell cycle-dependent manner. For example, at the onset of mitosis, mitochondria move away from the spindle region to the cell periphery. Later, in cytokinesis, the mitochondria network is organized into two clusters, one close to the cleavage furrow and the other at the cell pole (Kashatus et al., 2011; Lawrence and Mandato, 2013). The way mitochondria trafficking is regulated in dividing cells is yet to be understood. However, from the study

of the Miro/Milton/Motor protein complex, there are few key concepts that might be also true for the regulation of mitochondria trafficking during cell division. TFor instance, the direction of mitochondrial movement can be determined by the affinity of mitochondrial adaptors to motor proteins and their subcellular localization (van Spronsen et al., 2013). In neurons, Trak1 binds both kinesin and dynein, while TRAK2 preferentially interacts with dynein. In addition, retrograde movement of mitochondria in dendrites is more frequent compared to axons, where there is no preference for the direction of mitochondrial movement. This could be rationalized by the higher levels of Trak2 at the dendrites over axons, while the presence of Trak1 and Trak2 is similar in axons (van Spronsen et al., 2013).

Another factor regulating mitochondrial movement is cytosolic Calcium levels. Miro Ca^{2+} binding domains were linked to mitochondria motility. In fact, mitochondria stop moving upon Ca2+ elevation. This block in mitochondrial movement is mediated by the Ca^{2+}-sensing domains of Miro. Two alternative models explain how the signal is transduced at the molecular level (Saotome et al., 2008). The first model suggests kinesin disassociates from MT and interacts directly with the N-terminus of Ca2+-bound Miro (Wang and Schwarz, 2009). The alternative model poses that the block in mitochondria transport is due to the detachment of kinesin from the Miro-Milton complex (Macaskill et al., 2009). The mitochondrial GTPase Miro is ubiquitously expressed in a variety of different tissues (van Spronsen et al., 2013).

Moreover, accumulating evidence from yeast and human model cells suggests that Miro might be involved in extracurricular function besides mitochondrial trafficking. The first evidence for this comes from synthetic screen in budding yeast. This screen revealed a complex which tethers the mitochondria outer membrane and the ER (Kornmann et al., 2009). The protein complex is composed of five different proteins and one of them is Gem1p (Miro ortholog in yeast). Furthermore, Miro1 was found at the interface between the ER and mitochondria in mammalian cells (Kornmann et al., 2011). One interpretation could be that perhaps the ER membrane regulates mitochondria motility in Miro-dependent manner. In fact, the mitochondria and the ER were shown to move together on acetylated MTs (Friedman et al., 2010), which strengthens the hypothesis that ER-mitochondria motility could be regulated via Miro.

Besides motor protein-driven movement along microtubules, mitochondria are also attached to actin filaments. Notably, treatment with an MT-depolymerization agent was reported to have only a minor effect on mitochondria distribution and motility (Friedman

et al., 2010). One way to explain this observation is the possibility that the mitochondria move on actin cables in mammalian cells.

Unlike in budding yeast, evidence for actin-based mitochondria movement is missing in metazoans. However, some indirect evidence links the actin-based motor protein Myo19 to mitochondrial distribution and motility. Myo19 was shown to interact with the mitochondria via its protein cargo attachment domain. Moreover, Myo19 overexpression increased mitochondrial motility in neurons (Quintero et al., 2009). More recently, a possible role of Myo19 in mitochondria distribution and cell division was suggested. In this study, mitotic mitochondria partitioning failed in Myo19-silenced cells. In addition, the mitochondria were elongated and hyper-connected. Knocking down the mitochondria fusion factor Mfn2 could restore Myo19 phenotype (Rohn et al., 2014). These results suggest a role for Myo19 in mitochondria network dynamics integrity and cell cycle. However, the direct evidence for actin-based mitochondria motility by myosin is missing. Also, the mechanisms by which myosin interact with mitochondria and influence their movement are unknown.

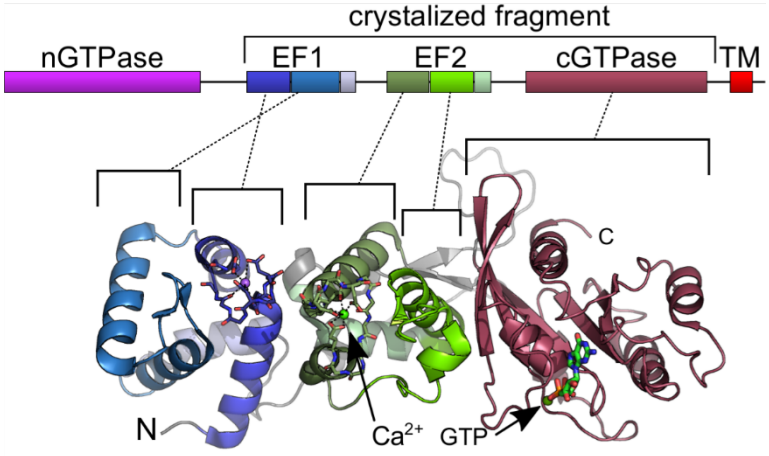

Introduction Figure 2: Top: Primary structure of Miro proteins. nGTPAse, N-terminal GTPase domain; cGTPase, C-terminal GTPase; EF1 and EF2, first and second EF-hand Ca^{2+}-binding motifs; TM, transmembrane segment. Bottom, crystal structure of *Drosophila* Miro. Only the indicated fragment was crystallized. Each Ca^{2+}-binding EF-hand is accompanied by a non-Ca^{2+}-binding homologous domain.

1.2. Mitochondria trafficking independent of motor proteins

Mitochondria move on cytoskeletal elements, and motor proteins are the driving forces of this movement. Yet, in fission yeast (*S.pombe*), an alternative pathway for mitochondria motility was found (Pon, 2011). In fission yeast, several linear bundles of antiparallel microtubules are organized along the cell axis, with the plus ends found at the cell extremities. The mitochondria tubules are dispersed along the cell axis parallel to the MT. When cells enter mitosis, the mitochondria are actively transported to the cell tip to ensure proper inheritance of the mitochondrial content. Surprisingly, a study by Yaffe and Vale reports an alternative way for mitochondria trafficking in a motor protein-independent manner. The researchers used time lapse total internal reflection microscopy (TIRF) to observe MT and mitochondria. They showed for the first time that mitochondria are attached to growing and shrinking MT ends (Yaffe et al., 2003).

In 2011, another study by Fu et al. discovered a protein named Mmb1p (mitochondria microtubule binder 1) that localizes both to the mitochondria and MTs. Mitochondria appear as aggregates asymmetrically distributed in the cell in the absence of Mmb1p. This aggregation leads to insufficient inheritance of the mitochondria and subsequent cell death (Fu et al., 2011).

In another study, kinesins or dyneins containing a mitochondria interaction sequence were introduced in Mmb1p-deleted cells (Fu et al., 2011). With this approach, the mitochondria aggregation phenotype was not rescued. On the other hand, a chimeric protein containing mitochondria- and MT-binding domain could replace Mmb1p for proper distribution of mitochondria network. This suggests that mitochondria distribution is dependent on MT dynamics in fission yeast (Fu et al., 2011; Li et al., 2015). Indeed, Mmbp1 was shown to associate with MT lattice. In addition, Mmbp1 stabilizes MTs by attenuation of the rescue and catastrophe events. This leads to stabilization of mitochondria in a static position and prevents morphological changes in the mitochondrial network.

Motor protein-independent mitochondrial transport has never been observed in any other model organism except fission yeast. However, there remains a possibility such processes could exist in higher eukaryotes too.

Another work suggested a different mechanism of mitochondrial trafficking mediated by dynamic MTs (Chiron et al., 2008). Here, they showed association of mitochondria with a conserved MT binding protein CLASP (Cytoplasmic linker associated protein), which belongs to the +TIP family (plus end-tracking proteins, see below). Deletion of CLASP led to altered mitochondrial morphology (Chiron et al., 2008) However, other studies failed to reproduce this observation and thus the involvement of CLASP in mitochondria trafficking needs to be further clarified (Pon, 2011).

Taken together, the current evidence suggests a unique motor protein-independent mode of organelle transport in fission yeast. Whether such processes exist in higher metazoans remains to be addressed.

1.3. The tip tracking machinery

In the cells, the MTs are not only influencing membrane trafficking but also dictate various cellular processes such as cell division, cell migration, and cell shape (for review see Jiang and Akhmanova, 2011). The MTs are forming a cylinder tubular structure composed of proximately thirteen laterally associated protofilaments (Nogales et al., 1998a, 1998b). Each protofilament consists of alpha and beta Tubulin dimers.. The MTs polymerise by "head to toe" association of the α / β -Tubulin dimers (Nogales et al., 1998a, 1998b). MTs are dynamic polymers which undergo multiple rounds of assembly and disassembly. Their dynamic properties provide the plasticity and the rapid reaction of the cells to internal and external signals, which results in fast morphological changes (Mitchison et al., 1986). MTs are also polarized, their minus end being located at the MTOC, and their plus end being generary localised at the periphery of the cell (Jiang and Akhmanova, 2011). The plus end MT asters explore the cytoplasm in a very dynamic manner. This rapid MT dynamics is defined by three phases, growth, pause and shrinkage (Li et al., 2002). The transition from growth to shrinkage is named catastrophe, where MT ceases growth and changes toward critical shrinkage phase, in which protofilaments are removed from the MT plus end (Mitchison and Kirschner, 1984). The transition from, shrinkage to growth is called rescue, when GTP-bound tubulin dimers are added at the plus-end of the microtubule. These growth and shrinkage states are accompanied by dynamic conformational changes of the MT plus-end. During MT polymerisation, the protofilaments at the MT ends are straight, whereas during MT depolymerization the protofilaments at the MT ends are curved. This dynamic transition is explained by conformational changes in microtubule dimers (Mitchison and Kirschner, 1984). Tubulin dimers bind two molecules of GTP. Alpha Tubulin binds GTP in unexchangeable conserved site while the GTP bound to β -tubulin is hydrolyzed to GDP shortly after assembly (Mitchison and Kirschner, 1984). The incorporation of Tubulin dimer into the protofilament is feasible in the GTP tubulin dimer conformation (Li et al., 2002). Following association, GTP hydrolysis happens very rapidly in the β -tubulin subunit. Hence, the MT lattice is enriched in Tubulin GDP formation. Rounds of hydrolysis of GTP bound β -tubulin and binding of tubulin dimer afford MTs ends structure conformational changes which determine the MT polymer assembly or disassembly state (Li et al., 2002). MT dynamics is dependent on the in-situ concentration of soluble dimers at the MT plus end. A high concentration of GTP -tubulin dimer will promote MT polymerization whereas a low concentration will promote catastrophe (Li et al., 2002). Several studies tested MT dynamics in-vitro. In these studies, MTs were purified, and the influence of soluble MT in

physiological concentrations result in stochastic rounds of MTs growth and shrinkage, This dynamic behaviour was entitled “dynamic instability” (Mitchison and Kirschner, 1984). However, a large set of in-vivo studies showed that MT dynamics is influenced by a collection of conserved MT regulatory proteins located along the MT lattice or at the MT ends.

As mentioned previously, organelle positioning and function are influenced by MT dynamics. Mitochondrial transport (only in fission yeast) and ER tubulation can be promoted by association with dynamic MTs (Fu et al., 2011, Grigoriev et al., 2008). The mechanism and function of this kind of membrane transport is far more established for the ER. The ER membrane associates with growing MTs via the ER resident membrane protein STIM1 and the plus-end tracking protein Eb1 (Grigoriev et al., 2008). Eb1 labeled in animal cells appears as a comet-like structure at the tip of growing microtubules. Possible explanations for this comet formation includes affinity of Eb1 for GTP cap at the MT tips or recognition of specific structural features such as tubulin sheets found at the growing tips (Jiang and Akhmanova, 2011).

Already in earlier *in vitro* reconstitution experiments with purified MT and microsomes, Waterman-Storer et al. described that the induction of MT growth can promote microsome movement, which is referred as Tip Attachment Complex (TAC) dynamics (Waterman-Storer et al., 1995). TAC dynamics depends on the ER membrane protein STIM1 and +TIP protein Eb1 (Grigoriev et al., 2008).

In case of ER transport by the TAC phenomenon, there are two physiological aspects reported. First, Ca^{2+} storage is regulated by subcellular positioning of STIM1. Following the depletion of ER Ca^{2+} levels, STIM1 moves to the plasma membrane. At the plasma membrane (PM) STIM1 associates with the effector PM Ca^{2+} channel ORAI, which allows Ca^{2+} entry to the cytosol, and its subsequent pumping into the ER lumen. The recruitment of STIM1 to the PM relies on Eb1 and MT dynamics since the treatment of cells with MT depolymerization agents prevents Ca2+ flux into the ER lumen (Smyth et al., 2007). The second aspect links ER organization and mitosis. In mitosis, the space between the spindle poles is devoid of ER membrane. This space void is achieved by the detachment of the ER membrane from the mitotic spindle, which is mediated by the dissociation of Eb1 from STIM1, following STIM1 phosphorylation (Smyth et al., 2012).

In summary, during cell cycle, organelles undergo massive reorganization. The mitochondria, in particular, are very dynamic organelles that constantly divide, fuse and get transported. These processes are critical for achieving its specific architecture, which in turn ensure accurate distribution of metabolism (e.g. ATP), buffering of Ca2+ and inheritance. There are at least two known mechanisms by which the mitochondria can be transported towards the cell periphery. First, motor protein-dependent transport and second, the transport by attaching MTs independent of motor protein. The molecular mechanism regulating mitochondria motility and its link to physiology are still under investigation.

2. Thesis overview

A synthetic screen in baker's yeast revealed a complex tethering the mitochondria and the Endoplasmic Reticulum (ER). This complex is called ERMES [ER-Mitochondria-Encounter-Structure], and consists of four structural and one regulatory protein (Kornmann, 2011). The structural proteins are only conserved in the fungi kingdom, while the fifth ERMES component, an atypical Rho-GTPase termed Gem1, is conserved from yeast to mammals, where it is known as MIRO (Kornmann et al., 2011). The initial goal of my project was to identify, and if possible, characterize a hypothetical mammalian tethering-complex between ER and mitochondria using Miro as bait. For identification of the ERMES homologues, MIRO was purified together with its associated proteins, which were subsequently identified using LC-MS/MS. Within the large variety of identified possible interactors, the most promising ones were selected for further examination. In the first experiments I was interested in the localization of the identified protein as well as in their effect on mitochondrial dynamics when absent. In order to answer the first question, I used specific antibodies to check for co-localization of Miro1 with the selected proteins. In addition, I took advantage of mitochondrial fluorescent markers to address the effect of the depletion or overexpression of these candidates on mitochondria dynamics and morphology. However, **none of the most promising candidates were found to localize together with Miro1 or to impact on the appearance of mitochondria**. These results led me to switch towards another, well-established approach, called SILAC, stable-isotope amino-acid labelling in culture. Using SILAC allows discriminating between post-lysis binding contaminants and Miro1 native interactions that were established before cell lysis. The outcome of this experiment allowed me to reject some of the formally detected potential interactions, and, in parallel, revealed few new targets for further investigation. However, this approach did not lead to the identification of ERMES-like proteins in mammalian cells. In this thesis dissertation I will focus one protein which was found to interact with Miro, the microtubule (MT)-binding protein Cenp-F (Centromeric protein F). Investigating the role of Cenp-F and Miro in mitochondria mobility led to a potential new mechanism of organelle transport in an MT dynamic-dependent manner. In the first part of the thesis, I will present my published study, which summarizes the discovery of Cenp-F as a Miro-associated protein and their combined function in mitochondria distribution in dividing cells. I could show that Cenp-F is involved in mitochondria trafficking, most likely by attaching mitochondria to growing MTs. Direct evidence was, however, missing. It was not clear whether Cenp-F, by itself, is sufficient for moving mitochondria along MTs, or this mobility is dependent on other factors, for example motor proteins. Interestingly, a very detailed in vitro work addressing this very question was just published by Vladimir Volkov and colleagues (Volkov et al., 2015). In this work the researchers showed that the purified MT-interacting domain of Cenp-F could follow de-

polymerizing MTs in vitro. Strikingly, Cenp-F could attach cargo (Glass beads in this case) to shortening MTs without additional proteins. In collaboration with Volkov, Martin Peterka (another Ph.D. student from the Kornmann group) and I set out to tackle the question whether Cenp-F is sufficient to transduce the force from polymerizing MTs to Cargos. In the second part of the result section, I will present that indeed, the purified carboxyl-terminal MT-interacting domain of Cenp-F can attach cargo – glass beads and isolated mitochondria – to growing and shrinking MTs. Moreover, I could further support the in vitro work with data from live cells in which full-length Cenp-F fused to GFP followed growing and shrinking MTs in cells. Although the molecular mechanism is not fully understood, this work reveals for the first time an adaptor protein that promote organelle motility by using the MTs as motor proteins.

3. Results - Mitotic redistribution of the mitochondrial network by Miro and Cenp-F

Gil Kanfer[1], Thibault Courtheoux[1], Martin Peterka[1], Sonja Meier[1], Martin Soste[1], Andre Melnik[1], Katarina Reis[2],Pontus Aspenstrom[2], Matthias Peter[1], Paola Picotti[1] & Benoit Kornmann[1]

1 Institute of Biochemistry, ETH Zu¨rich, 8093 Zurich, Switzerland.

2 Department of Microbiology, Tumor and Cell Biology, Karolinska InstitutetStockholm, Sweden.

Nature communication, DOI: 10.1038/ncomms9015

Contributions:

I am the first author of this publication, led the project and performed most of the experimental work, designed the study, and wrote the paper under the supervision of Prof. Dr. Benoit Kornmann.

nature COMMUNICATIONS

ARTICLE

Received 19 Jun 2015 | Accepted 8 Jul 2015 | Published 11 Aug 2015

DOI: 10.1038/ncomms9015 OPEN

Mitotic redistribution of the mitochondrial network by Miro and Cenp-F

Gil Kanfer[1], Thibault Courthéoux[1], Martin Peterka[1], Sonja Meier[1], Martin Soste[1], Andre Melnik[1], Katarina Reis[2], Pontus Aspenström[2], Matthias Peter[1], Paola Picotti[1] & Benoît Kornmann[1]

Although chromosome partitioning during mitosis is well studied, the molecular mechanisms that allow proper segregation of cytoplasmic organelles in human cells are poorly understood. Here we show that mitochondria interact with growing microtubule tips and are transported towards the daughter cell periphery at the end of mitosis. This phenomenon is promoted by the direct and cell cycle-dependent interaction of the mitochondrial protein Miro and the cytoskeletal-associated protein Cenp-F. Cenp-F is recruited to mitochondria by Miro at the time of cytokinesis and associates with microtubule growing tips. Cells devoid of Cenp-F or Miro show decreased spreading of the mitochondrial network as well as cytokinesis-specific defects in mitochondrial transport towards the cell periphery. Thus, Miro and Cenp-F promote anterograde mitochondrial movement and proper mitochondrial distribution in daughter cells.

[1] Institute of Biochemistry, ETH Zürich, 8093 Zürich, Switzerland. [2] Department of Microbiology, Tumor and Cell Biology, Karolinska Institutet, SE-171 77, Stockholm, Sweden. Correspondence and requests for materials should be addressed to B.K. (email: benoit.kornmann@bc.biol.ethz.ch).

Mitosis requires profound cytoskeletal reorganization to ensure correct chromosome partitioning. This causes marked changes in cell shape and in the distribution of the cytoplasmic organelles. For example, during mitosis, mitochondria fragment[1,2] and congress towards the dividing cell centre before partitioning into daughter cells through microtubule-based transport. This partitioning likely involves linking mitochondria to molecular motors.

To recruit molecular motors, mitochondria have specialized adaptors on their outer membrane. The best-characterized adaptor is the transmembrane calcium-binding GTPase Miro, which plays an essential role in mitochondrial trafficking along axons[3–6]. Yet, how mitochondria are distributed to daughter cells after mitosis remains unknown.

Results

Miro GTPases interact with the centromeric protein F. To identify Miro interactors, we established stable HEK293 cell lines that expressed doxycycline-inducible 3 × Flag-tagged versions of the two Miro paralogues encoded in the human genome—Miro1 and Miro2—and used them for immunoprecipitation (Supplementary Fig. 1A,B) coupled to mass spectrometry. This analysis identified Miro2 in FLAG-Miro1 pull-downs and vice versa, indicating that Miro1 and Miro2 are part of the same complex and underscoring the validity of our approach (Supplementary Data Set 1). This analysis also identified a large number of unrelated proteins, indicating possible unspecific interactions. We therefore devised a stable-isotope amino-acid labelling in culture (SILAC) strategy[7]. We mixed cells expressing Flag-tagged Miro1 with ^{15}N-^{13}C-Arg/^{15}N-^{13}C-Lys-labelled non-transgenic cells, prior to lysis and immunoprecipitation (Supplementary Fig. 1C). In such conditions, illegitimate proteins that bind Miro1 or the immunoprecipitation matrix consequent to cell lysis should derive from both the heavy-labelled and the non-labelled proteins, while *bona fide* interactors should be enriched for non-labelled proteins. Using this approach, we detected only three proteins (Supplementary Fig. 1D) that showed non-labelled peptides enrichment: Miro1, Miro2 and centromeric protein F (Cenp-F).

Cenp-F came as a surprise. It is a large (367 kDa) coiled-coil protein that accumulates during the G2 cell cycle phase, culminating during mitosis[8]. Cenp-F functions at the kinetochore and participates in nuclear envelope disassembly. Cenp-F interacts with several cytoskeletal components, such as Dynein motor complexes and microtubules themselves[9–13].

Cenp-F localizes at mitochondria–microtubule interfaces. To assess whether Cenp-F localized to the mitochondria, we generated a U2OS-derived stable cell line co-expressing a mitochondrial and an ER marker (mtBFP and sec61α-GFP, respectively), which we called KERMIT (for Kinesis of ER and MITochondria). Cenp-F displayed highly variable immunofluorescence staining from cell to cell (Fig. 1a), likely due to the fact that cells were at different cell cycle phases. We imaged Cenp-F together with cell cycle markers, including cyclin A that accumulates in G2 and is degraded in mitosis, phosphorylated histone H3 (Phospho-H3) that is a marker of mitotic chromatin and Aurora-B (Aur-B) that localizes to the midbody during cytokinesis[14]. Cenp-F showed expected localization patterns; Cenp-F was undetectable in G1 and was found in the nucleus, the nuclear envelope, the kinetochores and the midbody in G2, early prophase, (pro)metaphase and cytokinesis, respectively (Fig. 1b; Supplementary Fig. 2A,B). In addition, in S/G2, a fraction of Cenp-F was found on mitochondria (Fig. 1b, top right). Strikingly, at the end of mitosis, Cenp-F was strongly recruited to mitochondria (Fig. 1b, bottom). The profound difference in recruitment between early and late mitosis (Fig. 1c) was not merely due to differences in Cenp-F levels (Supplementary Fig. 2C), and must therefore indicate a regulated process.

Interestingly, during S/G2, Cenp-F was enriched at the distal tip of mitochondria projecting away from the cell centre (Fig. 1d; Supplementary Fig. 2D). This, together with the fact that Cenp-F is a microtubule-binding protein, suggested that Cenp-F mediated mitochondria–cytoskeleton interaction. We used structured-illumination super-resolution microscopy (3D-SIM) to assess the relationship between mitochondria, Cenp-F and microtubules. Microtubules are best conserved by methanol fixation. This fixation protocol, however, does not preserve the fluorescence of the mitochondrial marker in KERMIT cells (our observations). To circumvent this problem, we used U2OS cells stained with mitotracker Red. We imaged S/G2 cells, because (1) they were Cenp-F-positive and (2) the microtubule network is much better imaged in flat interphase cells, compared with round mitotic cells. Virtually all mitochondrial Cenp-F puncta colocalized with microtubules (Fig. 1e), indicating that Cenp-F is at the mitochondria–microtubules interface.

Miro directly recruits Cenp-F to mitochondria. We wondered whether Miro was responsible for recruiting Cenp-F to mitochondria. To achieve complete loss-of-function of both Miro1 and Miro2, we mutated Miro1 using the CRISPR/Cas9 technology in KERMIT cells[15]. We then knocked down Miro2 using specific small interfering RNAs (siRNAs). We generated four Miro1 CRISPR clones, bearing different homozygous mutations in exon 7 and 8. Two were used for subsequent studies (Supplementary Fig. 3A). Miro2 knockdown in Miro1-deficient cells (hereafter, Miro-less cells) led to a complete disappearance of Cenp-F from the mitochondria, even in cytokinetic cells (Figs 2a and 3b; ; Supplementary Fig. 3B), while the localization to the nucleus, nuclear envelope, kinetochores and midbody was unaffected (Supplementary Fig. 3B). Thus, Miro is necessary for Cenp-F recruitment to mitochondria. Conversely, overexpressing FLAG-Miro1 (Fig. 2b) or FLAG-Miro2 (Supplementary Fig. 3C) in KERMIT cells increased mitochondrial recruitment of Cenp-F, showing that Miro is also sufficient for Cenp-F mitochondrial recruitment.

Miro bears two calcium-binding EF hands that regulate its association to molecular motors[4], and two GTPase domains of unclear function[16]. To assess whether any of these domains were involved in Cenp-F recruitment, we transfected Miro-less cells with FLAG-Miro1 bearing mutations predicted to abolish GTPase activity and calcium binding[16]. Mutating the first GTPase domain (T18N) abrogated Cenp-F recruitment, while mutating the second domain (S462N) had no effect. Mutating the EF hands (E208K and E328K) strongly reduced Cenp-F recruitment (Fig. 2c). However, lowering cytosolic calcium level with EGTA and BAPTA-AM did not produce the same effect (Fig. 2d; Supplementary Fig. 3E), indicating that the predicted Miro calcium-binding mutants likely did not mimic calcium-free Miro, and suffered from additional defects. This finding reveals an important caveat in the usage of such mutants to mimic calcium-free Miro[4,5,16]. To define which part(s) of Cenp-F interacts with Miro, we fused all or parts of Cenp-F to GFP. Although GFP-Cenp-F[17] did not recapitulate all the features of endogenous Cenp-F localization, it was robustly recruited to mitochondria by FLAG-Miro1 co-overexpression (Supplementary Fig. 3F), allowing us to narrow down the interaction domain to a C-terminal fragment (Fig. 2e). For Cenp-F fragments showing

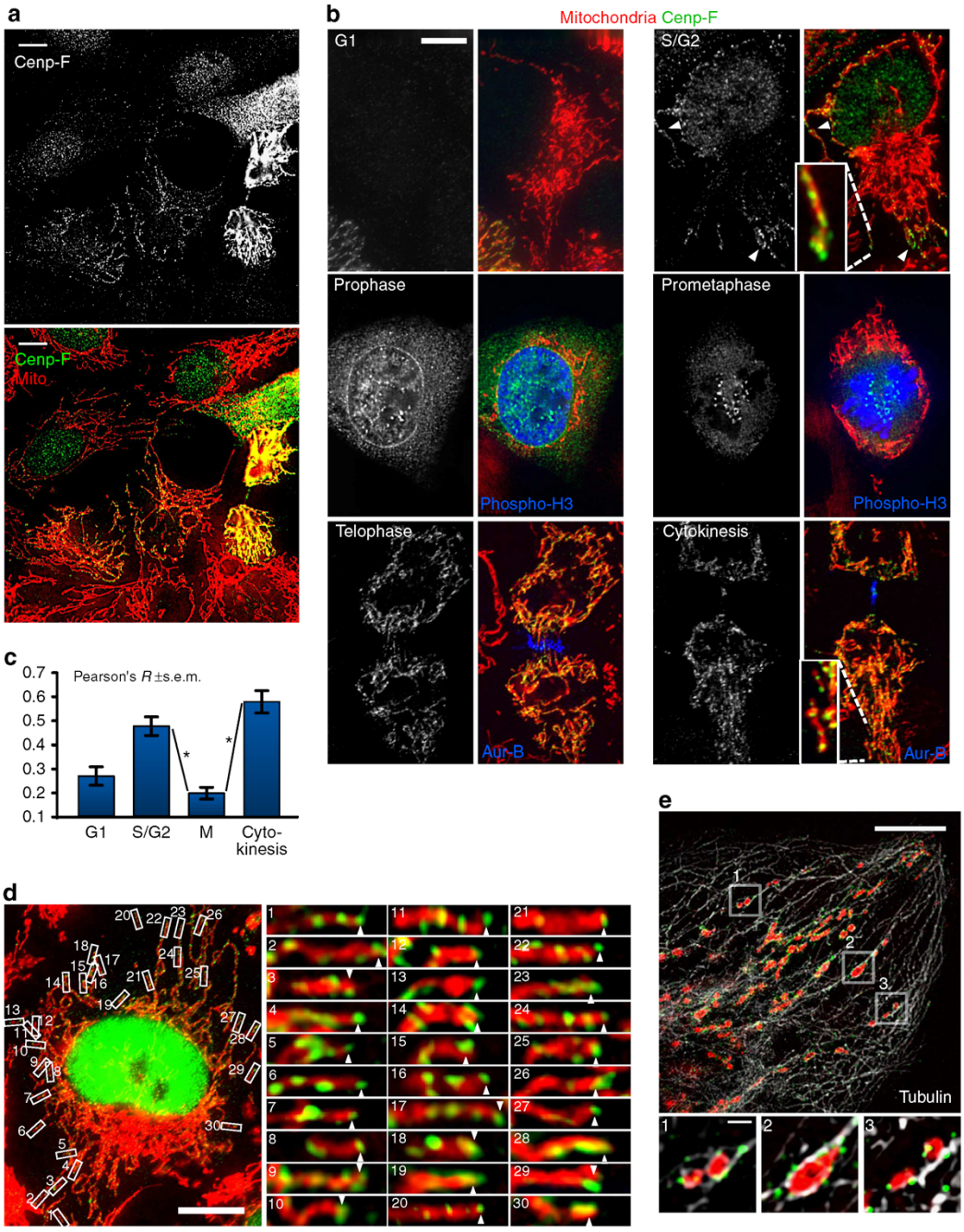

Figure 1 | Cenp-F localizes to mitochondria in a cell cycle-dependent manner. In all panels, mitochondria are shown in red and Cenp-F in green. (**a**) Cenp-F staining is heterogeneous in a field of unsynchronized cells. Immunofluorescence using an α-Cenp-F antibody (green in lower panel) of KERMIT cells expressing a mitochondrial marker (mtBFP, red in lower panel). Scale bar, 5 μm. (**b**) As in **a**. Where indicated, cells were labelled with cell-cycle markers: α-Phosphorylated histone H3 (phospho-H3, blue) α-Aurora-B (Aur-B, blue). Interphase cells were classified as G1 and S/G2 based on Cenp-F levels. Scale bar, 5 μm. (**c**) Quantification of Cenp-F-mitochondria colocalization in different cell cycle phases. M represents mitosis, from prometaphase to anaphase, *P value $<10^{-6}$ from a Mann–Whitney–Wilcoxon U-test. For quantifications, 2–4 regions were selected per cell. Number of selected regions: G1: 14; S/G2: 39, M: 48, cytokinesis: 17. The experiment was repeated at least three times. (**d**) Cenp-F localizes to mitochondrial tips. As in **a**. Scale bar, 10 μm. The right panels are higher magnifications of the boxed area. (**e**) Cenp-F colocalizes with mitochondria and microtubules. Structured-illumination microscopy of U2OS cells stained with mitotracker-red (red), Cenp-F (green) and tubulin-α (white). Scale bars, 5 μm (top panel), 500 nm (bottom).

mitochondrial recruitment in cells, we could reconstitute the interaction in pull-down (Fig. 2f) and yeast two-hybrid assays (Supplementary Fig. 3G). This latter assay showed that Cenp-F directly interacts with both Miro1 and Miro2, and allowed us to narrow the binding domain (Fig. 2g) to a highly conserved 40-amino-acid peptide (Fig. 2h).

Miro and Cenp-F are important for mitochondrial distribution. We hypothesized that Miro-dependent mitochondrial Cenp-F recruitment could serve in mitochondrial transport and distribution in the cell. This idea is consistent with a recent study reporting that mitochondria fail to spread to the cell periphery in Miro1 knockout mouse embryonic fibroblasts[6]. We observed that

indeed, mitochondria extended less towards the periphery in cells lacking both Miro paralogues (Fig. 3a, right). In our case, no phenotype was observed in cells lacking Miro1 only, indicating that the degree of redundancy of Miro1 and Miro2 may vary with cell type. Interestingly, the spreading defect observed in Miro-less cells was phenocopied in Cenp-F-silenced cells (Fig. 3a; Supplementary Fig. 3D).

Yet, because Cenp-F is strongly recruited to mitochondria during cytokinesis, we surmised that Miro/Cenp-F interaction would have a special role during this cell cycle phase. We imaged late cytokinetic wild-type, as well as Miro-less and Cenp-F-silenced KERMIT cells. In wild-type cells (Fig. 3b, left) or cells lacking only Miro1 (Miro1^{CRISPR}), the mitochondrial network adopted a stereotypical shape, where mitochondria were parallel and extended outwards and away from the division plane (arrowheads). In Miro-less cells, however, mitochondria remained clumped around the nucleus (shown by the ER marker in blue, Fig. 3b, right), and this was, again, phenocopied by Cenp-F silencing. Thus, Miro and Cenp-F are necessary for proper mitochondrial spreading after mitosis. Intriguingly, the mitochondrial spreading defect was accompanied by a defect in cellular spreading, which we measured as the minimal distance between the most distant ER signal and the nuclear envelope (Supplementary Fig. 4B). It was thus possible that the mitochondrial spreading defect observed both in interphase and cytokinesis in Cenp-F-silenced and Miro-less cells was caused by an altered cell shape. To ensure that the mitochondrial spreading defect was not due to a change in cell shape, we used Cytoo crossbow-shaped micropatterns to force cells into identical shapes. This allowed us to generate mitochondrial probabilistic density maps[18]. In cells lacking Miro or Cenp-F, mitochondria were more concentrated around the cell centre and failed to spread to the periphery (Fig. 3c). To assess the statistical significance of this phenotype, we computed the moment of inertia of the mitochondrial network around its centre of mass for every cell[19]. This metric, which reflects the spreading of the mitochondrial network, was reduced in cells lacking Miro or Cenp-F (Fig. 3d), confirming that Miro and Cenp-F are necessary for proper mitochondrial spreading, independent of cell spreading. To address whether the spreading defect was specific for a cell cycle phase, we co-stained cells with an anti-cyclin-A antibody. Interestingly, the spreading defect was visible in G1 as well as S/G2 cells (Supplementary Fig. 4A). This is surprising since Cenp-F is absent from G1, and indicates that G1 cells inherit a spreading defect from previous cell divisions.

Because of their reduced adherence, however, mitotic cells could not be forced into predetermined shapes by micropatterns. Therefore, whether the cytokinetic mitochondrial spreading defect is secondary to a change in cell shape remains unanswered. However, because of the results in interphase cells and since Miro proteins are mitochondrial, we consider more likely that defective mitochondrial spreading may, in fact, cause altered cell shape.

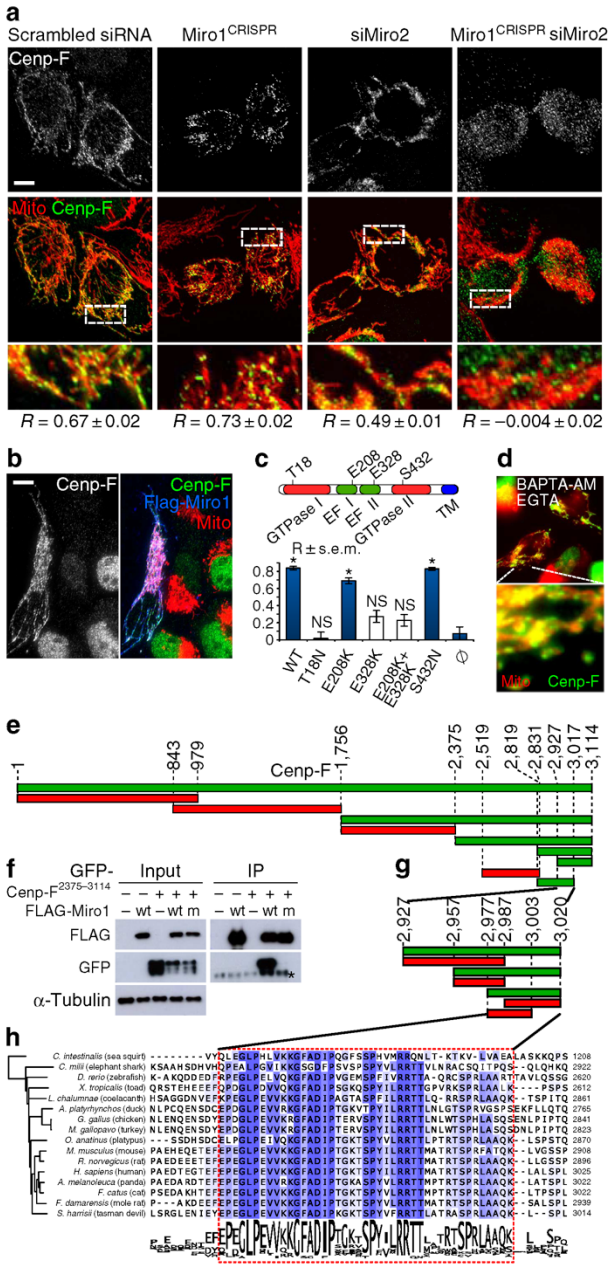

Figure 2 | Miro recruits Cenp-F to mitochondria. (**a**) Miro is necessary for Cenp-F mitochondrial recruitment. Localization of Cenp-F (green) and mitochondria (red) in the presence and absence of Miro1, Miro2 or both. Top: Cenp-F signal only. Middle: overlay. Bottom: magnification of the boxed areas. R: Pearson coefficient colocalization analysis ± s.e.m. Scale bar, 10 μm. Two to four regions were selected per cell. Number of selected regions: Miro1^{CRISPR}: 98; siMiro2: 36; Miro1^{CRISPR}-siMiro2: 34. The experiment was repeated at least four times. (**b**) Miro is sufficient for Cenp-F recruitment. Immunofluorescence of Miro-less cells overexpressing FLAG-Miro1 (blue). Green: Cenp-F, red: mitochondria. Scale bar, 10 μm. (**c**) Cenp-F recruitment to mitochondria by Miro1 mutants. Miro-less cells were transfected as in **b** with plasmids encoding the indicated mutants of Miro1. Recruitment was scored using the Pearson's *R* coefficient. Ø: untransfected cells. **P* value $<10^{-7}$ (compared with untransfected cells) from a Mann–Whitney–Wilcoxon *U*-test. NS, non-significant. Quantifications as in **a**. Number of selected regions: WT: 29; T18N: 17; E208K: 33; E328K: 28; E208K + E328K: 28; S432N: 31; ∅: 27. The experiment was repeated at least four times. (**d**) Cytosolic calcium withdrawal does not prevent Cenp-F mitochondrial recruitment. Cells treated with EGTA and BAPTA-AM to chelate extra- and intracellular calcium were imaged as in **a**. (**e**) Mapping of the Miro-interaction domain on Cenp-F. KERMIT cells were cotransfected with FLAG-Miro and GFP fusion of indicated Cenp-F fragments. Green fragments are recruited to mitochondria. Red ones are not. (**f**) Co-immunoprecipitation of transiently transfected Cenp-F fragment (amino acids 2375–3144) and wild-type (wt) and calcium-binding mutant (m) Miro1. * IgG shedding from the beads. (**g**) Yeast two-hybrid mapping of the Miro-interaction domain on Cenp-F. Green fragments are positive for interaction. Red ones are not. (**h**) Alignment of the Miro-binding domain of Cenp-F in chordates. The phylogenetic tree is generated by neighbour joining using percentage identity.

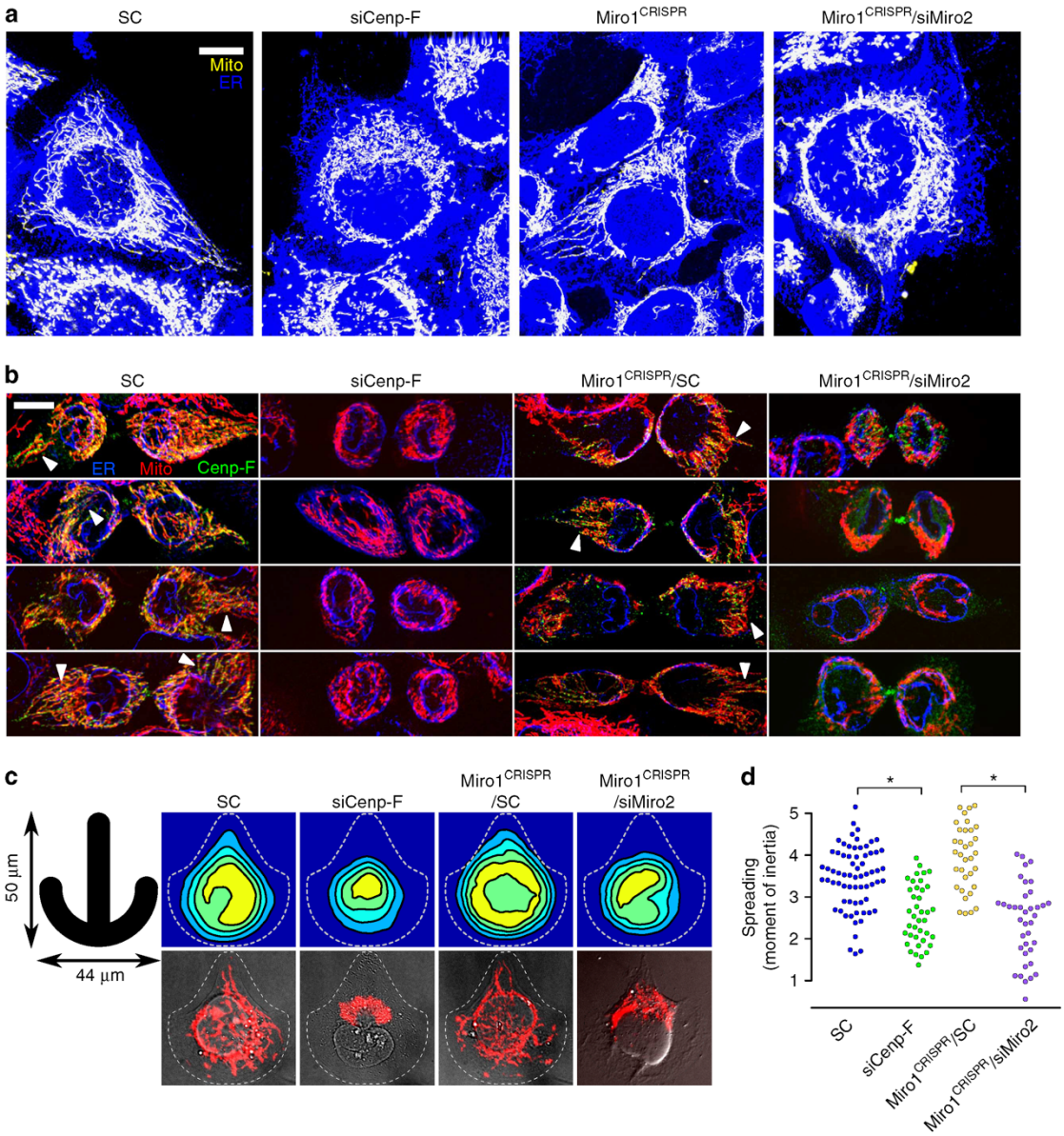

Figure 3 | Miro and Cenp-F influence mitochondrial distribution. (**a**) KERMIT cells of the indicated genotype with the indicated treatment, imaged both for mitochondria (mtBFP, yellow) and the ER (sec-61α-GFP, blue), which indicates cell boundaries. SC, scrambled siRNA. Scale bar, 10 µm. (**b**) Immunofluorescence of cytokinetic KERMIT cells with α-Cenp-F antibody. Arrowheads indicate bundles of parallel mitochondria. Scale bar, 10 µm. (**c**) Live KERMIT cells of the indicated genotype with the indicated treatment were seeded on crossbow-shaped micropatterns (left). Top: probability density maps of the position of the mitochondrial network. Bottom: example cells. The dashed line shows typical cell boundaries. (**d**) Measurement of the moment of inertia of the mitochondrial network of the cells in **c**. $^*P<10^{-5}$ from a Mann–Whitney–Wilcoxon *U*-test. The experiment has been repeated at least three times.

Mitochondria distribution is linked to microtubule dynamics. Both phenotypes observed in interphase and in cytokinesis indicated a defect in anterograde transport of mitochondria. This is paradoxical because Cenp-F is known to interact with Dynein retrograde motor complexes[11]. Dynein needs to be sent to the periphery before transporting cargo towards the cell centre. This involves association with growing microtubule tips[20], a phenomenon known as tip-tracking[21]. Cenp-F binds to the microtubule tips at the kinetochores[22], and associates with the microtubule end-binding protein 1 (EB1)[23]. We wondered whether Miro/Cenp-F could mediate anterograde mitochondrial movement through tip association. We imaged EB1 and Cenp-F using 3D-SIM. We focused on S/G2 cells, since they showed both appropriate Cenp-F signals and a flat morphology conducive to optical imaging. EB1 had a characteristic comet-like staining that marks the microtubule growing tips (Fig. 4a)[20]. In S/G2 cells showing a typical nuclear Cenp-F staining, Cenp-F was also often found in puncta at the extreme tips of EB1 comets (Fig. 4a). We found that 40% of all EB1 comets had visible Cenp-F staining at their tips. This proportion rose to 80% in cytokinetic cells (Supplementary Fig. 4C). To assess the significance of this localization, we computed the proportion of Cenp-F foci located in the vicinity of EB1 comet tips (less than three pixels, that is, the microscope resolution limit), and found that this proportion was much higher than that computed for random points on the microtubules ($P<10^{-7}$ using a permutation test).

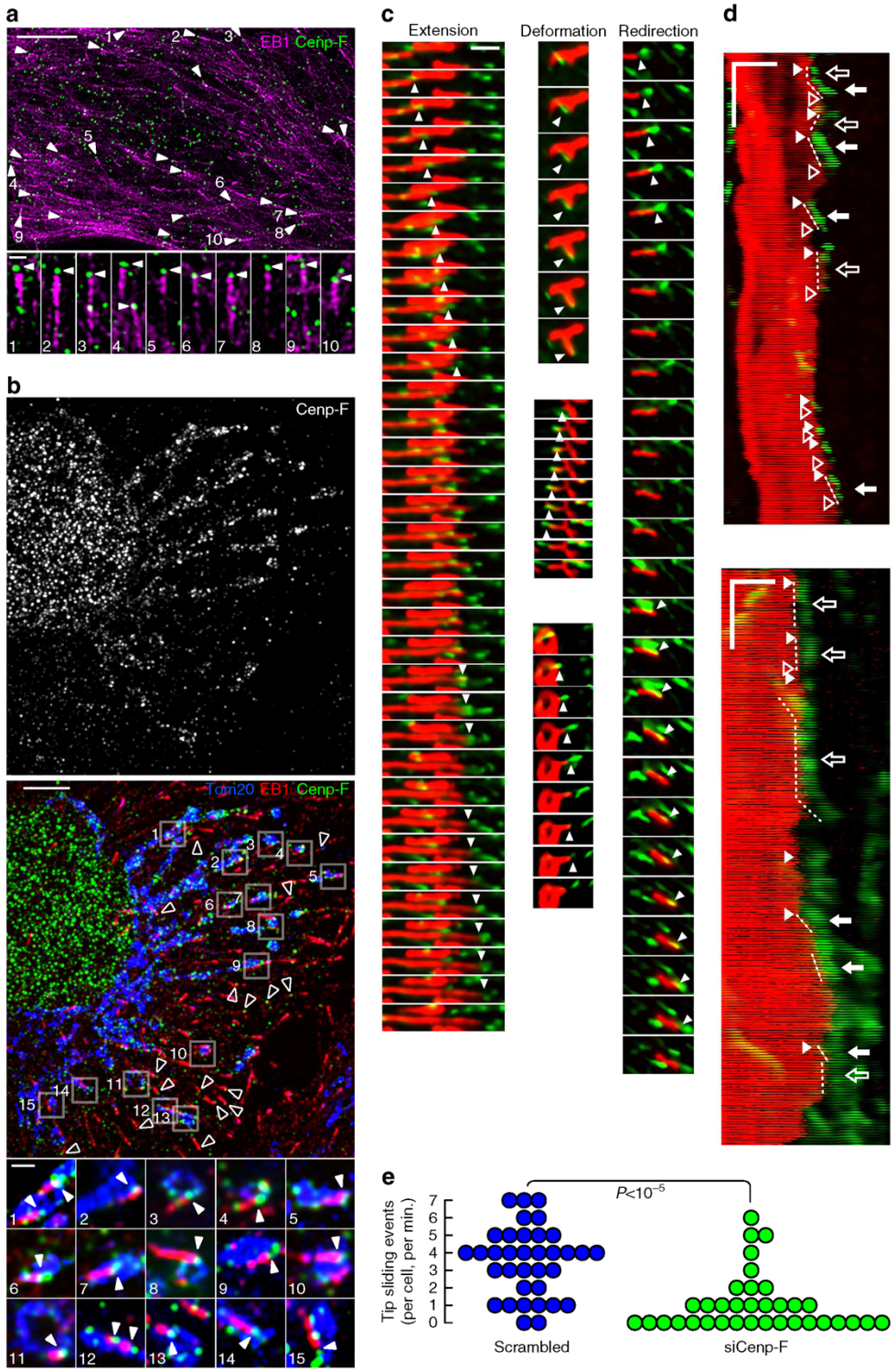

Figure 4 | Mitochondria are connected to microtubule tips. (**a**) Structured-illumination microscopy of Cenp-F and EB1 in U2OS cells. Top: arrowheads represent example EB1 comets that have clear Cenp-F signal at their tips. Scale bar, 5 μm. Bottom: magnification of some of these comets. Scale bar, 500 nm. (**b**) As in **a**. Mitochondria were additionally revealed using an α-Tom20 antibody. Boxed areas in the top panel are magnified in the lower panels. Arrowheads represent Cenp-F signal at the tip of comets and on the mitochondria. Open arrowheads in top panel indicate EB1 comets that have Cenp-F signal at their tips, but are not on mitochondria. Note that the upper panel is a Z-projection across 2 μm, while the lower panels are individual sections. Scale bar, 5 μm (top), 500 nm (bottom). (**c**) Time-lapse images G2-synchronized of U2OS cells expressing GFP-EB1 (green) and mt-dsRED (red). Arrowheads show tip-tracking events. Timescale is 800 ms per frame. Scale bar, 2 μm. (**d**) Kymographs of time-lapse experiments as in **c**, showing that additionally to mitochondria tip-tracking events (plain arrows), microtubule rescue (plain arrowheads), pauses (open arrows) and catastrophes (open arrowheads) events are enriched at mitochondria tips. Scale bar, *x*: 2 μm, *y*: 10 s (0.4 s per frame). (**e**) Quantification of mitochondria tip-tracking events in cells treated or not with siRNA against Cenp-F. *P* value is from a Mann–Whitney–Wilcoxon *U*-test. The experiment has been repeated three times.

Cenp-F localization ahead of EB1 comets is remarkable and contrary to expectations for a hypothetical EB1-binding protein. This localization pattern is, however, not unprecedented: the CytosKeleton Associated Protein 5 (CKAP5/Ch-TOG) was also shown to lie at the tip of EB1 comets[24]. We compared the localization of Cenp-F and CKAP5/Ch-TOG, relative to EB1 and microtubules, and found both proteins to localize very similarly (Supplementary Fig. 4D–I).

We imaged mitochondria using an α-Tom20 antibody, together with EB1 and Cenp-F, and found that the comets whose tips were on mitochondria showed Cenp-F staining (Fig. 4b). These results were also true in cytokinetic cells (Supplementary Fig. 4C).

To test whether mitochondria could be moving together with growing microtubule tips, we imaged live G2-synchronized U2OS cells, which expressed GFP-EB1 and a mitochondrial marker (mt-dsRed). We could indeed observe numerous events where mitochondria moved along with growing microtubules. Such events were associated with extension, deformation and reorientation of individual mitochondria (Fig. 4c arrowheads; Supplementary Movie 1). Cenp-F was necessary for these events since their frequency was markedly reduced upon Cenp-F knockdown (Fig. 4e). Interestingly, we also observed that mitochondrial tips were local hotspots for microtubule dynamics events. Figure 4d and Supplementary Fig. 5 show that, in addition to coordinated microtubule tips and mitochondrial movements (plain arrows), rescue events (plain arrowheads), pauses (open arrows) and catastrophes (open arrowhead) happen preferentially at mitochondrial tips.

Discussion

Thus, Miro-dependent Cenp-F recruitment governs intracellular mitochondrial distribution. We propose that Miro–Cenp-F interaction connects mitochondria to the tips of growing microtubules, causing mitochondria to track microtubule tips. The observation of tip-tracking mitochondrial movement is unprecedented, but is reminiscent of ER tip-tracking movements[25]. Both types of movement suggest that association with polymerizing microtubules can generate mechanical forces for membrane extension, deformation and reorientation[26]. It is unclear how such forces are generated, since plus-tip-bound proteins are usually turned over upon microtubule growth, and not dragged by the growing tip. A possibility is that motors, such as kinesins are involved in tip tracking. For instance, Cenp-E is a known tip-tracking kinesin[27]. It is worth noting that the mitochondria tip-tracking events that we observe are shorter than published ER tip-tracking events. This may be due to the fact that mitochondria are larger than ER tubules (~500 versus ~50 nm diameter) and therefore, more difficult to transport.

In turn, we observe that mitochondria influence local microtubule dynamics by promoting rescues, pauses and catastrophes. It is unclear how mitochondria can promote these events. One model is that the dragging forces imposed on growing microtubules by attached mitochondria may lead to pauses and catastrophes. Conversely, high Cenp-F local concentration at mitochondria tips may locally promote microtubule rescue.

It is intriguing that Cenp-F, a protein involved in chromosome segregation during mitosis, functions at mitochondria. Adaptors expressed during mitosis to move chromosomes may be reused for transporting other cargoes, such as organelles, at different cell cycle phases. Adaptor reuse for different structures, at different moments may emerge as a common theme. Indeed, we found that Cenp-F was often associated with EB1 comets even when it was not associated with mitochondria (Fig. 4b, open arrowheads; Supplementary Fig. 4C), suggesting that Cenp-F may also be involved in the anterograde transport of other cargoes. Intracellular signals may temporally and spatially direct the motors and adaptors to the appropriate cargoes. Such signals may be integrated either on Miro first GTPase domain, or directly on Cenp-F Miro-binding peptide, which harbours serine and threonine residues that are phosphorylated during the cell cycle[28–30]. These signals may promote or inhibit Miro binding in a timely fashion.

This unsuspected connection between mitochondria, Cenp-F and microtubule will need to be clarified by future investigations. In particular, understanding how Cenp-F is connected to microtubule tips will be highly interesting to understand not only mitochondrial inheritance but also other Cenp-F-dependent processes, such as kinetochore assembly and nuclear envelope breakdown.

Although our observations were made in symmetrically dividing cancer cells, the mechanisms described herein might be of particular importance during development, especially in asymmetrically dividing stem cells. Cenp-F mutations cause congenital malformation and microcephaly in humans[31]. The aetiology of these diseases is unclear and may pertain, at least in part, to Cenp-F mitochondrial function.

Methods

Plasmids. pAc-Sec61α-GFP[32] was a kind gift from Gia Voeltz (University of Boulder, USA). GFP-Cenp-F plasmid[17] was provided by Stephen Taylor (University of Manchester, UK). pcDNA3.1-mtBFP was generated by inserting mtBFP sequence digested with HindIII Xba1 into pcDNA3.1 + plasmid. pcDNA5/FRT/TO-3XFlag-6his-Miro1 and pcDNA5/FRT/TO-3XFlag-6his-Miro2 were cloned by PCR amplification of Miro1 and Miro2 CDSs using primers #1 and #3 (see Supplementary Table 1), and 2# and #4, respectively, using complementary DNA clones as templates (IMAGE clones 40118340 and 4859240, respectively), followed by reamplification using primer #5, #3 and #5, #4, respectively. The PCR products were cloned using Gateway into the pcDNA5/FRT/TO plasmid (Invitrogen). GTPase and EF-hand mutants of Miro1 were generated by site-directed mutagenesis of the pcDNA5/FRT/TO-3XFlag-6his-Miro1 plasmid using primers #10 and #11 for the T18N mutation, #12 and #13 for the E208K mutation, #14 and #15 for the E328K mutation and #16 and #17 for the S432N mutation. Constructs containing different Cenp-F fragments (residues 1–979, 843–1764, 1756–3114, 1756–2375, 2375–3114, 2519–2831, 2719–2831 and 2819–3017) were prepared by PCR using the indicated primers (#22–#34, respectively), and using the GFP-Cenp-F plasmid as a template, followed by cloning into the pcDNA5/frt/to plasmid vector within BamHI and NotI restriction sites. Miro1 CRISPR plasmids (pX330-Miro1ex7 and pX330-Miro1ex8) were generated by cloning annealed oligos (#6, #7 and #8, #9, respectively), designed by the CRISPR design tool into pX330, as described[15].

Cell culture and transfection. HEK293 and U2OS cells were grown at 37 °C in DMEM (Life Technologies) supplemented with 10% FCS, 100 μg ml^{-1} streptomycin, 100 U ml^{-1} penicillin and 1% L-glutamine. To establish the KERMIT cell line, U2OS cells were cotransfected with linearized mtBFP and pAc-Sec61α-GFP. Individual clones were selected in 0.4 μg ml^{-1} G418 and maintenance was performed in 0.2 μg ml^{-1}.

The 3 × flag-6 × HIS-Miro1/2 cell lines were created by cotransfection of pcDNA5/FRT/TO vectors encoding 3 × flag-6 × HIS-Miro1/2 with pOG44 into T-Rex-293 cells (Life Technologies), according to the manufacturer's protocol. The clones were selected in 100 μg ml^{-1} Hygromycin (Invitrogen). For stimulating transgene expression, cells were treated with 10 nM doxycycline for 24 − 48 h.

GFP-EB1-expressing cells were generated by cotransfection of pcDNA5/FRT/TO-EGFP-EB1 (kind gift from Jochen Beck, ETH Zurich) into T-Rex-U2OS cells (Life Technologies), according to the manufacturer's protocol.

Flag-miro purification and mass spectrometry. T-Rex-293 expressing 3 × Flag-6 × HIS-Miro1/2 were harvested and homogenized in lysis buffer (20 mM Hepes, 150 mM potassium acetate, 2 mM magnesium acetate, 0.1 mM phenylmethyl sulphonyl fluoride, 1 μg ml^{-1} leupeptin, 1 μg ml^{-1} aprotinin and 1 μg ml^{-1} pepsatin), containing 2% Triton-100 ×. Whole-cell extracts were incubated with 4% M2-Flag-coated magnetic beads (Sigma). The beads were thereafter washed six times with ice-cold lysis buffer, containing 0.2% digitonin and eluted with the same buffer containing 150 ng ml^{-1} 3 × Flag peptide. Samples were then diluted fivefold with 8 M urea and 0.1 M ammonium bicarbonate and reduced using 12 mM dithiothreitol, at 32 °C for 30 min followed by alkylation with 40 mM iodoacetamide at room temperature for 45 min. The samples were diluted fivefold with 0.1 M ammonium bicarbonate and proteins were digested to peptides by adding 1 μg of trypsin (Promega) and incubating overnight at 32 °C. A column

Quantification of microtubule tip-tracking events. Events where mitochondria move in a coordinate fashion with EB1 comets were counted manually after randomizing the 'scrambled' and 'siCenp-F' movies to avoid biases.

References

1. Kashatus, D. F. *et al.* RALA and RALBP1 regulate mitochondrial fission at mitosis. *Nat. Cell Biol.* **13,** 1108–1115 (2011).
2. Taguchi, N., Ishihara, N., Jofuku, A., Oka, T. & Mihara, K. Mitotic phosphorylation of dynamin-related GTPase Drp1 participates in mitochondrial fission. *J. Biol. Chem.* **282,** 11521–11529 (2007).
3. Guo, X. *et al.* The GTPase dMiro is required for axonal transport of mitochondria to Drosophila synapses. *Neuron* **47,** 379–393 (2005).
4. Wang, X. & Schwarz, T. L. The mechanism of Ca2+ -dependent regulation of kinesin-mediated mitochondrial motility. *Cell* **136,** 163–174 (2009).
5. Saotome, M. *et al.* Bidirectional Ca2+-dependent control of mitochondrial dynamics by the Miro GTPase. *Proc. Natl Acad. Sci. USA* **105,** 20728–20733 (2008).
6. Nguyen, T. T. *et al.* Loss of Miro1-directed mitochondrial movement results in a novel murine model for neuron disease. *Proc. Natl Acad. Sci. USA* 3631–3640 (2014).
7. Ong, S.-E. Stable isotope labeling by amino acids in cell culture, SILAC, as a simple and accurate approach to expression proteomics. *Mol. Cell. Proteomics* **1,** 376–386 (2002).
8. Zhu, X. *et al.* Characterization of a novel 350-kilodalton nuclear phosphoprotein that is specifically involved in mitotic-phase progression. *Mol. Cell. Biol.* **15,** 5017–5029 (1995).
9. Liao, H., Winkfein, R. J., Mack, G., Rattner, J. B. & Yen, T. J. CENP-F is a protein of the nuclear matrix that assembles onto kinetochores at late G2 and is rapidly degraded after mitosis. *J. Cell Biol.* **130,** 507–518 (1995).
10. Bolhy, S. *et al.* A Nup133-dependent NPC-anchored network tethers centrosomes to the nuclear envelope in prophase. *J. Cell Biol.* **192,** 855–871 (2011).
11. Vergnolle, M. a S. & Taylor, S. S. Cenp-F links kinetochores to Ndel1/Nde1/Lis1/dynein microtubule motor complexes. *Curr. Biol.* **17,** 1173–1179 (2007).
12. Feng, J., Huang, H. & Yen, T. J. CENP-F is a novel microtubule-binding protein that is essential for kinetochore attachments and affects the duration of the mitotic checkpoint delay. *Chromosoma* **115,** 320–329 (2006).
13. Musinipally, V., Howes, S., Alushin, G. M. & Nogales, E. The microtubule binding properties of CENP-E's C-terminus and CENP-F. *J. Mol. Biol.* **425,** 4427–4441 (2013).
14. Adams, R. R., Carmena, M. & Earnshaw, W. C. Chromosomal passengers and the (aurora) ABCs of mitosis. *Trends Cell Biol.* **11,** 49–54 (2001).
15. Cong, L. *et al.* Multiplex genome engineering using CRISPR/Cas systems. *Science* **339,** 819–823 (2013).
16. Pransson, A., Ruusala, A. & Aspenström, P. Atypical Rho GTPases have roles in mitochondrial homeostasis and apoptosis. *J. Biol. Chem.* **278,** 6495–6502 (2003).
17. Gurden, M. D. J. *et al.* Cdc20 is required for the post-anaphase, KEN-dependent degradation of centromere protein F. *J. Cell Sci.* **123,** 321–330 (2010).
18. Schauer, K. *et al.* Probabilistic density maps to study global endomembrane organization. *Nat. Methods* **7,** 560–566 (2010).
19. Tolić-Nørrelykke, S. F., Rasmussen, M. B., Pavone, F. S., Berg-Sørensen, K. & Oddershede, L. B. Stepwise bending of DNA by a single TATA-box binding protein. *Biophys. J.* **90,** 3694–3703 (2006).
20. Vaughan, K. T., Tynan, S. H., Paulkner, N. E., Echeverri, C. J. & Vallee, R. B. Colocalization of cytoplasmic dynein with dynactin and CLIP-170 at microtubule distal ends. *J. Cell Sci.* **112** Pt 1, 1437–1447 (1999).
21. Akhmanova, A. & Steinmetz, M. O. Microtubule ±TIPs at a glance. *J. Cell Sci.* **123,** 3415–3419 (2010).
22. Hussein, D. & Taylor, S. S. Farnesylation of Cenp-F is required for G2/M progression and degradation after mitosis. *J. Cell Sci.* **115,** 3403–3414 (2002).
23. Jiang, K. *et al.* A Proteome-wide screen for mammalian SxIP motif-containing microtubule plus-end tracking proteins. *Curr. Biol.* **22,** 1800–1807 (2012).
24. Nakamura, S. *et al.* Dissecting the nanoscale distributions and functions of microtubule-end-binding proteins EB1 and ch-TOG in interphase HeLa cells. *PLoS ONE* **7,** e51442 (2012).
25. Waterman-Storer, C. M. & Salmon, E. D. Endoplasmic reticulum membrane tubules are distributed by microtubules in living cells using three distinct mechanisms. *Curr. Biol.* **8,** 798–807 (1998).
26. Grigoriev, I. *et al.* STIM1 Is a MT-Plus-End-Tracking Protein Involved in Remodeling of the ER. *Curr. Biol.* **18,** 177–182 (2008).
27. Gudimchuk, N. *et al.* Kinetochore kinesin CENP-E is a processive bi-directional tracker of dynamic microtubule tips. *Nat. Cell Biol.* **15,** 1079–1088 (2013).
28. Dephoure, N. *et al.* A quantitative atlas of mitotic phosphorylation. *Proc. Natl Acad. Sci. USA* **105,** 10762–10767 (2008).
29. Kettenbach, A. N. *et al.* Quantitative phosphoproteomics identifies substrates and functional modules of Aurora and Polo-like kinase activities in mitotic cells. *Sci. Signal* **4,** rs5 (2011).
30. Malik, R. *et al.* Quantitative analysis of the human spindle phosphoproteome at distinct mitotic stages. *J. Proteome Res.* **8,** 4553–4563 (2009).
31. Waters, a. M. *et al.* The kinetochore protein, CENPF, is mutated in human ciliopathy and microcephaly phenotypes. *J. Med. Genet.* 147–156 (2015).
32. Friedman, J. R., Webster, B. M., Mastronarde, D. N., Verhey, K. J. & Voeltz, G. K. ER sliding dynamics and ER-mitochondrial contacts occur on acetylated microtubules. *J. Cell Biol.* **190,** 363–375 (2010).
33. Cox, J. *et al.* A practical guide to the MaxQuant computational platform for SILAC-based quantitative proteomics. *Nat. Protoc.* **4,** 698–705 (2009).
34. Golemis, E. A. *et al.* Interaction trap/two-hybrid system to identify interacting proteins. *Curr. Protoc. Mol. Biol.* **Chapter 20,** Unit: 20.1 (2008).
35. Serebriiskii, I. G. & Golemis, E. A. Uses of lacZ to study gene function: evaluation of beta-galactosidase assays employed in the yeast two-hybrid system. *Anal. Biochem.* **285,** 1–15 (2000).

Acknowledgements

We thank Alicia Smith, Martin Jinek, Agnès Michel, Arun Thomas and the whole Kornmann lab for critical comments, Constance Ciaudo, Stephen Taylor and Gia Voeltz for reagents, Simon Nørrelykke for data analyses and the ETH Institute of Biochemistry staff members for their help. Imaging was performed at the Scientific Center for Optical and Electron Microscopy (ScopeM) of the ETH Zurich. This project was supported with funds from the ETH Zurich (to B.K. and M. Peter), the Swiss National Research Foundation professor (to B.K., P.P. and M. Peter) the European Research Council (to B.K., P.P. and M. Peter), the Swedish Research Council (K.R. and P.A.) and the Promedica Stiftung (P.P.).

Author contributions

G.K. led the project and performed most of the experimental work. T.C. and M. Peter performed and analysed the 3D-SIM microscopy experiments. M. Peterka performed the yeast two-hybrid experiments. S.M. performed the Cenp-F truncation experiments. M.S., A.M. and P.P. performed and analysed the mass spectrometry assays. K.R. and P.A. participated in the Miro:Cenp-F interaction studies. G.K. and B.K. designed the study and wrote the paper. All authors discussed the results and commented on the manuscript.

Additional information

Supplementary Information accompanies this paper at http://www.nature.com/naturecommunications

Competing financial interests: The authors declare no competing financial interests.

Reprints and permission information is available online at http://npg.nature.com/reprintsandpermissions/

How to cite this article: Kanfer, G. *et al.* Mitotic redistribution of the mitochondrial network by Miro and Cenp-F. *Nat. Commun.* 6:8015 doi: 10.1038/ncomms9015 (2015).

SUPPLEMENTARY FIGURES

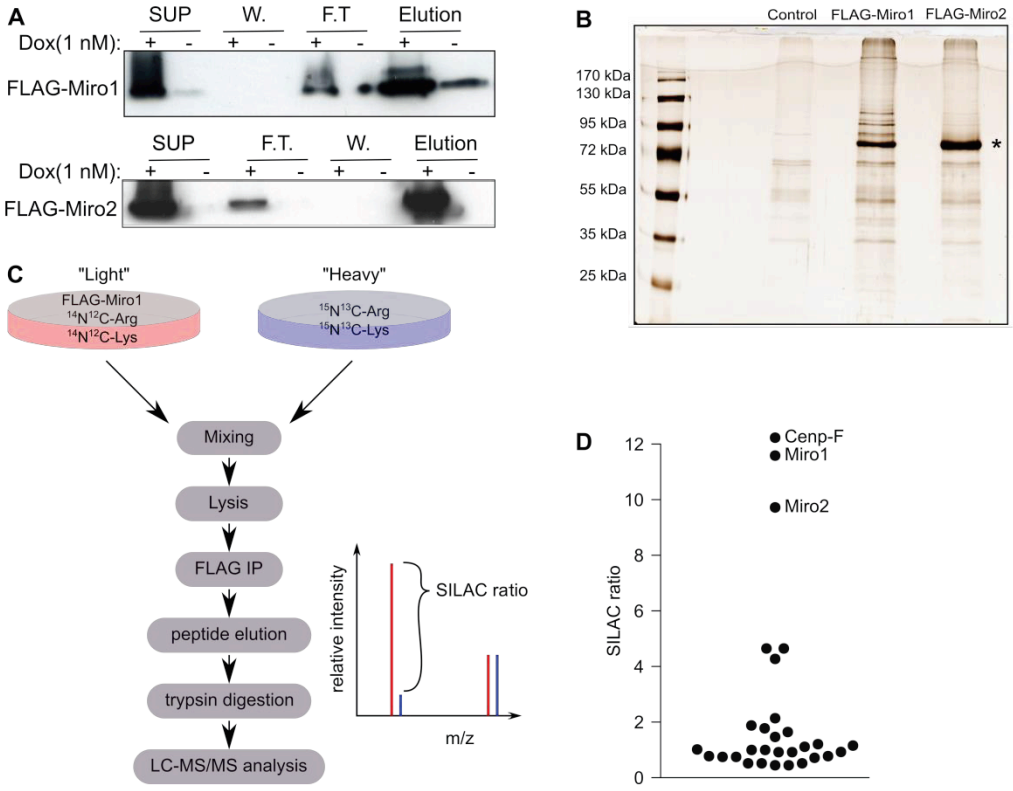

SUPPLEMENTARY FIG. 1

Purification of Miro interacting proteins.
(A) Western blotting with an α-Flag antibody of the following fractions from HEK293 cells expressing FLAG-Miro1 or FLAG-Miro2: whole cell lysate supernatant (SUP), flow-through unbound to the beads (F.T.), last wash (W) and elution. The expression of the transgene has been induced (+) or not (-) by the addition of 1 nM doxycycline (Dox).
(B) Silver-stained SDS-Page of the elutions from normal HEK293 (control), FLAG-Miro1 or FLAG-Miro2 expressing cells. The band indicated by an asterisk is the appropriate size for being FLAG-Miro.
(C) Stable isotope labeling with amino acid in culture (SILAC) strategy to discriminate proteins bound to Miro *in vivo* from those binding as a consequence of cell lysis. Cells expressing FLAG-Miro1 are cultured in a medium containing non-labeled Arginine and Lysine, while wild type cells are cultured in a medium containing ^{15}N-^{13}C ("heavy")-labeled Arginine and Lysine. "Light"- and "heavy"-labeled cells are mixed before lysis, immunoprecipitation, and mass-spectrometry detection. The heavy label causes a mass shift of 8 Da for Lysine tryptic peptides and 10 Da for Arginine tryptic peptides. Proteins that were bound to Miro1 before lysis should be exclusively light-labeled, while proteins that bound to Miro1 after lysis should be equally light- and heavy-labeled. The SILAC ratio can thus be used as a proxy for specificity.
(D) Bee swarm plot of the SILAC ratios for proteins identified with high confidence in the immunoprecipitate.

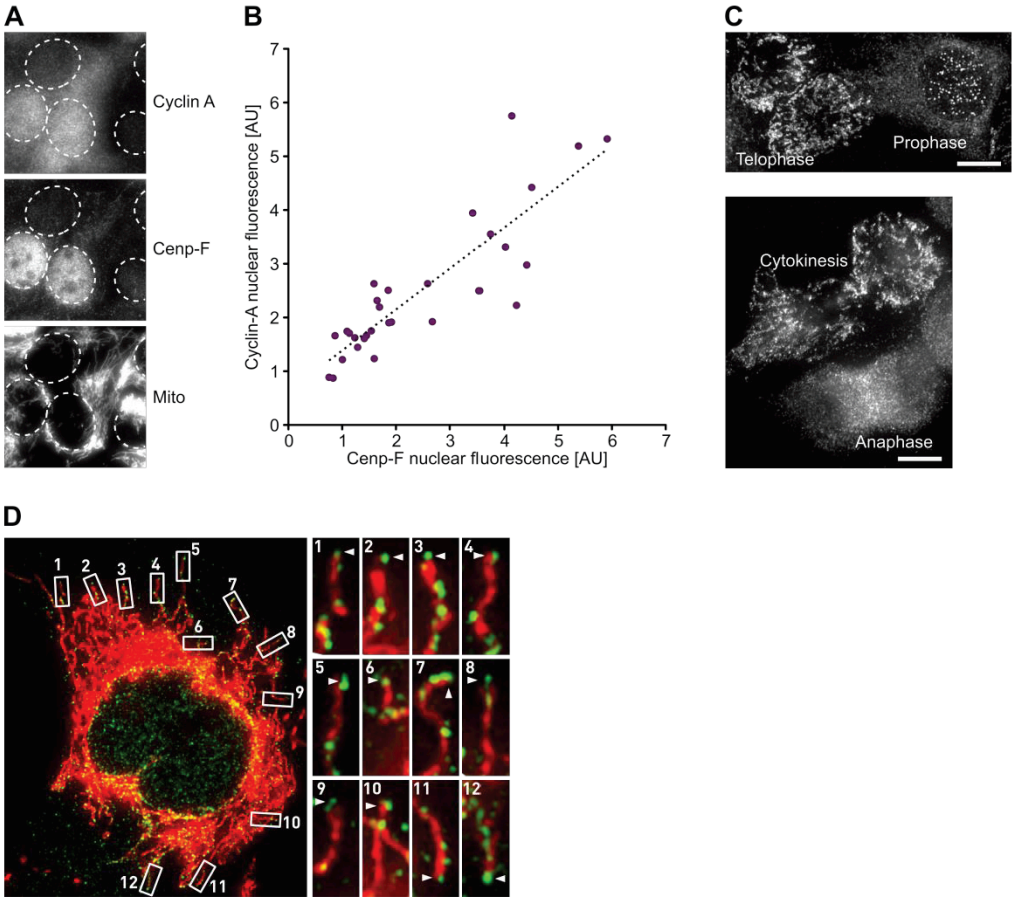

SUPPLEMENTARY FIG. 2

Cenp-F accumulates in the nucleus parallel to S/G2-specific protein Cyclin A
(A) Immunofluorescence of KERMIT cells with α-Cyclin A and α-Cenp-F antibody. Nuclei of the cells in the field of view are indicated by a dashed outline. The images represent average intensity projections over the whole thickness of the cells.
(B) Quantification of the fluorescence intensities of the nucleus in the Cenp-F channel (x-axis) and in the Cyclin A channel (y-axis). Each point represents one cell. AU: arbitrary units.
(C) Immunofluorescence of Cenp-F in cells undergoing mitosis. Two examples in which two mitotic cells were found in the same field of view show that the profound difference in Cenp-F recruitment between early and late mitosis is not simply due to variations in Cenp-F levels. Late mitosis cells (telophase and cytokinesis) show filamentous Cenp-F staining indicative of mitochondrial recruitment. By contrast early mitosis cells show diffuse staining (anaphase) or kinetochore and nuclear envelope staining (prophase). Scale bar, 10 µm.
(D) Late G2 cell imaged as in Fig. 1. Cenp-F staining is found at the nuclear envelope and the mitochondria, and is enriched at the distal tip of the mitochondria.

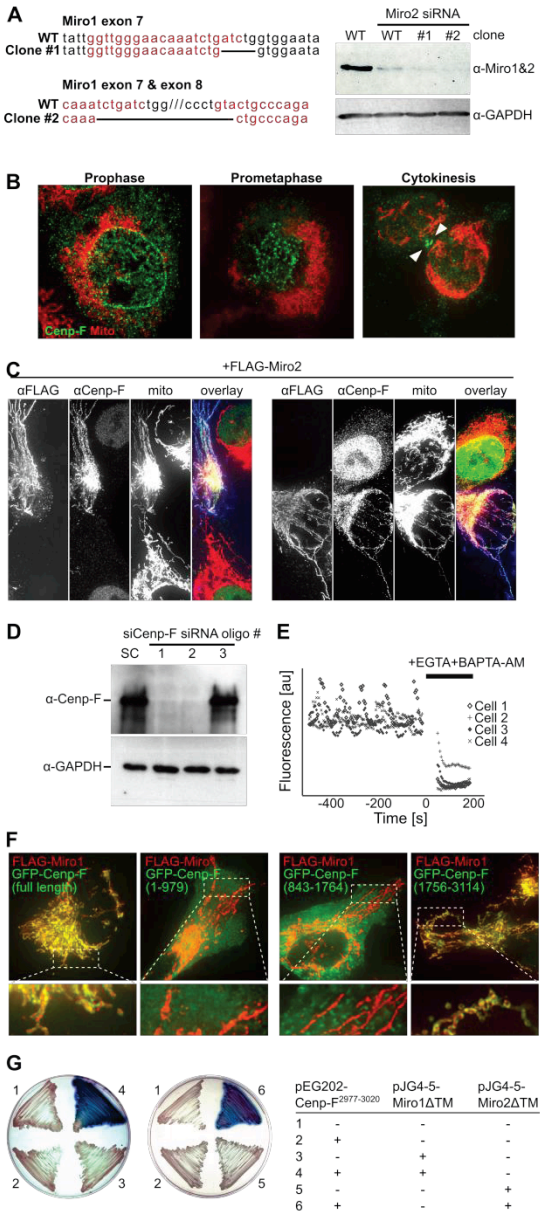

SUPPLEMENTARY FIG. 3

Interaction of Miro and Cenp-F.

(A) Left: genetic lesions induced in clone #1 and #2 by CRISPR/Cas9 engineering. Red sequences are those used for generating the CRISPR guide RNA. Clone #1 bears a 5 bp deletion causing a frameshift in exon 7. Clone #2 bears a deletion spanning from exon 7 to exon 8, causing a deletion of 54 aminoacids and a frame-shift. Right, western blotting of whole cell protein extracts from normal KERMIT cells (WT), the same cells treated with siRNA against Miro2, or cells from Clone #1 and #2 treated with Miro2 siRNA. Top, detection with α-Miro antibody. Although this antibody is sold as an α-Miro1 antibody, it is raised against a peptide that is conserved between Miro1 and Miro2, and therefore recognises both. Most of the western signal actually comes from Miro2. Bottom: an α-GAPDH antibody is used as a loading control.

(B) Immunofluorescence of miro-less KERMIT cells showing unaffected Cenp-F localisation to the nuclear envelope in prophase (left), to kinetochores in prometaphase (middle) and to the midbody in cytokinesis (right).

(C) As in Fig. 2B, except that a FLAG-Miro2-encoding expression plasmid (instead of FLAG-Miro1) was transfected. FLAG-Miro2: blue, Cenp-F:green, mtBFP: red, in the overlay panel.

(D) Western blotting of whole cell protein extracts from KERMIT cells treated with scrambled siRNA (SC), or siRNA against Cenp-F (1, 2, 3). siRNA 3 obviously did not work and was not used further.

(E) EGTA +BAPTA-AM treatment effectively depletes cytosolic calcium and suppresses calcium oscillations. Cells loaded with fluorescent calcium indicator (Oregon Green Bapta-AM) were imaged in normal growth medium. EGTA and BAPTA-AM are added at timepoint 0. Measurements for four cells are shown. Cell 1 and 3 show spontaneous calcium oscillations.

(F) A FLAG-Miro1 expression plasmid was cotransfected with plasmids expressing GFP-fusion of full length or indicated fragments of Cenp-F. Cells were then fixed and stained with an anti-FLAG antibody. The full-length and the C-terminal fragment of Cenp-F are robustly recruited to mitochondria by FLAG-Miro1 overexpression. Bottom panels correspond to magnifications of the top panel (indicated by a white dashed box).

(G) Yeast-two hybrid assay by X-Gal overlay, using yeast strains bearing the indicated plasmids or their empty counterpart (pEG202 and pJG4-5, respectively).

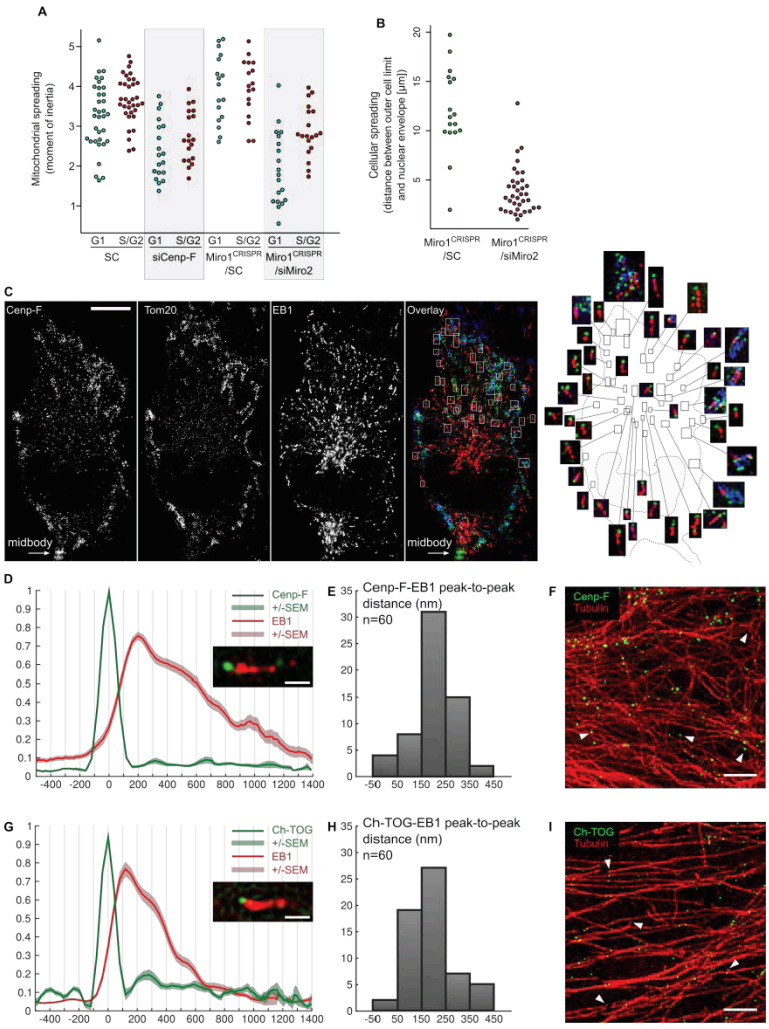

SUPPLEMENTARY FIG. 4

(A) Same data as in Fig. 3D except that cells were categorised as G1 or S/G2 according to the expression level of CyclinA.

(B) Miro-less cells have a cell spreading defect in cytokinesis. KERMIT cells were fixed, cytokinetic cells were imaged and the cellular spreading (defined as the minimal distance between the most distant point of the cell and the nuclear envelope) was measured in Miro1^{CRISPR} KERMIT cells (left) or Miro-less cells (right).

(C) Cytokinetic cell imaged as in Fig. 4B. Right, magnification of comets showing Cenp-F signal at their tips, which colocalises, or not with mitochondria. Scale bar, 5 µm.

(D, G) Comparison of Cenp-F and ch-TOG localisation. 3D-SIM immunofluorescence images of U2OS cells stained with Cenp-F and EB1 (D), or ch-TOG and EB1 (G) were acquired. The signal of each protein along the length of the comet was measured by line scanning. The position of maximal Cenp-F (respectively ch-TOG) signal was set at 0 nm. The intensities ± SEM are plotted. Scale bar, 500 nm.

(E, H) Peak-to-peak distance between the point of maximum Cenp-F (E) or ch-TOG (H) intensity and the point of maximal EB1 signal.

(F, I) 3D-SIM immunofluorescence images of U2OS cells stained with Cenp-F (F, green) or ch-TOG (I, green) and tubulin-α (red). Arrowheads indicate Cenp-F or ch-TOG signal at microtubule tips. Scale bar, 2 µm.

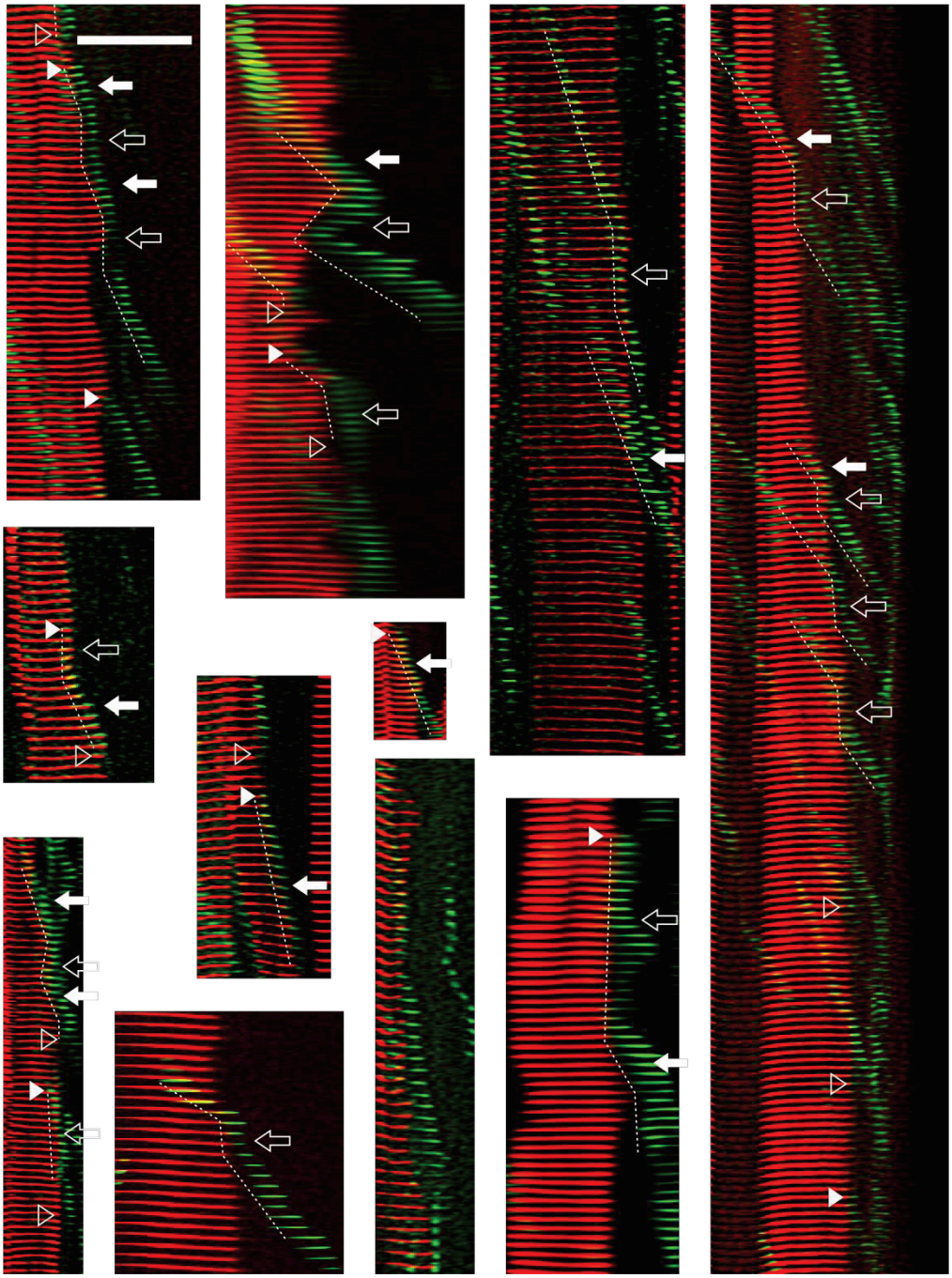

SUPPLEMENTARY FIG. 5

Representative kymographs of mitochondria (red) and EB1 (green) imaged as in Fig. 4C-D. Scale bar, 2 µm. Each step is 400 ms. Plain arrowheads: rescue event, open arrowheads: catastrophe, plain arrow: mitochondria-microtubule coordinated movements, open arrow: microtubule pausing at mitochondrial tips.

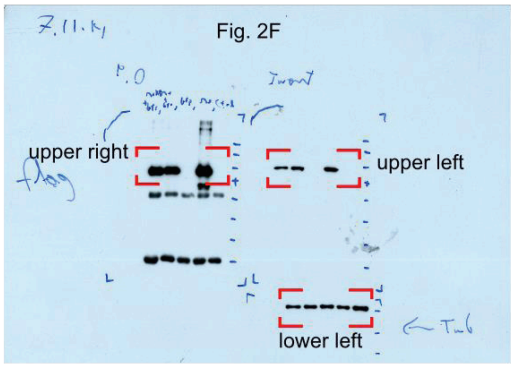

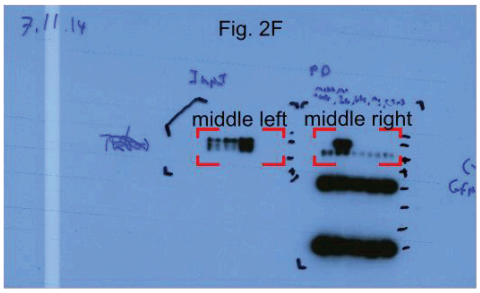

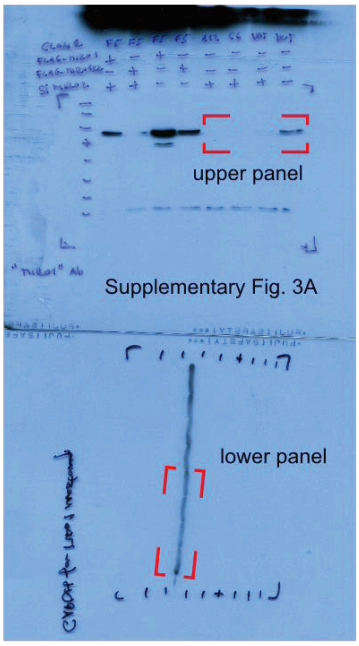

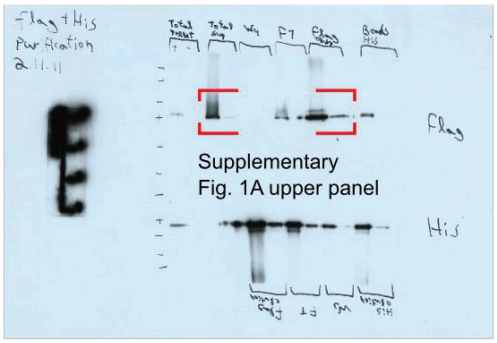

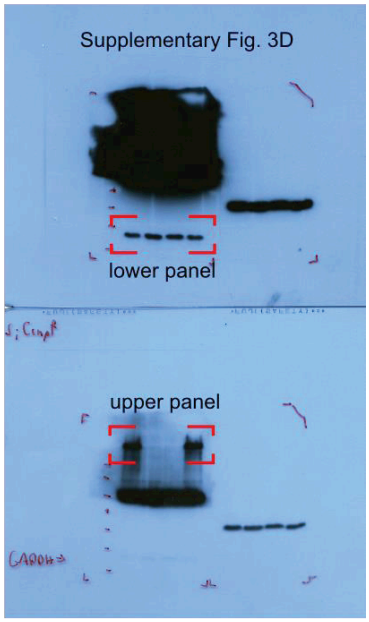

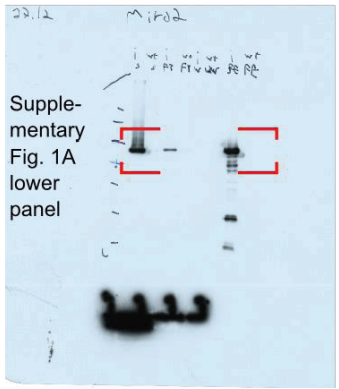

SUPPLEMENTARY FIG. 6

Non-cropped western blots for Fig. 2F and Supplementary Figs. 1A, 3A and 3D.

SUPPLEMENTARY TABLE 1:

Primers used in this study

#	Name	Sequence
1	3flag6hisMiro1	gactacaaggaccatgacggtgattacaaggatcatgacatcgactacaaggatgacgat gacaagcatcatcaccatcaccatggtatgaagaaagacgtgcg
2	3flag6hisMiro2	gactacaaggaccatgacggtgattacaaggatcatgacatcgactacaaggatgacgat gacaagcatcatcaccatcaccatggtatgaggcgggacgtgcgc
3	revMiro1Attb	ggggaccactttgtacaagaaagctgggtgtcatcgctgtttcaata
4	revMiro2attb	ggggaccactttgtacaagaaagctgggtgtcactggctcttcacca
5	Attbkozakflag	ggggacaagtttgtacaaaaaagcaggcttcaccatggactacaaggaccatgac
6	CRISPRmiro1ex7s	caccGGTTGGGAACAAATCTGATC
7	CRISPRmiro1ex7as	aaacGATCAGATTTGTTCCCAACC
8	CRISPRmiro1ex8s	caccCCTTCTCCTCTGGGCAGTAC
9	CRISPRmiro1ex8as	aaacGTACTGCCCAGAGGAGAAGG
10	hMiro1_T18N_F	cctagagttgggaagaactcactgattatgtc
11	hMiro1_T18N_R	gacataatcagtgagttcttcccaactctagg
12	hMiro1_E208K_F	ggtactctcaatgatgctaaactcaacttctttcag
13	hMiro1_E208K_R	ctgaaagaagttgagtttagcatcattgagagtacc
14	hMiro1_E328K_F	gctttgtcacctgataagcttaaagatttatttaaag
15	hMiro1_E328K_R	ctttaaataaatctttaagcttatcaggtgacaaagc
16	hMiro1_S432K_F	gaaaaactgtgggaaaaacggagttcttcaggc
17	hMiro1_S432K_R	gcctgaagaactccgtttttcccacagtttttc
18	CenpF2977F	GTTGGGGTTATTCGCAACGGCGACTGGCTGGAATTCgagccaga gggacttccagaa
19	CenpF3020R	TCGCCCGGAATTAGCTTGGCTGCAGGTCGACTCGAGtcataacttct gtgcagccaggcg
20	Y2H_pJG4-5_MIRO1_F	TACCCTTATGATGTGCCAGATTATGCCTCTCCCGAATTCGGCC GAatgaagaaagacgtgcggatcctgc
21	Y2H_pJG4-5_MIRO1_R	TGATTGGAGACTTGACCAAACCTCTGGCGAAGAAGTCCAAAGC TTtcaaagccaaaacgtggagctcttg
22	cenpf1_197bamh1F	gagaGGATCCATGAGCTGGGCTTTGG
23	cenpf1_197Not1R	tatGCGGCCGCtcaaagagtcccattctctt
24	cenpf_843-1764_fw	gagaGGATCCAAACAGATGAACTCAGACCTG
25	cenpf_843-1764_rv	taatGCGGCCGCtcaCCCCAGGAAATCCATAG
26	cenpf_1756_F	gagtGGATCCGGTCCTAATGCTTTGGTA
27	cenpf_3114_R	gtttGCGGCCGCtcactggaccttacagtt
28	cenpf_2375_fw	gagtGGATCCATGACCCAAAGTCTGAGA
29	cenpf_2519_fwd	gagtGGATCCAAGGATGAAGAAATCAGTAG
30	cenpf_2831_rev	tatGCGGCCGCtcaAGTACCTGTTTTCTGCTTCT
31	cenpf_2719_fw	gagaGGATCCCAGTATGAAGTAGAAATCCAG
32	cenpf_2831_rev	tatGCGGCCGCtcaAGTACCTGTTTTCTGCTTCT
33	cenpf_2819_fwd	gagtGGATCCCAAGCTGCACAGGAGAA
34	cenpf_3017_rev	tatGCGGCCGCtcaGGATAGCGCTAACTTCTG
35	CenpF2927F	GTTGGGGTTATTCGCAACGGCGACTGGCTGGAATTCaaagcttca ggcaagaggcaa
36	CenpF2957F	GTTGGGGTTATTCGCAACGGCGACTGGCTGGAATTCagcaagaa agcagtcatgagt
37	CenpF2977F	GTTGGGGTTATTCGCAACGGCGACTGGCTGGAATTCgagccaga gggacttccagaa
38	CenpF2987F	GTTGGGGTTATTCGCAACGGCGACTGGCTGGAATTCaaagggtttg ctgacatcccg
39	CenpF2987R	TCGCCCGGAATTAGCTTGGCTGCAGGTCGACTCGAGtcactttaca acttctggaagtcc
40	CenpF3003R	TCGCCCGGAATTAGCTTGGCTGCAGGTCGACTCGAGtcatcgcag gatatatgggctagt
41	Y2H_pJG_MIRO2_F	TACCCTTATGATGTGCCAGATTATGCCTCTCCCGAATTCGGCC GAatgaggcgggacgtgcgcatcctgt
42	Y2H_pJG_MIRO2_R	TGATTGGAGACTTGACCAAACCTCTGGCGAAGAAGTCCAAAGC

		TTtcaccggagccagaaggaagaggg
43	fw_Cenpf1_bhamh1	ccccctcgaggtcgacggtatcgataagcttgataGGATCCGCGATGAGCTGGGC
44	rev_Cenpf1	GCTGCAAAATACTTCATCTACACTGCAC
45	fw_cenpf2	AGTCTGCAGGAGGAGAATCTGACCAGGAAAGAAACC
46	rev_cenpf2_not	cggccgctctagaactagtggatcccccgggctgcgcggccgcTCACTGGACCTTACAGTTCT
47	Fw_GFP	CAAACCAGTGCAGTGTAGATGAAGTATTTTGCAGCatggtgagcaagggcgagga
48	Rev_GFP	GTTTCTTTCCTGGTCAGATTCTCCTCCTGCAGACTcttgtacagctcgtccatgc

SUPPLEMENTARY NOTES

SUPPLEMENTARY NOTE 1

ImageJ script to outline single cells and process the mitochondrial network for momentum of inertia analysis

```
name=getInfo("image.filename") rename("dd");
run("Split Channels");
//close non mitochondrial images run("Close");
run("Close");
//remove background, do a Z-projection (C1-dd is the mitochondria
channel, C2-dd is the ER channel )
selectWindow("C1-dd");
run("Subtract Background...", "rolling=12 stack");
run("Z Project...", "start=1 stop=40 projection=[Max Intensity]");
run("Subtract...", "value=100");
run("Enhance Contrast", "saturated=0.35");
selectWindow("C2-dd");
run("Z Project...", "start=1 stop=40 projection=[Max Intensity]");
run("Enhance Contrast", "saturated=0.35");
run("Merge Channels...", "c1=MAX_C1-dd c2=MAX_C2-dd create");
selectWindow("C2-dd");
close();
selectWindow("C1-dd");
close();
///// //setTool("polygon");
///loop repeated for as many cells as present on the picture.
ans=1;
i=0 while (ans>0){
      i=i+1;
      waitForUser("select the outline of a cell");
      run("Measure");
      run("Duplicate...", "title=Composite-1 duplicate channels=1");
      setBackgroundColor(0, 0, 0);
      run("Clear Outside");
      saveAs("Tiff", name+i+".tif");
      run("Close");
      Dialog.create("Test");
      Dialog.addMessage("do you have more cells to outline?")
      Dialog.addCheckbox("yes!", true) Dialog.show();
      ans=Dialog.getCheckbox();
      }
```

SUPPLEMENTARY NOTES

SUPPLEMENTARY NOTE 1

ImageJ script to outline single cells and process the mitochondrial network for momentum of inertia analysis

```
name=getInfo("image.filename") rename("dd");
run("Split Channels");
//close non mitochondrial images run("Close");
run("Close");
//remove background, do a Z-projection (C1-dd is the mitochondria
channel, C2-dd is the ER channel )
selectWindow("C1-dd");
run("Subtract Background...", "rolling=12 stack");
run("Z Project...", "start=1 stop=40 projection=[Max Intensity]");
run("Subtract...", "value=100");
run("Enhance Contrast", "saturated=0.35");
selectWindow("C2-dd");
run("Z Project...", "start=1 stop=40 projection=[Max Intensity]");
run("Enhance Contrast", "saturated=0.35");
run("Merge Channels...", "c1=MAX_C1-dd c2=MAX_C2-dd create");
selectWindow("C2-dd");
close();
selectWindow("C1-dd");
close();
///// //setTool("polygon");
///loop repeated for as many cells as present on the picture.
ans=1;
i=0 while (ans>0){
      i=i+1;
      waitForUser("select the outline of a cell");
      run("Measure");
      run("Duplicate...", "title=Composite-1 duplicate channels=1");
      setBackgroundColor(0, 0, 0);
      run("Clear Outside");
      saveAs("Tiff", name+i+".tif");
      run("Close");
      Dialog.create("Test");
      Dialog.addMessage("do you have more cells to outline?")
      Dialog.addCheckbox("yes!", true) Dialog.show();
      ans=Dialog.getCheckbox();
      }
```

SUPPLEMENTARY NOTE 3

MatLab script to calculate the distance of eb1 comet to the closest Cenp-F focus. It uses three variables: eb1, list of XY coordinates for the tips of Eb1 comets; cenpf, list of XY coordinates of Cenp-F foci obtained by the "Analyse particles.." procedure in ImageJ; mt, list of XY coordinates for random points on microtubules (likewise acquired using the "Analyse particles.." in ImageJ.

```
clear disteb1 distmt
%for each eb1 comet, calculate the distance to the closest cenpf
focus
for ii=1:length(eb1)
      disteb1(ii)=min(sqrt((cenpf(:,1)-eb1(ii,1)).^2+(cenpf(:,2)-
      eb1(ii,2)).^2));
end
%for each point on microtubules, calculate the distance to the
closest cenpf focus
for ii=1:length(mt)
      distmt(ii)=min(sqrt((cenpf(:,1)-mt(ii,1)).^2+(cenpf(:,2)-
      mt(ii,2)).^2));
end
clear data
clear dist1p dist2p dist3p dist4p

%permutation test to find the probability that the eb1-cenp-f
distances can be the result of a random draw.
iteration=10000000
for ii=1:iteration
%make a random draw of points on the microtubules
      for kk=1:length(disteb1)
        data(kk)=distmt(round(rand*(length(distmt)-1))+1);
      end
      %find the proportions of that are smaller than 1, 2, 3 or 4
      pixels
      dist1p(ii)=length(find(data<1));
      dist2p(ii)=length(find(data<2));
      dist3p(ii)=length(find(data<3));
      dist4p(ii)=length(find(data<4));
end
clear onep twop threep fourp ii kk a b c d
%Compare the random draw to the data for eb1 comets.
a=length(find(disteb1<1))
b=length(find(disteb1<2))
c=length(find(disteb1<3))
d=length(find(disteb1<4))
length(find(dist1p>=a))/iteration
length(find(dist2p>=b))/iteration
length(find(dist3p>=c))/iteration
length(find(dist4p>=d))/iteration
```

4. Results - Cenp-F attaches cargo to growing microtubule ends

On the basis of the published article presented in this thesis, a few loose ends remained. This section addresses questions such as – how is mitochondrial network distribution mediated by Miro-Cenp-F at the molecular level? Are motor proteins required, in addition to Cenp-F, for mitochondria mobility?

4.1. Mitochondrial distribution mediated by Miro-Cenp-F

In proliferating cells, mitochondria are dynamic and dispersed in the cytoplasm. Mitochondria spreading is associated with several factors and the mitochondrial Rho GTPase Miro is crucial for the regulation of mitochondrial trafficking in neurons (Schwarz, 2013). Mitochondria distribution was previously shown to be, at least in part, mediated by Cenp-F, which was found to be recruited to the mitochondria by Miro. In particular, Miro and Cenp-F are acting in very similar manners, since mitochondria distribution was dysregulated in cells where Miro or Cenp-F had been depleted. In fact, in cells in which Miro1 expression was completely deleted by CRISPR knockout and Miro2 expression was reduced by siRNAs, the collapsed mitochondria network could be rescued by overexpression of Miro1. However, upon , redistribution ofthe mitochondria network failedupon expression of Miro1 mutants, which harbored mutations previously shown to block Cenp-F recruitment (e.g. Miro1 with point mutations in the N-terminus GTPase or Ca2+-binding domain) (Fig.5a). In contrast, disrupting the C-terminal GTPase domain, which does not influence the ability of Miro to recruit Cenp-F to the mitochondria, rescued the mitochondrial phenotype. The effect of Cenp-F on mitochondria distribution is most likely related to mitochondria transportation. Therefore, we tested whether mitochondria dynamics is influenced by Cenp-F disruption. We visualized mitochondria in U2OS cells using mitochondria-localized blue fluorescent protein following knockdown of Cenp-F by siRNA. We measured mitochondria dynamics by following mitochondria position for 16 seconds (Fig. 5b). Analysis of these time-lapse images by a co-localization assay showed a significant reduction in mitochondrial mobility in Cenp-F knockdown cells.

Fig. 5

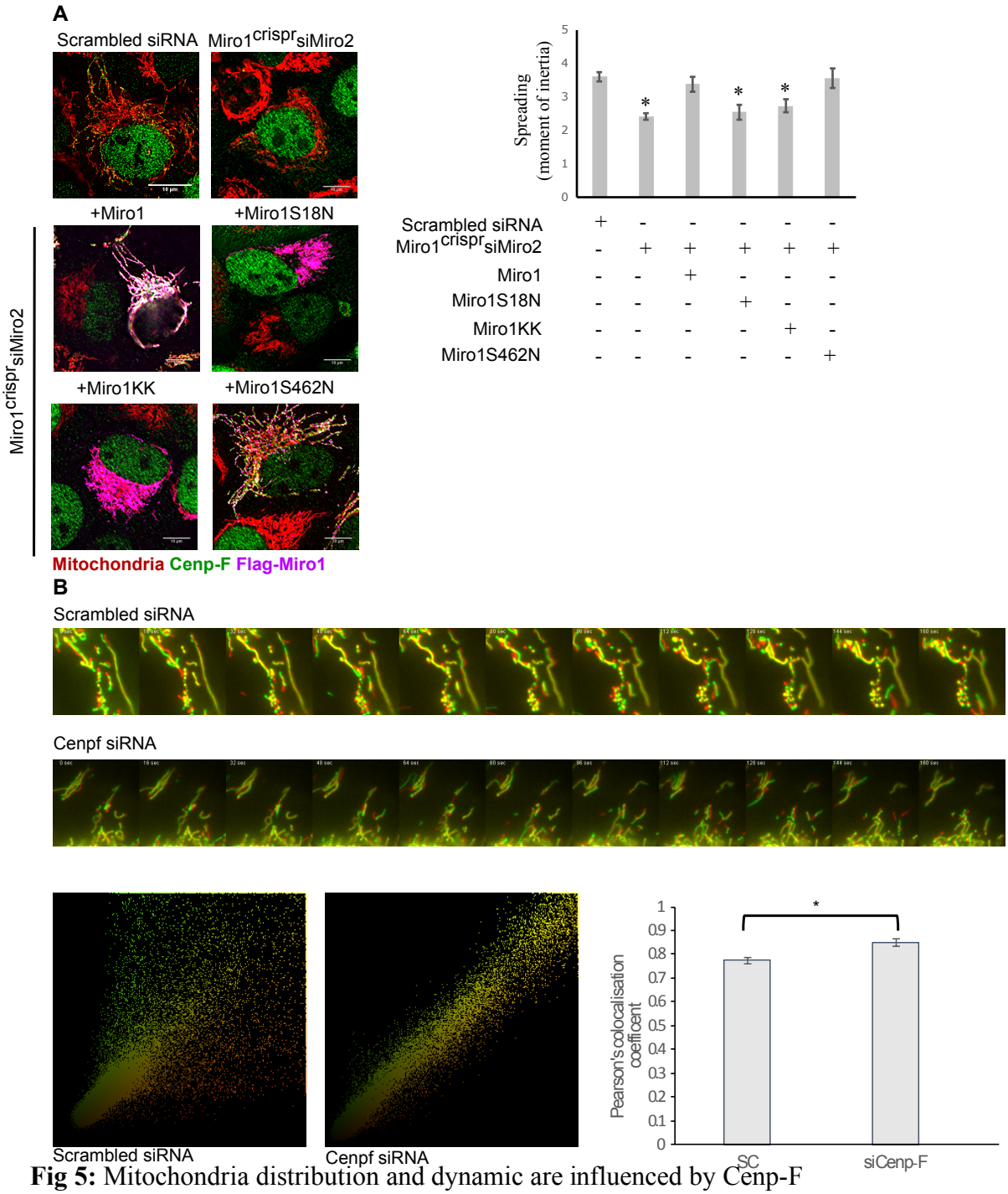

Fig 5: Mitochondria distribution and dynamic are influenced by Cenp-F

a) Miro rescues mitochondria collapse by Cenp-F recruitment to mitochondria. Immunofluorescence of U2OS (left panel) or Miro-less cells expressing Flag-Miro1X (contains the indicated mutations). Localization of Cenp-F (green), mtBFP (Red), Flag-Miro1X (Magenta). Scale bar, 10µm. b) Cenp-F disruption decreases mitochondria dynamics. Merged images of U2OS cells expressing mitoBFP at time t0 (green) and time t 0 + 16 sec (red). Upper panel, scrambled siRNA-treated cells. Lower panel, cells treated with Cenp-F siRNA (30nM) for 48 hours. B) Scatter plot of fluorescence intensities where X axies is time t 0 + 16 sec and Y axis is Time t 0. The treatments are indicated below the image, the colocalization coefficient was determined by Pearson's colocalization test using ImageJ plugin - Pearson – Spearman correlation colocalization plugin (French et al., 2008). The mean Pearson colocalization coefficient calculated for 15 cells for each treatment, * p value < 10^{-2} from Mann-Whithney-Wilcoxon U test. Scale bar, 2µm.

4.2. Cenp-F mediated mitochondrial distribution appears independent of Cenp-E, Nudel and MTs organization

Since Miro promotes distribution by attaching mitochondria to motor proteins, we assessed whether the mechanism of mitochondria transport by Miro-Cenp-F is motor protein-dependent. First, we tested the minus end-directed motor protein Dynein. Previously, Cenp-F was shown to associate with Dynein via the nuclear distribution protein nudE1-like 1 (NudeI) (Vergnolle and Taylor, 2007). Recently, these proteins were shown to influence mitochondrial retrograde movement in neuronal axons (Shao et al., 2013). Hence, we determined Cenp-F recruitment and mitochondrial distribution in cells depleted of NudeI by siRNA (Fig 6a). Disrupting NudeI did not significantly alter mitochondrial distribution nor affect the mitochondrial localization of Cenp-F. Besides Dynein, the kinesin Cenp-E was found to directly bind Cenp-F at the kinetochore (Chan et al., 1998; Maton et al., 2015; Musinipally et al., 2013). Therefore, we tested the influence of Cenp-E depletion on mitochondrial redistribution after cytokinesis (Fig. 6a). As for Nudel, disrupting Cenp-E expression did not affect post-mitotic distribution of mitochondria in U2OS cells. However, since the reduction of NudeI and Cenp-E were not measured in the current study, the influence of these proteins on mitochondria movement by Cenp-F remains to be determined.

MTs play a central role in mitochondrial network organization, and because Cenp-F was previously shown to promote MT polymerization in vitro and also in vivo (Feng et al., 2006; Moynihan et al., 2009), we assessed if the defect in mitochondria spreading in cells lacking Cenp-F or Miro were due to changes in overall MT network. Cells were treated with nocodozole, a MT depolymerizing drug, for one hour. Subsequently, the nocodazole was washed out and after two minutes of incubation cells were fixed and immunostained with specific Tubulin antibody (Fig. 6b). In contrast to previous studies, no significant alteration in MT assembly was detected, neither in cells depleted of Cenp-F by siRNA nor in cellsexpressing Miro1. Thus, the mechanism mediating mitochondria distribution by Cenp-F is unlikely due to changes in MT dynamics in cells.

Fig. 6

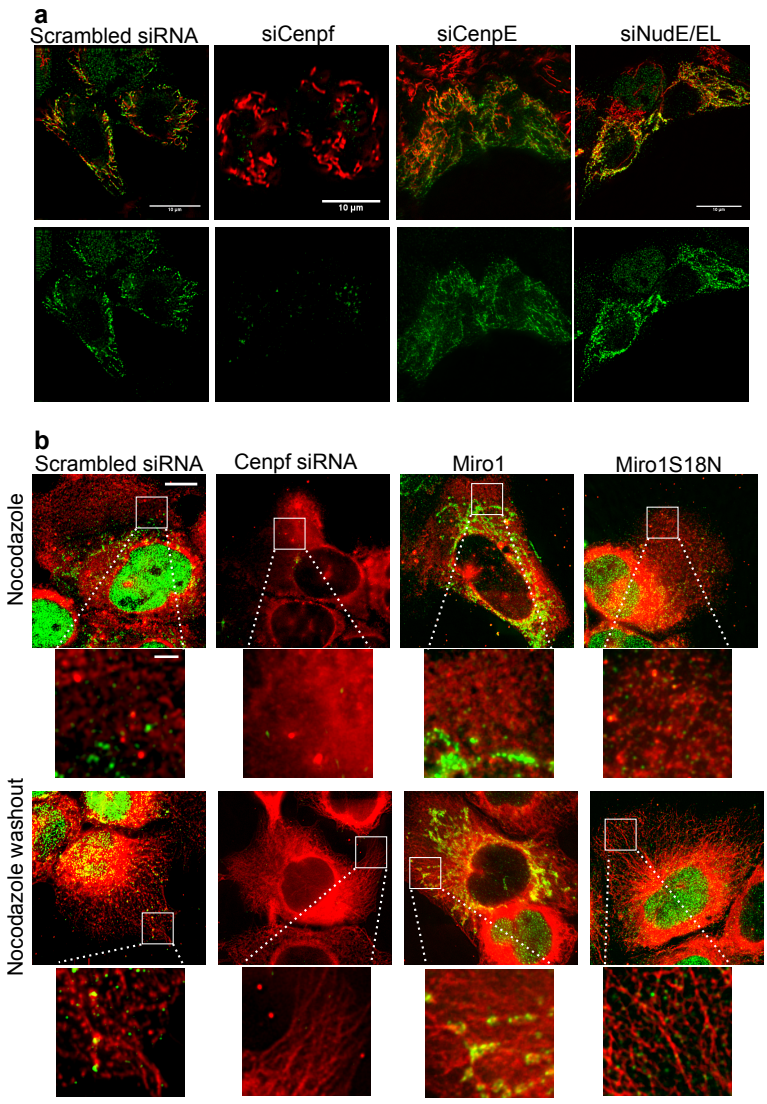

Figure 6: Mitochondrial redistribution is not influenced by Cenp-f adaptors proteins.

a) Immunofluorescence of U2OS expressing mitoBFP (red) stained with Cenp-F antibody (green). Indicated proteins were depleted with 30nM siRNA for 48 hours . Scale bar, 10 µm. b) Cells which were silenced for Cenp-F or expressed Flag-Miro1X were treated with 10 µM nocodazole and fixed directly (upper panel) or nocodozole was washed out (bottom panel) and cells were fixed after 2 minutes. MTs and Cenp-F were stained with specific antibody.

4.3. CENP-F and mitochondria colocalize with the tips of MTs in live U2OS cells and follow MT growth and shrinkage

Interphase microtubules carry a number of proteins on their growing tips, including EB proteins (EB1, 2 and 3), CLIP170 and others (reviewed in [Jiang & Akhmanova, 2011]), which interact with specific structural features of the GTP-bound tubulin at the polymerizing MT tip [Zhang et al., 2015]. Cenp-F has been associated with growing microtubules in fixed cells, but in vitro, Cenp-F has been shown to associate with shrinking microtubules. Because microtubules can switch between growth and shrinkage in a dynamic fashion, we wanted to observe Cenp-F localization relative to dynamic microtubules in live cells. Expression of a N-terminally tagged GFP-Cenp-F did not recapitulate the sub-cellular localization of endogenous Cenp-F (Fig. 7b, left panel). This might be due to the fact that Cenp-F N-terminus bears a MT-binding domain, that may no longer be functional in the GFP fusion. Since the C-terminus of Cenp-F bears an important farnesylation motif, it is not a better place to fuse a GFP. Instead, we took advantage of the fact that in mammalian cells, Cenp-F expresses two different splice variants which differ in that one comprises exon 19, while the other skips it. We reasoned that the space left by the skipped exon 19 could be a good location to insert an internal GFP (Fig. 7a). Internally tagged Cenp-F (hereafter named Cenp-F^GFP) recapitulated faithfully the localization of endogenous Cenp-F, as it localized to mitochondria (Fig 7b), nucleus, nuclear envelope and kinetochores (not shown), as expected. Because the Cenp-F^GFP was overexpressed, an excess of free protein localized uniformly to the cytoplasm. Using total internal fluorescence microscopy, however, allowed to focus on a small proportion of the Cenp-F^GFP molecules associated with the microtubules in closest contact with the plasma membrane. Cenp-F^GFP was cotransfected with RFP-EB1 to specifically mark growing microtubules (Fig 7c). We could observe Cenp-F^GFP foci at the tip of growing microtubules, slightly ahead of EB1 comets, in agreement with what we had observed in fixed cells. Moreover, these foci followed microtubule growth, indicating that Cenp-F tracks growing microtubules. To visualize also shrinking microtubules, we imaged Cenp-F^GFP together with SIR-tub, a dye that marks all microtubules (Fig 7d). Events of Cenp-F tracking shrinking microtubules could also be observed, although the speed of microtubule depolymerization made it difficult to follow such events for more than 2-3 frames (2 s per frame.) Thus, Cenp-F can track both growing and shrinking microtubules in vivo.

Fig. 7

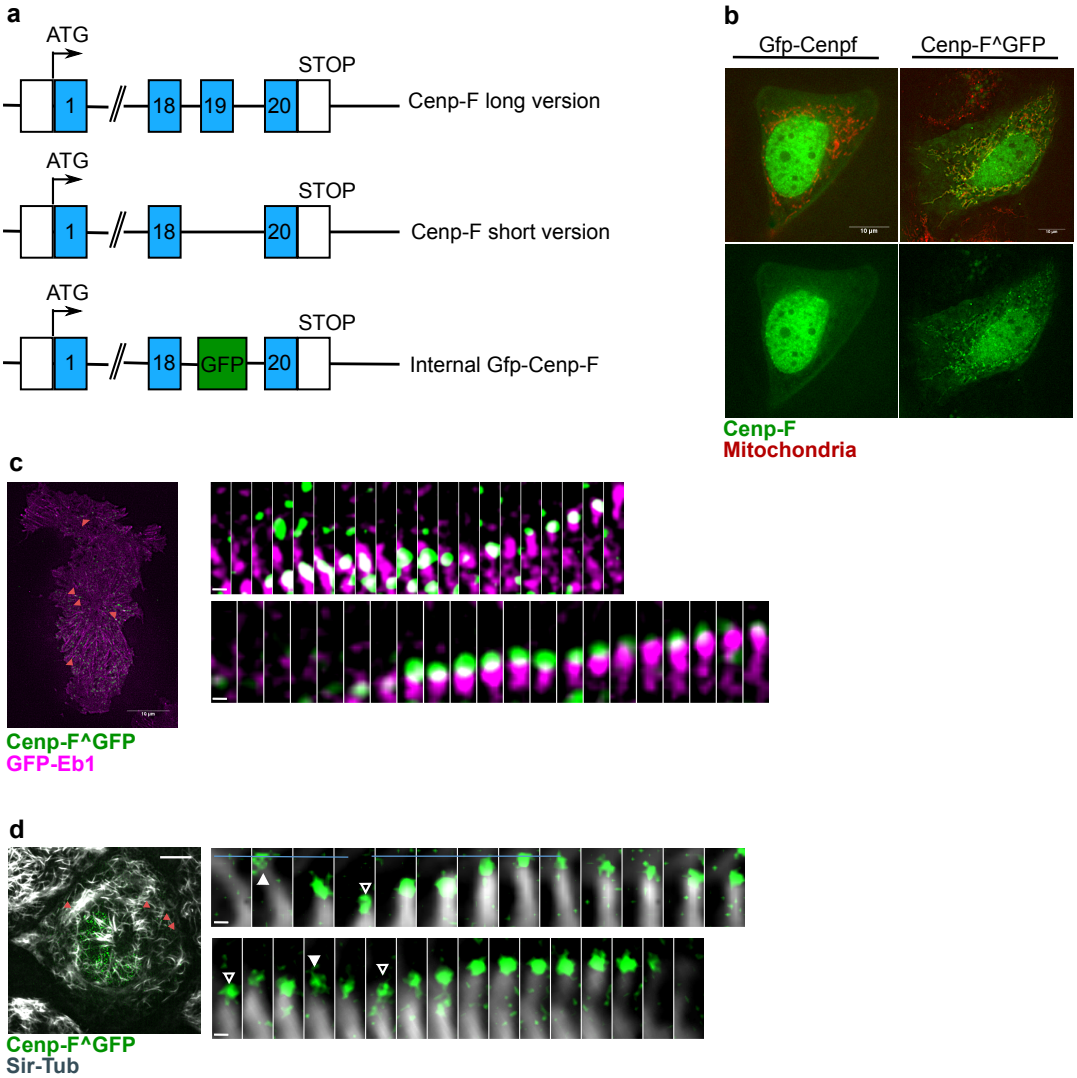

Figure 7: Cenp-F tracks growing and shrinking microtubule ends in-vivo

a) GFP internal tagging by replacing exon19 with GFP. Blue boxes indicate exons.

b) Internal tagged GFP Cenp-F (designated as Cenp-F^GFP, in green) localizes to the mitochondria (mitoBFP in red, left panel) in comparison to amino-terminally tagged Cenp-F(right panel). c) Cenp-F moves ahead of Eb1. Time lapse images of U2OS cells expressing RFP-Eb1(magenta) and Cenp-F^GFP (green). Time scale is 400 ms/ frame. d) Cenp-F follows growing and shrinking MT ends. U2OS cells were transfected with Cenp-F^GFP (green) and stained with 1µM Sir-Tubulin (grey). Time scale is 2 s/frame. Red arrowheads in top panel indicate Cenp-F foci in front of MT end or Eb1 comets. In the left panel, open arrowheads indicate microtubule recue, plain arrowheads indicate catastrophes. Scale bar, 10 µm for the whole cells and 0.5 µm for the single events.

4.4. CENP-F fragments load at the growing MT tips, but do not follow the growth

Most microtubule tip-tracking proteins do so by association with the GTP-tubulin-binding EB proteins. Cenp-F, however appears to track microtubules through a different mechanism since, 1) it does not colocalize with the EB1 comet but appears to bind microtubules closer to their tips, and 2) it can follow shrinking microtubules, which have lost the GTP-tubulin cap and their EB proteins. This prompted us to test if the microtubules-binding domains of Cenp-F had tip-tracking capability in isolation. To assess whether single molecules of Cenp-F can follow MT growth as well as MT shrinkage, we used an *in vitro* reconstitution approach. Dynamic MT extensions were grown using purified, fluorescently labeled tubulin from GMPPCP-stabilized, coverslip-anchored MT seeds in the presence of previously characterized recombinant MT-binding domains of Cenp-F, fused to superfold GFP(-tagged CENP-F fragments, N436-sfGFP and sfGFP-2592C)(Volkov et al., 2015) (Fig. 8a). Kymographs of dynamic MT extensions (Fig. 8b) showed two types of interactions with MTs: (1) some GFP-tagged molecules were loaded at the MT lattice and diffused rapidly along MTs before disappearing; and (2) some GFP-molecules were loaded at the growing MT tip, but did not track the growing tips. Instead, they remained stably associated at the site where they were loaded and stayed bound until MTshortening. These events were observed for both the N- and C-terminal fragments (Fig. 8b). We have not observed any detectable movement with the MT tip for any of the two fragments used. Thus, individual MT-binding domains of Cenp-F do not appear to have intrinsic tip-tracking capability in our *in vitro* system. Previous studies showed that Cenp-F fragment influences MT dynamics, hence we quantified the growth and shrinkage speed of MT in presence of N436-sfGFP and sfGFP-2592C. Consistent with our *in vivo* data, we could not observe significant changes in MT dynamics in the presence of the Cenp-F fragments (Fig 8c).

Fig. 8

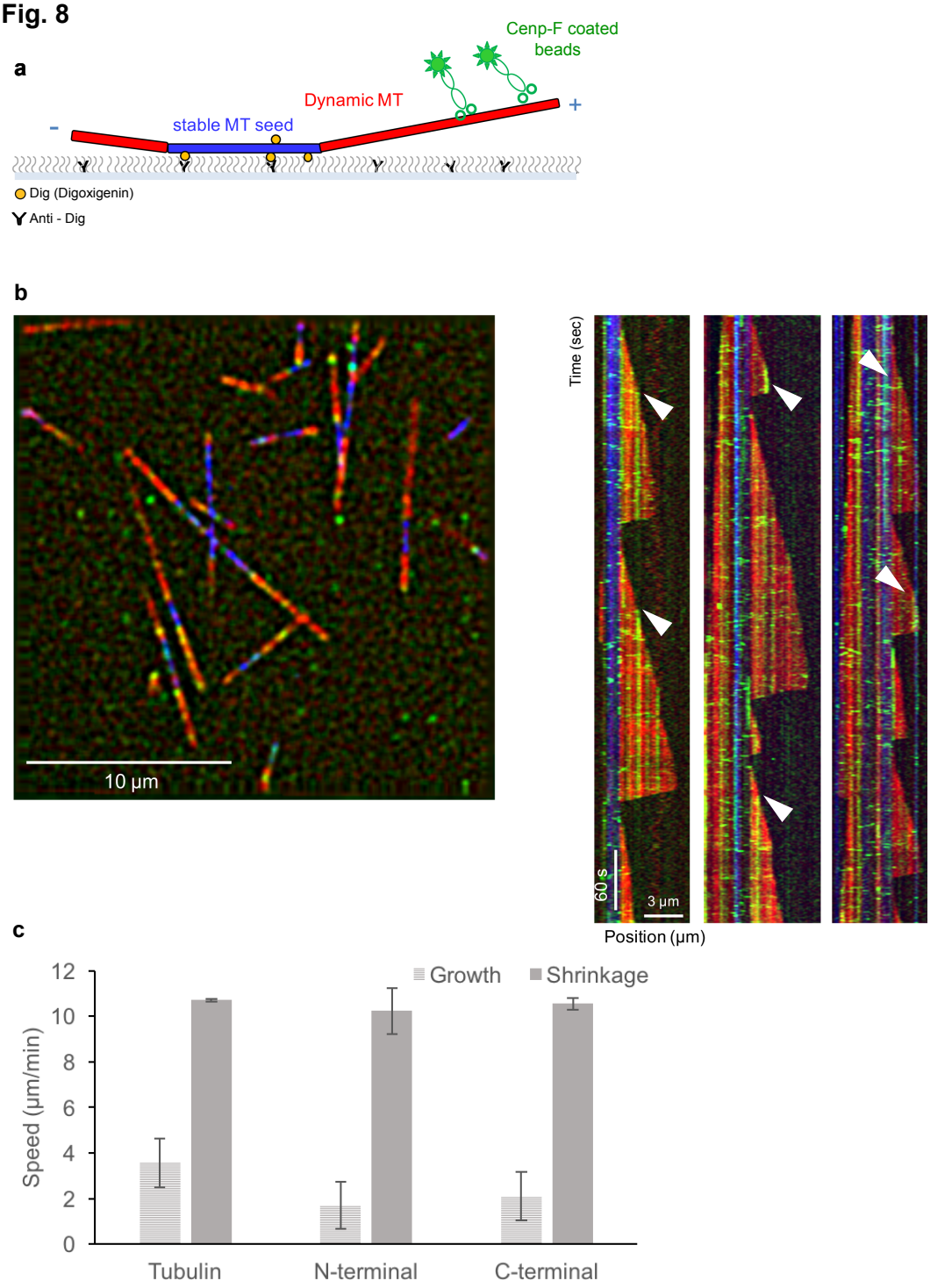

Figure 8: Isolated MT interaction domains appear at tip of growing MTs but fail to track dynamic MT ti

a) Schematic representation of the experimental setup used to investigate MT dynamics and isolated Cenp-F-MT interact domains. b) left panel, still image of seed MT (blue) with dynamic MTs (red) in the presence of 2µM sfGFP-2592C (gree Right, example Kymograph from a time-lapse video. Isolated MT interaction domains are enriched at the tip (arrowheads) fail to follow MT tips. Time scale is 400 msec per frame, Scale bar, x:3µm, y: 60s. c) Bar graph of MT growth and shrinka speed. The mean +/-SEM of MT growth speed in the absence of purified fragment (n=10) or in the presence of N436sf-G (n=25) or in the presence of sfGFP-2592C (n=27) were 3.5 ± 1.07 µm/min, 1.7 ± 1 µm/min, 2.1 ± 0.21 respectively. The me +/-SEM of growth MT speed for MT in the absence of purify fragment (n=13) or in the presence N436sf-GFP (n=10) or in presence of sfGFP-2592C (n=19) were 3.5 ± 1.07 µm/min, 1.7 ± 1 µm/min, 2.1 ± 0.21 respectively. The mean +/- SEM shrinkage MTs speed for MT in the absence of purified fragment (n=13) or in the presence N436sf-GFP (n=10) or in the prese

4.5. Beads coated with the 2592C fragment follow growing MT tips

Though Cenp-F fragments did not follow MT growth, a recent study showed that beads coated with Cenp-F fragments can track shrinking MTs. Hence, we attached GFP fused Cenp-F MT-binding fragments to the surface of 1-μm microbeads in order to track the beads and MT dynamics using a total internal reflection microscope (TIRF). sfGFP-2592C coated beads were attached to growing and shrinking MTs, in contrast to N436-sfGFP coated beads which were strongly bound to MT seed or to the MT wall (data not shown). Given the fact that sfGFP-2592C can promote cargo movement by attaching beads to MT, and since this fragment contains a Miro interaction motif, we tested whether sfGFP-2592C could also promote mitochondria transport. To reconstitute this reaction *in vitro* we prepared crude mitochondria extracts from U2OS cells overexpressing Miro1 and mitoBFP in the presence or absence of endogenous Cenp-F. Subsequently, we incubated the extracts with recombinant sfGFP-2592C and added these to the flow chambers with fluorescently labeled, dynamic MTs extending from coverslip-anchored stable MT seeds (Fig. 9b). Particles with blue (mitoBFP) and green (sfGFP-2592C) fluorescence were bound to the MT extensions, and we observed movement of these particles with the tips of both growing and shortening MTs (Fig. 9c). The CENP-F-coupled mitochondrial particles moved over 2.4 ± 0.4 μm (n = 16, mean ± SEM) with MT shortening and over 0.8 ± 0.1 μm (n = 11) with MT growth.

Fig. 9

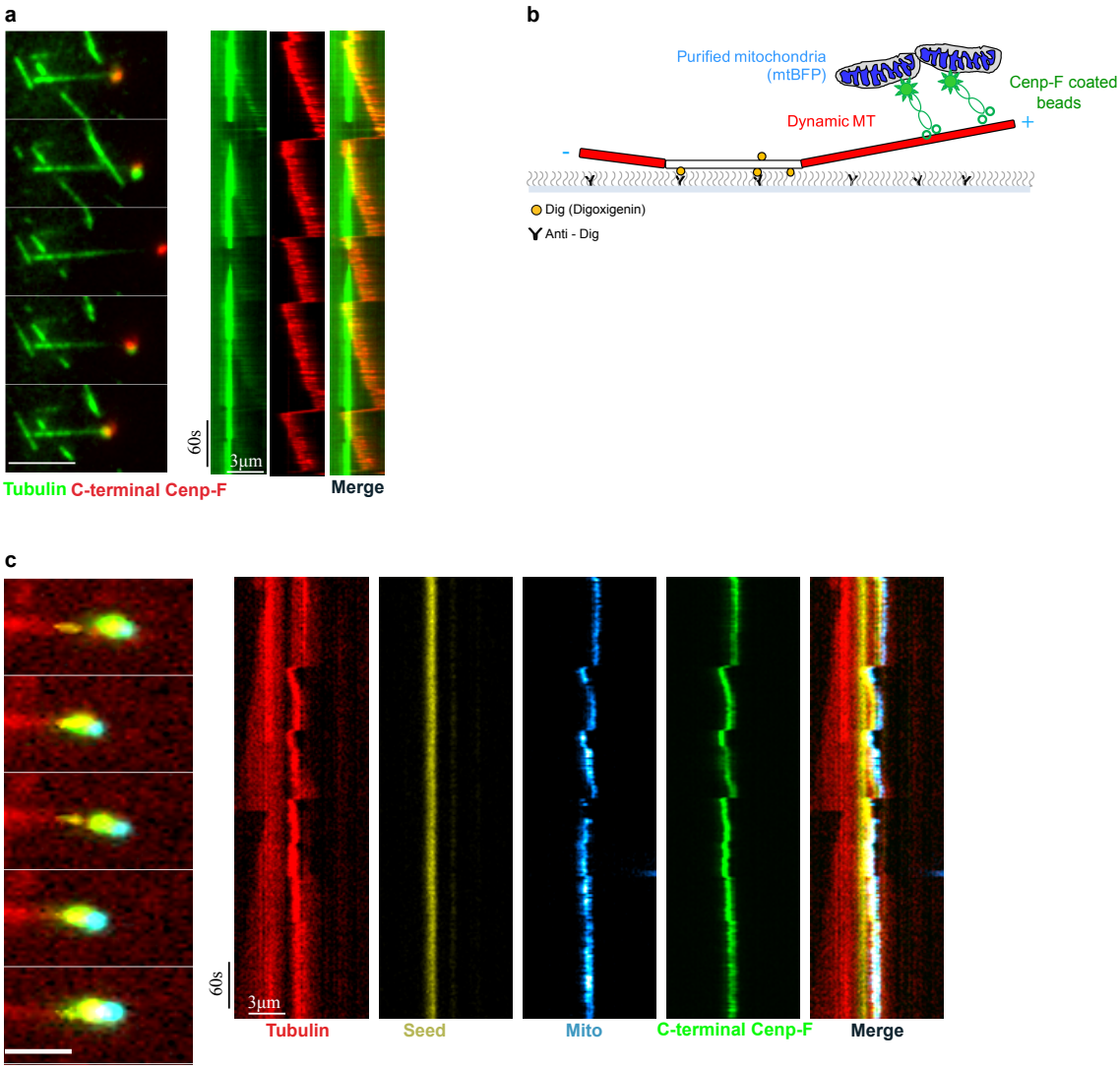

Figure 9: Cargos are attached to dynamics microtubule tips by sfGFP-2592C

a) Left panel, selected frames from time-lapse movies of fluorescently labeled MT extensions (green) and beads coated with sfGFP-2592C (red). Kymographs of the corresponding video. Time scale, 1 s/frame, scale bar x:3µm y:60sec. b) Schematic representation of the experimental setup used for investigating MT dynamics in presence of the isolated Cenp-F MT interaction domain and isolated mitochondria from Miro1 overexpressing cells. c) Left panel, selected frames from time lapse movies of fluorescently labeled MT extensions (red) and beads coated with sfGFP-2592C (red) MT seeds (yellow) and isolated mitochondria (cyan). Right panels, Kymographs of the corresponding video, time scale 1 sec per frame, scale bar x:3µm y:60sec.

5. Discussion

In cells, mitochondria are organized as dynamic interconnected networks which are maintained by a balance between fission, fusion and transport. In the course of the cell division cycle, the mitochondria undergo a dramatic alteration in distribution. This alteration is mediated by the Rho GTPase Miro which attaches the mitochondria to the MTs and facilitates mitochondria spreading. Here I show that the redistribution of the mitochondria by Miro is mediated by a cell-cycle-dependent association of MTs with the protein Cenp-F. Miro recruits Cenp-F to the mitochondria by recognizing a Cenp-F forty-four amino-acid sequence. The Cenp-F-Miro interaction promotes mitochondria transport by coupling the mitochondria to growing MTs.

Although the mechanism behind Cenp-F-mediated mitochondria movement has been clarified in this work, some fundamental aspects remain unclear. For instance, how is mitochondria spreading by Miro-Cenp-F regulated? Why is mitochondria distribution altered during cell-cycle? How does mitochondria localization relate to cell development and differentiation? Is Cenp-F-mediated mitochondrial distribution relevant in the development of cancer malignancies?

5.1. Cell-cycle dependent interaction between the mitochondria and the cytoskeleton changes mitochondria distribution

Mitochondria morphology changes during cell cycle. Although the recruitment of fusion and fission factors to the mitochondria in dividing cells, and particularly in mitosis, is covered extensively, the impact of organelle transport and trafficking mechanisms on mitochondria morphology in dividing cells has been poorly addressed. In fact, the involvement of Cenp-F (also called Mitosin) in mitochondria distribution is the first molecular evidence that mitochondrial transport is linked to the cell-cycle. Cenp-F is a large 367 kDa MT binding protein. Cenp-F was first defined as a component of the outer kinetochore (Casiano et al., 1995; Rattner et al., 1993). Cenp-F expression profile is very dynamic. Cenp-F expression initiates during S phase, increases through G2 and culminates at mitosis before quickly decreasing in G1. Parallel to protein expression, the sub-cellular localization of Cenp-F also changes during the course of the cell-cycle. It binds to the nuclear envelope during the G2/M transition, is enriched at the kinetochores during mitosis and re-localizes to the mid-body in cytokinesis (Hussein and Taylor, 2002; Liao et al.,

1995). In S/G2 the protein is found at the nuclear matrix while a cytosolic subpopulation is present in distal mitochondria, proximal to the cell borders. Cenp-F re-localization to mitochondria is further enhanced during cytokinesis, before Cenp-F expression is reduced in G1 (Fig. 1b). The recruitment of Cenp-F to the mitochondria by the outer mitochondria membrane protein Miro is achieved by direct interaction of the two proteins (Fig. 2g). Deletion of either Miro or Cenp-F results in mitochondrial dynamics reduction and collapsing of the mitochondria network to the cell center, indicating that these proteins are acting in similar pathways (Fig. 2a and Fig. 5b). It seems that neither the loss of Miro nor Cenp-F depletion affects cell cycle progression, at least in the U2OS cells used in the current study (Fig. 10a). The mechanism that relocates Cenp-F from the kinetochores at anaphase, to mitochondria during cytokinesis is yet to be found. This transition is certainly tightly regulated and likely due to sensing of unknown signals. (Kanfer et al,. 2015). Therefore, it is highly intriguing to identify the key players driving Cenp-F spatiotemporal translocation at specific cell-cycle stages. A first hint comes from the identification of the conserved forty-four amino-acid Cenp-F sequence recognized by Miro (Fig. 2h). This sequence contains consensus phosphorylation motifs of cell-cycle kinases, such as Cdk1 and Aurora B. Notably, previous works have identified Aurora and Cdk1 as master regulators of the mitochondria fission prior to mitosis (Kashatus et al., 2011; Taguchi et al., 2007). Hence, it is tempting to surmise that Cenp-F mitochondrial recruitment could be triggered by cell-cycle specific kinases. Another hint derives from studies in mouse. The Cenp-F homolog (designated as Lek1) was found to interact with another central cell-cycle factor - the canonical tumor-suppressor gene retinoblastoma (RB) (Ashe et al., 2004; Papadimou et al., 2005; Robertson et al., 2008). Although it is not clear whether the association with RB promotes cell-cycle progression, the fact that Lek1 interacts with RB through a domain that partially overlaps with the Cenp-F Miro interaction motif suggests a possible competition between RB and Miro for Cenp-F binding. Moreover, it was shown that a subpopulation of RB can be found in mitochondrial fraction where it stimulates programmed cell death by interacting with the pro-apoptotic protein BAX (Hilgendorf et al., 2013). Although the study is missing experimental evidence supporting a role for Cenp-F during apoptosis, the co-localization and interaction of Cenp-F and RB at the mitochondria suggests a role for Cenp-F in programmed cell death. Finally, recent work has found that the cell cycle kinase Cdk1 phosphorylates Cenp-F and promotes its nuclear envelope localization prior to mitosis (Baffet et al., 2015). Although the recruitment of Cenp-F to mitochondria occurs in various stages, (sooner than nuclear envelope recruitment and after anaphase), it is interesting to explore the potential role of Cdks in the

context of Cenp-F recruitment to mitochondria.

5.2. Mechanism of mitochondria transport by Cenp-F and Miro

Cenp-F is a MT-interacting protein. Cenp-F was first described as part of the outer kinetochore, where it stabilizes MTs and kinetochores interaction in mitosis (Chan et al., 1998; Feng et al., 2006; Hussein and Taylor, 2002; Musinipally et al., 2013; Volkov et al., 2015). The ablation of Cenp-F results in mitotic delay, chromosomes misalignment and failed assembly of full kinetochore (Bomont et al., 2005; Holt et al., 2005). Even though these observations emphasize the role for Cenp-F in mitosis, down-regulation of Cenp-F by RNAi only delays but does not completely disrupt progression of mitosis. Indeed, a variety of studies have demonstrated a broad role of Cenp-F behind its function in mitosis (Varis et al., 2006). For instance, a subpopulation of Cenp-F was shown to localize to the NE while another sub-population of the protein was found at centrosomes (Bolhy et al., 2011; Moynihan et al., 2009; Waters et al., 2015). Likewise, another study performed in MEFs also demonstrated Cenp-F localization to the centrosomes, where MT nucleation was found to be influenced by Cenp-F, supporting a role for Cenp-F in promoting MT growth (Moynihan et al., 2009). These results are inconsistent with the current study, in which MTs growth rates were shown to be similar between WT and Cenp-F RNAi cells (Fig. 6b and Fig. 8c). The discrepancy might come from the usage of different cell-line systems or of different organisms. The claim that Cenp-F can be involved in MT dynamics is supported by the unique localization of Cenp-F at the very tip of growing MTs ends (Fig. 4a,b), ahead of EB protein comets. In fact, there are only two more known MT-associated proteins which localize at the extreme MT tips, the MT microtubule-associated proteins Ch-Tog and CLASP (Al-Bassam and Chang, 2011). Ch-TOG acts as MT polymerase by accelerating MT assembly. An earlier study in which isolated MTs were exposed to glass beads coated with purified Ch-Tog has demonstrated that cargo movement can be coupled to dynamic MTs by Ch-Tog (Trushko et al., 2013). However, unlike the current study which supports mitochondria transport by Cenp-F in vivo, whether Ch-Tog can promote organelle transport in cells remains unknown. It is also not clear how Cenp-F transduces the force from the MT dynamics to moving cargoes. Since the structure and function of Ch-Tog was investigated elaborately, Ch-Tog can serve as a model to study the mechanism of Cenp-F-driven mitochondria transport at the molecular level. Another player which might participate in cargo movement by Cenp-F and MT tips is the MT plus end tip protein CLASP. CLASP promotes MT rescue and suppresses MT catastrophe events. There are two reasons to study CLASP in the context

of Cenp-F-mediated mitochondrial dynamics: first, CLASP was found to interact with a Cenp-F homolog in C.elegans (Cheeseman et al., 2005). Second, CLASP -dependent mitochondrial trafficking on dynamic MTs was demonstrated in fission yeast (Chiron et al., 2008). Although Cenp-F, Ch-Tog and CLASP can track dynamic MT ends, the ability to exert force from both growing and shrinking MTs has so far only been demonstrated for Cenp-F. In addition to attachment to dynamic MTs, there is also the possibility that the force necessary to move cargo is generated by motor proteins. Indeed, previous studies have connected Cenp-F and MT based motor proteins. First, Cenp-F interacts with the plus-end-directed MT motor Cenp-E (Chan et al., 1998; Maton et al., 2015; Musinipally et al., 2013). Both proteins were found to be part of the outer kinetochore structure and share similar functions during mitosis. The downregulation of Cenp-E by RNAi influenced neither Cenp-F mitochondrial localization nor mitochondria spreading (Fig. 6a), indicating that Cenp-E most likely does not participate in mitochondrial transport by Cenp-F. Second, Cenp-F was also found to recruit Dynein by binding proteins of the Nuclear distribution family Nude/Nudel/Lis1, which are critical components of the cytoplasmic Dynein complex (McKenney et al., 2014; Vergnolle and Taylor, 2007). This functional recruitment of Dynein complex by Cenp-F was shown to be a critical step in the process of Nuclear envelope break down, which happens at the G2/M transition. However, as was demonstrated with Cenp-E, the down-regulation of Nude/Nudel by RNAi resulted neither in Cenp-F mitochondrial mislocalization nor in altered mitochondrial network distribution (Fig. 6a). However, disrupting Nude/Nudel1/Lis1 expression in neurons blocked mitochondria retrograde transport in dendrites (Shao et al., 2013). Since Cenp-F is expressed in mouse brain and plays a role in neuronal progenitor stem cells, it will be interesting to test whether Cenp-F can promote mitochondria transport in neurons by attaching to the Dynein complex (Dees et al., 2012).

In agreement with the results presented in current study, recent work by Volkov and others also shows that Cenp-F can follow MT ends and couple cargo transport in vitro (Volkov et al., 2015). In this case, the researchers suggest that Cenp-F contributes to pulling chromosome following anaphase by attaching the kinetochores to the disassembling MTs. More specifically, they show that Cenp-F is enriched in pulldown of curled MTs, which are thought to harbor the shape of shrinking MTs. These experiments were conducted in vitro, unlike in the current work where Cenp-F ability to follow MT growth was supported by in vivo experiments. Evidence from living cells showing that Cenp-F follows kinetochores during chromosome segregation is still missing, but those two complementary approaches point for the first time that MT can serve as a motor for

pulling and pushing cargoes. The mechanism of action still needs to be clarified at the molecular level and the possible involvement of motor proteins in this process should be tested in living cells.

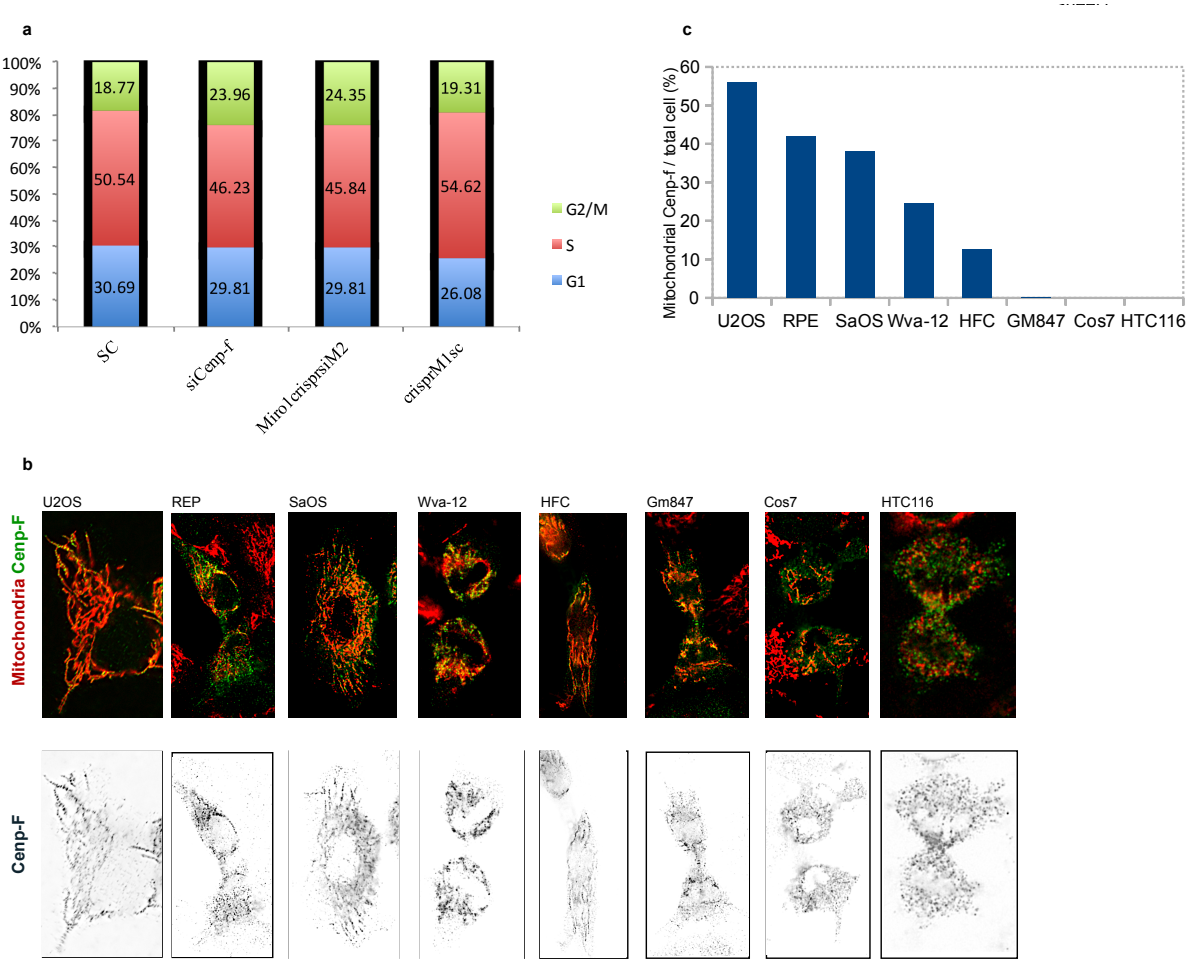

Figure 10: Cenp-F, cell-cycle and cancer cell-lines

a. Cell cycle analysis performed by FACS on SK-N-MC cells.
b. Immunofluorescence of cancer-cell line stained with Cenp-F antibody (green) and Tom20(red).
c. Quantification of Cenp-F translocate to the mitochondria. Over 100 cells were counted for the different cell-lines

5.3. Cenp-F and Miro role in cellular development and cancer

The recruitment of Cenp-F to the mitochondria in a cell cycle-dependent manner, establishes the first connection between mitochondrial transport and cell-division progression . However, despite the fact that Cenp-F is related to mitosis, and that mitochondria spreading is regulated by Cenp-F expression and localization, Cenp-F down-regulation does not influence cell cycle progression (Fig 10a). In-fact, the link between mitochondrial network organization and cell-cycle progression is missing. On the other hand, more studies report on possible roles for mitochondrial network organization in stem cell differentiation and development. For instance, a link was observed between mitochondria fission/fusion dynamics during the process of oogenesis. In this case, Mitochondria fission was found to be essential for cell-cycle exit and differentiation of a posterior follicle cell in the fruit fly (Drosophila). Moreover, hyperelongation of the mitochondrial network results in premature differentiation (Mitra et al., 2012). Similarly, the sub-cellular position of mature cells prior to stem like-cells differentiation correlated with mitochondrial function and stemness (Prigione et al,. 2010; Varum et al,. 2011; St Joun JC,. 2005; Mandal S,. 2011; Katajisto,. 2015).

Cenp-F was also found to play an important role in development. In the embryonic mouse, Cenp-F protein expression is ubiquitous but increased in the heart and brain (Dees et al., 2012). Attempts to create a globally targeted deletion of Cenp-F results in embryonic stem cells with significant duplication defects, such that the lines could not be expanded beyond the eight-cell stage (Toralová et al., 2009). It is not clear whether this phenotype is due to the role of Cenp-F at kinetochores or at mitochondria distribution. One way to address this point would be to engineer separation of functions alleles of Cenp-F in mice. A point mutation in Miro interaction motif of Cenp-F prevents Cenp-F mitochondrial recruitment, presumably without affecting its other roles.

Besides its role in development, Cenp-F is also overexpressed in various cancers such as lung cancer, breast cancer, Non-Hodgkin lymphomia, mantle cell lymphoma and in prostate cancer (Ma et al., 2006). Although this protein is expressed in cancer cells and plays a role in KT-MT attachment during mitosis, Cenp-F function in malignancy process is still not clear. In particularly, in a variety of different cancer cell lines, Cenp-F is found in the nucleus, but Cenp-F mitochondrial localisation was displayed in only a fraction of these cells (Fig. 10b and c). Protein regulation can explain the discrepancies in Cenp-F subcellular positioning in the different cancer cells as different cancer models activate

various sets of protein and signaling pathways (Fig. 10b and c). In-fact, it is not clear at all whether Cenp-F mitochondrial role is engaged in the process of cancer development. Until recently, the connections between mitochondria and cancer were related mainly to metabolism. The connection between cancer invasion and a decrease in mitochondrial respiration is established and has been named "the Warburg effect" (Warburg, 1956; Wallace, 2012). Recent work indicates a role for mitochondria dynamic in tumor invasion. This study suggests a correlation between tumor penetration and mitochondria division (Fission et al., 2015). In addition, mitochondria positioning was also linked to an increase in tumor cell motility and invasion (Caino et al., 2015). In this study the researchers show that upon stimulus, cancer cells redistribute their mitochondria to the cell periphery (Caino et al., 2015). Specifically, they show a correlation between mitochondria with higher respiration profile and their specific sub-cellular localization at the cell periphery, probably for supplying energy for the highly demanding actin cytoskeleton which promotes cell motility. This observation suggests an active mechanism which separates the mitochondria according to their respiration and transports more functionally active mitochondria to the cell periphery, most likely by attaching mitochondria to MTs. It would be intriguing to test whether Cenp-F is involved in this type of selective transport of mitochondria. Supporting possible role of Cenp-F in cancer cell migration comes from a study which identified Cenp-F as a master regulator of prostate cancer (Aytes et al., 2014), where Cenp-F down-regulation was shown to block cell motility and to reduce tumor malignancy.

Materials and methods

Cell Culture, Transfection and plasmids

U2OS cells were grown at 37° C in DMEM (Life Technologies) supplemented with 10% F.C.S., 100 µg/ml streptomycin, 100 U/ml penicillin, and 1% L-glutamine. To establish the KERMIT cell line, U2OS cells were cotransfected with linearised mtBFP and pAc-Sec61α-GFP. Individual clones were selected in 0.4 µg/ml G418 and maintenance was performed in 0.2 µg/ml. To visualize microtubules, U2OS cells were stained with Sir-Tubulin, by incubating for 1 hour for with 1 µM of Sir-Tub (supplemented with 10uM Verapamil) in warm DMEM in 37° C. To visualize microtubule growth, cells were transfected with 0.5 µg of Eb1-RFP, human EB1 fused to monomeric RFP was a gift from Tim Mitchison & Jennifer Tirnauer (Addgene plasmid # 39323). Additional cancer cell lines which were used in this work, RPE, SaOS, Wva-12, Gm847, HTC116 were kind gifts from Claus Azzalin. pAc-Sec61α-GFP32 was a kind gift from Gia Voeltz (University of Boulder, USA). GFP-Cenp-F plasmid17 was provided by Stephen Taylor (University of Manchester, UK). pcDNA3.1-mtBFP was generated by inserting mtBFP sequence digested with HindIII Xba1 into pcDNA3.1+ plasmid. pcDNA5/FRT/TO-3XFlag-6his-Miro1 and pcDNA5/FRT/TO-3XFlag-6his-Miro2 were cloned by PCR amplification of Miro1 and Miro2 CDSs using primers #1 and #3 (see Supplementary Table 1), and 2# and #4, respectively, using cDNA clones as templates (IMAGE clones 40118340 and 4859240, respectively), followed by reamplification using primer #5, #3 and #5, #4, respectively. The PCR products were cloned using Gateway into the pcDNA5/FRT/TO plasmid (Invitrogen). GTPase and EF-hand mutants of Miro-1 were generated by site-directed mutagenesis of the pcDNA5/FRT/TO-3XFlag-6his-Miro1 plasmid using primers #10 and #11 for the T18N mutation, #12 and #13 for the E208K mutation, #14 and #15 for the E328K mutation, and #16 and #17 for the S432N mutation. Constructs containing different Cenp-F fragments (residues 1 to 979, 843 to 1764, 1756 to 3114, 1756 to 2375, 2375 to 3114, 2519 to 2831, 2719 to 2831, 2819 to 3017) were prepared by PCR using the indicated primers (#22-#34, respectively), and using the GFP-Cenp-F plasmid as a template, followed by cloning into the pcDNA5/frt/to plasmid vector within BamHI and NotI restriction sites. Miro-1 CRISPR plasmids (pX330-Miro1ex7 and pX330-Miro1ex8) were generated by cloning annealed oligos (#6, #7 and #8, #9, respectively), designed by the CRISPR design tool into pX330, as described by Cong et al. Science. 2013.

Gap- repair-cloning

For internal tagging of Cenp-F, the pcDNA5/FRT-GFP Cenp-F plasmid was used as a template. Cenp-F N-terminal fragment and C-terminal (from amino acid 1 – 1523 and 1523 – 3114 , respectively) were PCR amplified with overlapping homologous regions for the yeast plasmid pRS426, which was linearized by EcoRI, and homologous regions for the N and C terminus sequences of eGFP. Cells were transformed with the PCR amplified fragments and the linearized pRS426 plasmid to promote recombination of the desired Cenp-F sequence. Since pRS426 contains LEU2, yeast cells were grown on SD-Leu selection medium for 3 days. The repaired plasmid was extracted as followed: cells were grown in suitable medium to OD600=0.5 – 0.8. 1.5ml of suspension was centrifuged and washed with ddH2O. To rescue the plasmid, the solution was resuspended in 250µl of "resuspension solution" (from plasmid miniprep kit), 250ul of glass beads and homogenize by vortexing for 3-5min. After adding and mixing with 250 µl "lysis solution" for 3min the solution was neutralized using 350ul of "Neutralization Solution". Cell debris was removed by fast centrifugation, The subsequent steps of column purification were performed as suggested by the manufacturer after cell breakage. 1-2 µl of the elution product was used to transform E. coli DH5α. After sequencing the extracted plasmid, the repaired sequence was digested with Not1 and BamH1 and reintroduced into pcDNA5FRT/TO plasmid. 2 µg of extracted plasmid was transfected into U2OS cells.

Purification of CENP-F constructs

The N436-sfGFP and the sfGFP-2592C were purified as previously describe (Volkov et al,. 2015). Briefly, Cell pellets were resuspended in lysis buffer (50 mM NaH2PO4, pH 6.9, 300 mM NaCl, 10 mM imidazole, and 250 µg/ml Pefabloc SC) and a series of sonication steps were applied for cell breaking. 0.25% Tween-20 was added and the lysate was centrifuged at 10,000g for 20 min at 4° C. Clarified lysates were passed through a Ni-NTA column (Qiagen, 31014) and after 1 hr incubation, the column was washed with buffer (50 mM NaH2PO4, pH 6.9, 500 mM NaCl, and 20 mM imidazole), and the proteins were eluted with elution buffer (50 mM NaH2PO4, pH 6.9, 300 mM NaCl, and 250 mM imidazole). Eluted fractions were desalted on a Zeba Desalting Spin Column that had been equilibrated with BRB80 buffer plus 150 mM NaCl. CENP-F fragments were additionally purified using ion-exchange chromatography. Ni-NTA fractions were

desalted into 50 mM NaH2PO4, pH 6.6 (N436-sfGFP) or 7.0 (2592C and sfGFP- 2592C), with 0.1 M NaCl; applied to a 1 ml HiTrap SP HP column (GE Healthcare); washed with 10 ml of the same buffer; and eluted with a linear gradient from 0.1 to 1 M NaCl in the same buffer. Peak fractions were snap frozen in liquid nitrogen.

Crude Mitochondria isolation

U2OS cells stably expressing mitochondria-BFP were grown to 80-95% Confluence. Mitochondrial purification was performed with some modifications as described previously (Wieckowski, M.R., 2008). Cells were harvested by trypsinization and washed with PBS twice. Cells were centrifuged at 300g for 5 min, the pellet was resuspended in Mito homogenization solution (225mM mannitol, 75mM sucrose ,30mM tris ph7.4, 0.1mM EGTA), the solution was homogenized by 25 strokes with glass douncer and centrifuged at 600g for 5 minutes. After the pellet was discarded, the supernatant was spun again at 7000g for 10 min in 40C. Next, the supernatant was discarded and the pellet was collected, and resuspended in mitochondria homogenization solution 2 (225mM mannitol, 75mM sucrose 30mM tris ph7.4). Followed a fast spin of 10,000 g for 10 min, the crude isolated mitochondria pellet was finally resuspended in the mitochondrial re-suspension buffer (250mM mannitol, 5mM HEPES (ph 7.4) 0.5mM EGTA).

Preparation of assembled tubulin

Tubulin was prepared from pig brains by two polymerization cycles (Castoldi and Popov, 2003 and Weingarten et al., 1974), frozen in assembly buffer (100 mM MES, pH 6.4, 1 mM EGTA, and 1 mM MgSO4, plus 1.5 mM GTP), and stored at −80° C until needed. Briefly, after removing the blood vessels from the brain, 700 g of tissue was resuspended in 500 µl of MES buffer and homogenized. The homogenized cold solution was centrifuged at 9000RPM at 40C (SS-34 Fixed Angle Rotor, Thermo Scientific). The supernatant was mixed with half a volume of glycerol, 5mM MgCl2, 0.25mM GTP, 2.00mM ATP, the solution was incubated at 370C for promoting MTs polymerization. After 45 mintues, the solution was spun at 235,000g for 30min in 37C0 using 45Ti Fixed Angle Rotor Ultracentrifuge (Beckman Coulter, 365672, 331362). The pellet was collected and resuspended with 100ml of cold depolymerization buffer (MES buffer + 0.25mM GTP, 1.5mM ATP, 1mM DTT), after 30 minutes the solution was centrifuged again at 40,000RPM at 4 ° C using cold 71Ti Fixed Angle Rotor Ultracentrifuge

(Beckman Coulter, 365672, 331362). Another round of polymerization was performed to increase sample purity.

Characterization Cenp-F interaction with growing MTs

Following isolation, tubulin was labeled with Alexa Fluor® 647 NHS Ester (A-20006, ThermoFisher), rhodamine (Molecular Probes), or DIG (Molecular Probes) as described previously (Hyman et al., 1991). The behavior of Cenp-F and growing MTs was tracked by TIRF illumination, modified from Volkov et al., 2014. Briefly, to create tubulin seeds, 5µl of unlabeled Tubulin (10mg/ml) were mixed with 2.5µl rhodamine-Tubulin(5mg/ml), 2.5µl DIG-tubulin (5mg/ml) and 1µl GMPCPP (10mM), incubated for 15 min in 37° C and supplemented with 39µl of BRB buffer (1mM EGTA, 80mM Pipes (pH 6.9), 4mM MgCl2, GTP 1mM, DTT 1mM pH 6.9,). The seeds solution was mixed and spun at max speed for 15min at the room temperature. The pellet was resuspended in 25µl of BRB.

To preform the MT growth assay, stabilized, rhodamine-labeled MTs were attached with anti-DIG antibodies to the silanized coverslips passivated with Pluronic F-127. A solution of CENP-F fragment in BRB80 supplemented with 2 mM dithiothreitol, 0.1 mg/ml glucose oxidase, 68 µg/ml catalase, 20 mM glucose, 0.5% 2-mercaptoethanol and 12µM of Alexa Fluor® 647-labeled Tubulin was continuously pumped through the flow chamber at 20 µl/min. For testing MTs dynamic and beads, the beads were coated with the sfGFPCenp-F fragment. Glass beads [Str 1-µm glass COOH-modified beads (Bangs Laboratories)] were coated with streptavidin (Thermo Fisher Scientific) and then with biotinylated anti-Penta-His antibodies (QIAGEN) as described previously (Grishchuk et al., 2008, Volkov et al., 2015). 6xHis-tagged CENP-F fragments were then attached to these beads, washed, spun and mixed with Cenp-F fragment. The coated beads were introduced into the flow chambers together with 12µM of Alexa-647-labeled tubulin promote MT growth. To test mitochondria and MTs dynamics, isolated mitochondria were centrifuged at 10,000g for 10 min and resuspended in 200µl of BRB. They were then mixed with Cenp-F fragment and mixed by rotation for 40min in the cold room. After spinning the mitochondria-Cenp-F solution at 10,000g for 10 min, the pellet was resuspended in 5µl BRB80 buffer.

Flow chambers were equilibrated at 37° C during the acquisition. Images were acquired every second using a Leica TIRF microscope (DMI6000B, inverted), equipped with with a 100× HCX PlanApo 1.47 NA TIRF objective and an Andor iXon EM CCD camera

(front illuminated, 8x8 μm2 pixel size). The system was incubated at 37° C in a Cube Incubator (LIFE IMAGING SERVICES GmbH, Switzerland). 405 nm, 488 nm, 561 nm and 647 nm lasers were used.

Immunofluorescence and Imaging

Cells were seeded on 18 mm cover-slips in 6-well vessels and optionally transfected with 6 μl lipofectamine-2000 (Invitrogen). On the next day, wells were optionally stained with 2 μM MitoTracker-Red-CM-H2Ros (Invitrogen) and washed in phosphate-buffered saline (PBS; 12mM phosphate, 137 mM NaCl, 3 mM KCl, pH 7.4). For optimal mitochondria imaging, cells were fixed with 4% paraformaldehyde in PHEM buffer (60 mM Pipes, pH 6.8, 25 mM Hepes, pH 7.4, 10 mM EGTA, 5 mM MgCl) for 10 min. Coverslips were washed three times in PBS and permeabilized in 0.5% NP-40, then washed three times with PBS and blocked in blocking solution (PBS + 10% fetal calf serum + 10 mg/ml BSA). For optimal cytoskeleton imaging, cells were fixed using 100% methanol (-200C for 8 minutes). Fixed cells were rinsed with PBS and incubated in blocking solution (5% FCS in PBS). Primary antibodies were added to the blocking solution and incubated for one hour. Antibody concentration: rabbit anti-Miro1 (HPA010687, sigma) 1:500; mouse anti-Miro1 (WH0055288M1, Sigma) 1:500; mouse anti-Tom20 (clone 4F3, Abnova) 1:100; mouse anti-Phospho-H3 (ser 10, 9706, Cell signaling) 1:1000; mouse anti-Aurora B (611082/3, BD Biosciences) 1:1000; rabbit anti-Cenp-F (ab5, Abcam) 1:300; mouse anti-Cenp-F (610768, BD Biosciences) 1:500; mouse anti-alpha-Tubulin (B-5-1-2, Sigma) 1:1000; rat anti-EB1 (KT51, Absea) 1:1000. Wide-field microscopy of fixed samples was conducted on a DeltaVision Microscope (IX-71; Olympus) connected to a camera (Roper CoolSnap HQ2, Photometrics), using a differential interference contrast Plan Apochromat 60X, NA 1.42 oil PlanApoN immersion objective. 3D image stacks were acquired in 0.2- μm steps using DAPI-FITC-TRC-CY5 filter set (Chroma). The 3D image stacks were deconvoluted with softWoRx (Applied Precision, LLC). For Microtubule visualisation, fixed cells were imaged using a DeltaVision OMX 3D-SIM Super-Resolution system controlled by DV-OMX software (Applied Precision). Images were captured at 0.125-μm step size with a UNIPLANAPO 100×/1.4 numerical aperture (NA) objective, using 1.514 immersion oil. The 405 nm-channel images were acquired for 100 ms at 1% laser strength, 488 nm-channel images for 50 ms at 10% strength, 561 nm-channel images for 50 ms at 100% strength, and 642 nm-channel images for 50 ms at 100% strength. Images were processed using softWoRx

(Applied Precision) and IMARIS 3D imaging software (Bitplane, Saint Paul, MN). Colocalization analyses were performed using Daniel J White, Tom Kazimiers and Johannes Schindelin ImageJ plugin Coloc 2. Analysed regions of interest excluded the nucleus. All experiments have been repeated a minimum of three times, with consistent results.

RNAi

Oligonucleotides for siRNA synthesised against the target sequence of Cenp-F (oligo #1: 5'-CAGGAAAGACTAGCCCATATA-3', oligo #2: 5'-CAGAATCTTAGTAGTCAAGTA-3', oligo #3 (ineffective): 5'-CTGGTGATGGATTAACATATA-3', oligo #4: 5'-ACCGAGAG-AAATTGACTTCTA-3'), Miro2 (oligo #1 5'-AAGGCAGAGCTTTGGGCCAAA-3', oligo #2 5'-GAGGTTGGGTTCCTGA-TTAAA-3'), and scrambled siRNA 5′ -TTCTCCGAACGTGTCACGT-3’ were purchased from Qiagen. siRNA transfection was performed using Lipofectamine RNAiMAX (life technologies) according to the manufacturer, at a final concentration of 30 nM.

CRISPR/Cas9 Mutagenesis

To mutate endogenous Miro1, KERMIT cells were seeded on a 10 cm plate and cotransfected with 16.2 µg pX330-Miro1ex7, 16.2 µg pX330-Miro1ex8 and 3.6 µg HcRed plasmid (kind gift of Juan Gerez, ETH Zurich). 48 hours post transfection, RFP-positive cells were sorted by FACS and seeded on 10 cm plate at low density. Next, isolated colonies were transferred to 96 well plate and genotyped.

Mitochondrial Spreading Measurement

To analyse mitochondrial spreading we imaged and processed control and experimental cells identically, using ImageJ (Supplementary appendix 1). Indicated cells were seeded onto 22-mm2 micropatterned glass coverslip (Cytoo, Grenoble, France), according to the manufacturer's protocol. At least 34 cells per condition were analysed. The centre of mass (CofM) of the mitochondrial network was calculated using the following equation: where XYi represents the XY coordinate of each pixel and Ii represents the intensity of each pixel. Second, to determine the moment of inertia (M) of the mitochondrial network, the distance of each pixel to the CofM was computed: The measurement was performed by a MatLab function (Supplementary appendix 2).

Quantification of Cenp-F Enrichment at Microtubule Tips

To assess if Cenp-F localisation at growing microtubule tips was due to chance, we devised the following analysis (Supplementary appendix 3, Kanfer et al,. 2015). Three channel images (EB1, Cenp-F, microtubules) were analysed. Only cytoplasmic areas were considered. First, using ImageJ, the position of the tips of EB1 comets (typically around 30 per image) were manually determined. The channel for Cenp-F was hidden during this manual step to avoid bias. We determined the position of Cenp-F foci automatically using the "Find Maxima..." procedure (typically around 1000 per images). We assessed the extent of comet tip and Cenp-F colocalisation by counting the number of comets closer than 3 pixels (~100nm from a Cenp-F focus). To assess if the EB1-Cenp-F distances could be the result of a random draw, the distance of the closest Cenp-F focus was measured for random points of the microtubule network (typically 3000 per image) picked using the "Find Maxima..." procedure. Then random points (same number of points as the number of EB1 comets) were drawn 107 times from this pool and the number of those colocalising with Cenp-F was calculated. The p-value equals the number of time that the draw picked more random points colocalising with Cenp-F foci than observed for comet tips, divided by the number of attempts.

Quantification of Microtubule Tip Tracking Events

Events where mitochondria move in a coordinate fashion with EB1 comets were counted manually after randomising the "scrambled" and "siCenp-F" movies to avoid biases.

Statistics

All statistical tests herein were performed using non-parametric Mann-Whitney-Wilcoxon U tests.

Flag-Miro Purification and Mass Spectrometry

T-Rex™-293 expressing 3XFlag-6XHIS-Miro1/2 were harvested and homogenised in lysis buffer (20 mM Hepes, 150 mM potassium acetate, 2 mM Magnesium acetate, 0.1mM PMSF, 1 μg/ml Leupeptin, 1 μg/ml Aprotinin, 1 μg/ml Pepstatin), containing 2% Triton-100X. Whole cell extracts were incubated with 4% M2-Flag coated magnetic beads (sigma). The beads where thereafter washed six times with ice cold lysis buffer, containing 0.2% digitonin and eluted with the same buffer containing 150 ng/μl 3X Flag peptide. Samples were then diluted five fold with 8 M urea and 0.1 M ammonium

bicarbonate and reduced using 12 mM DTT, at 32° C for 30 min followed by alkylation with 40mM iodoacetamide at room temperature for 45 min. The samples were diluted five fold with 0.1 M ammonium bicarbonate and proteins were digested to peptides by adding 1 µg of trypsin (Promega) and incubating overnight at 32° C. A column packed with C-18 material (The Nest Group) was used to purify and concentrate peptides. The peptide samples were analyzed on a 5600TripleTOF mass spectrometer (ABSciex) equipped with a nanoelectrospray ion source. Chromatographic separation of peptides was performed using an Eksigent Ultra nano LC system (ABSciex) coupled to a 15 cm fused silica emitter, 75 µm diameter, packed with a Magic C18 AQ 5 µm resin (Michrom BioResources). Peptides were loaded on the column from a cooled (4 ° C) Eksigent autosampler and separated with a linear gradient of acetonitrile/water, containing 0.1% formic acid, at a flow rate of 300 nl/min. A gradient from 5 to 35% acetonitrile over 120 min was used. The mass spectrometer was operated in data-dependent acquisition mode. For TOF analyses, the accumulation time was set to 0.299995s, and the mass range to 400 – 1250 Da. Peptides with 2 – 5 charges and signals exceeding 150 cps were selected for fragmentation. Per cycle, up to 20 precursor ions were monitored and excluded for 20s after one occurrence. The product ion analysis was performed with an accumulation time of 0.149998s, and a mass range of 170 – 1500 Da in a high sensitivity mode. The total cycle time was 3.35s. Raw data was converted from WIFF format to MGF format (Matrix Science) using the AB SCIEX MS data converter (version 1.1 beta). Peak lists in .mgf format were searched against a human protein database downloaded from Uniprot (http://www.uniprot.org/, September 2009) with Sorcerer™-SEQUEST® (Thermo Electron). Trypsin was set as the digesting protease with the tolerance of two missed cleavages, one non-tryptic terminus and not allowing for cleavages of KP and RP peptide bonds. The monoisotopic peptide and fragment mass tolerances were set to 50 ppm and 0.8 Da respectively. Carbamidomethylation of cysteins (+57.0214 Da) was defined as a fixed modification and the oxidation of methionines (+15.99492) as a variable modification. Protein identifications were statistically analyzed with ProteinProphet (v3.0) and filtered to a cut-off of 0.9 ProteinProphet probability, which corresponded to a FDR <1%, calculated based on a target-decoy approach. For SILAC labeling, Hek293 cells were grown for 6 generations in DMEM without arginine and lysine, and supplemented with either Arg0/lys0 for 3XFlag6HMiro1 cells or Arg10 (13C6 15N4)/Lys8 (13C6 15N2) for the Hek293t-rex (control) cells. ”Heavy” and “Light”-labeled cells were harvested and directly combined in equal amounts before

lysis. Flag purification, peptide preparation, and analysis by mass spectrometry was preformed as above. For each peptide in which a light and heavy form was detected, the light to heavy ratio was determined by manually measuring the area under the curve using PeakViewer(version 2.3.3). Light and Heavy peptides were identified and their ratios were calculated by MaxQuant33. The results are compiled in Supplementary Table 1, Kanfer et al,. 2015.

Yeast Two Hybrid Assay

The assay was performed according to standard protocol (Golemis, E. A. et al. 2008). Briefly, LexA-fused Cenp-F bait plasmid was created by gap-repair cloning of PCR-amplified C-terminal fragment of Cenp-F (amino acids 2977-3020, primers #18 and #19, see Supplementary Table 1) into pEG202 vector linearised with NotI. The prey plasmid was created by gap-repair cloning of Miro1 (without transmembrane domain, amino acids 1-594, primers #20 and #21) or Miro2 (amino acids 1-592, primers #41 and #42) into pJG4-5 vector linearised with XhoI. Both plasmids were transformed into yeast strain EGY48 containing reporter plasmid pSH18-34, which encodes lacZ reporter gene under control of LexA operators. Strain with empty bait and prey plasmids and strains with either Cenp-F-bait or Miro1-prey plasmid alone were used as controls. Transformants were grown on -Ura/-Trp/-His media containing galactose to induce expression of prey protein. The transcription of lacZ reporter was then assessed by X-gal overlay assay (Serebriiskii, I. G. & Golemis, E. A., 2000).

CRISPR/Cas9 Mutagenesis

To mutate endogenous Miro1, KERMIT cells were seeded on a 10 cm plate and cotransfected with 16.2 µg pX330-Miro1ex7, 16.2 µg pX330-Miro1ex8 and 3.6 µg HcRed plasmid (kind gift of Juan Gerez, ETH Zurich). 48 hours post transfection RFP-positive cells were sorted by FACS and seeded upon 10cm plate at low density. Next, isolated colonies were transferred to 96 well plate and genotyped.

Live Cell Imaging

Inducible GFP-EB1 expressing cells were stimulated with 10nM Doxycycline for 16-24 h before imaging. G2 synchronisation was performed by arresting cells with 2 µM thymidine 16 h before imaging. For visualisation of the mitochondria, cells were transfected with mtDsRed plasmid prior for Doxycycline induction. Mitochondria and

GFP-EB1 were imaged live at 370C using a DeltaVision OMX 3D-SIM Super-Resolution system controlled by DV-OMX software (Applied Precision), in epifluorescence mode. Images were captured with an UNIPLANAPO 100×/1.4 numerical aperture objective, using 1.514 immersion oil. Images were acquired every 400 ms sec for maximum of 2 min. All experiments have been repeated a minimum of three times, with consistent results.

Cell-cycle analysis

Cells with the indicated treatment were trypsinized and fixed in 70% ethanol overnight at -200C. Following a 30 min blocking incubation in PBS 5% FCS 0.25% Triton X‐100, cells were resuspended for 30 min at 37° C in a solution containing 50 µg/ml propidium iodide, 20 µg/ml ribonuclease and 38 mM Na3Citrate (pH 7.5). Flow‐cytometry was performed with a FACScalibur flow cytometer (BD Biosciences) using the CellQuest software. Data analysis was performed using the FlowJo software.

Abbreviation

Cenp-F, Centromer protein F

Miro, Mitochondria Rho

Eb1, End Binding Protein 1

Clasp, Cytoplasmic linker associated protein

Ch-Tog, colonic and hepatic tumor over-expressed gene

Mfn, Mitofusins

Drp1, Dynamin-related protein

TAC, tip attachment complex

+TIPs, Plus end-tracking proteins

G1 and G2 phases, gap 1 and gap 2 phases

KT, kinetochores

Tirf, Total internal reflication

SIM, structure illumination

SILAC, stable-isotope amino-acid labelling in culture

Cenp-E, centromere protein E

NudeI, nuclear distribution protein nudE1-like 1

Cdk, Cyclin-dependent kinase

Crispr, Clustered regularly-interspaced short palindromic repeats

ER, endoplasmic reticulum

RB, retinoblastoma protein

Bax, BCL2-Associated X Protein

OMM, Outer-mitochondrial membrane

MT, microtubule

MTOC, microtubule organization center

References

Acharya, U., Mallabiabarrena, A., Acharya, J.K., and Malhotra, V. (1998). Signaling via Mitogen-Activated Protein Kinase Kinase (MEK1) Is Required for Golgi Fragmentation during Mitosis. Cell *92*, 183–192.

Altmann, K., Frank, M., Neumann, D., Jakobs, S., and Westermann, B. (2008). The class V myosin motor protein, Myo2, plays a major role in mitochondrial motility in Saccharomyces cerevisiae. J. Cell Biol. *181*, 119–130.

Al-Bassam, J., and Chang, F. (2011). Regulation of microtubule dynamics by TOG-domain proteins XMAP215/Dis1 and CLASP. Trends Cell Biol. 21, 604 – 614.

Ashe, M., Pabon-Peña, L., Dees, E., Price, K.L., and Bader, D. (2004). LEK1 Is a Potential Inhibitor of Pocket Protein-mediated Cellular Processes. J. Biol. Chem. 279, 664 – 676.

Aytes, A., Mitrofanova, A., Lefebvre, C., Alvarez, M.J., Castillo-Martin, M., Zheng, T., Eastham, J. a, Gopalan, A., Pienta, K.J., Shen, M.M., et al. (2014). Cross-species regulatory network analysis identifies a synergistic interaction between FOXM1 and CENPF that drives prostate cancer malignancy. Cancer Cell 25, 638 – 651.

Van Bergeijk, P., Adrian, M., Hoogenraad, C.C., and Kapitein, L.C. (2015). Optogenetic control of organelle transport and positioning. Nature.

Baffet, A.D., Hu, D.J., and Vallee, R.B. (2015). Cdk1 Activates Pre-mitotic Nuclear Envelope Dynein Recruitment and Apical Nuclear Migration in Neural Stem Cells. Dev. Cell 33, 1 – 15.

Bolhy, S., Bouhlel, I., Dultz, E., Nayak, T., Zuccolo, M., Gatti, X., Vallee, R., Ellenberg, J., and Doye, V. (2011). A Nup133-dependent NPC-anchored network tethers centrosomes to the nuclear envelope in prophase. J. Cell Biol. 192, 855 – 871.

Bomont, P., Maddox, P., Shah, J. V, Desai, A.B., and Cleveland, D.W. (2005). Unstable microtubule capture at kinetochores depleted of the centromere-associated protein CENP-F. EMBO J. 24, 3927 – 3939.

Boldogh, I.R., Yang, H.C., Nowakowski, W.D., Karmon, S.L., Hays, L.G., Yates, J.R., and Pon, L. a (2001). Arp2/3 complex and actin dynamics are required for actin-based mitochondrial motility in yeast. Proc. Natl. Acad. Sci. U. S. A. *98*, 3162–3167.

Braschi, E., Zunino, R., and McBride, H.M. (2009). MAPL is a new mitochondrial SUMO E3 ligase that regulates mitochondrial fission. EMBO Rep. *10*, 748–754.

Burkhardt, J.K., Echeverri, C.J., Nilsson, T., and Vallee, R.B. (1997). Overexpression of the dynamitin (p50) subunit of the dynactin complex disrupts dynein-dependent maintenance of membrane organelle distribution. J. Cell Biol. *139*, 469–484.

Caino, M.C., Ghosh, J.C., Chae, Y.C., Vaira, V., Rivadeneira, D.B., Faversani, A.,

Rampini, P., Kossenkov, A. V., Aird, K.M., Zhang, R., et al. (2015). PI3K therapy reprograms mitochondrial trafficking to fuel tumor cell invasion. Proc. Natl. Acad. Sci. 112, 201500722.

Casiano, C.A., Rene, L.H., Peebles, C., Covini, G., and Tan, E.M. (1995). A u t o i m m u n i t y to the cell cycle-dependent centromere protein p330dlCENP-F in disorders associated with cell proliferation. 575 – 586.

Chan, G.K.T., Schaar, B.T., and Yen, T.J. (1998). Characterization of the kinetochore binding domain of CENP-E reveals interactions with the kinetochore proteins CENP-F and hBUBR1. J. Cell Biol. 143, 49 – 63.

Cheeseman, I.M., MacLeod, I., Yates, J.R., Oegema, K., and Desai, A. (2005). The CENP-F-like proteins HCP-1 and HCP-2 target CLASP to kinetochores to mediate chromosome segregation. Curr. Biol. 15, 771 – 777.

Chiron, S., Bobkova, A., Zhou, H., and Yaffe, M.P. (2008). CLASP regulates mitochondrial distribution in Schizosaccharomyces pombe. J. Cell Biol. 182, 41 – 49.

Chernyakov, I., Santiago-Tirado, F., and Bretscher, A. (2013). Active segregation of yeast mitochondria by Myo2 is essential and mediated by Mmr1 and Ypt11. Curr. Biol. *23*, 1818–1824.

Chiron, S., Bobkova, A., Zhou, H., and Yaffe, M.P. (2008). CLASP regulates mitochondrial distribution in Schizosaccharomyces pombe. J. Cell Biol. *182*, 41–49.

Christiansen EG. (1949) Orientation of the mitochondria during mitosis. Nature. 163, 361.

Collot, M., Louvard, D., and Singer, S.J. (1984). Lysosomes are associated with microtubules and not with intermediate filaments in cultured fibroblasts. Proc. Natl. Acad. Sci. U. S. A. *81*, 788–792.

Dees, E., Miller, P.M., Moynihan, K.L., Pooley, R.D., Hunt, R.P., Galindo, C.L., Rottman, J.N., and Bader, D.M. (2012). Cardiac-specific deletion of the microtubule-binding protein CENP-F causes dilated cardiomyopathy. Dis. Model. Mech. 5, 468 – 480.

Friedman, J.R., Webster, B.M., Mastronarde, D.N., Verhey, K.J., and Voeltz, G.K. (2010). ER sliding dynamics and ER-mitochondrial contacts occur on acetylated microtubules. J. Cell Biol. *190*, 363–375.

Fransson, A., Ruusala, A., and Aspenström, P. (2003). Atypical Rho GTPases have roles in mitochondrial homeostasis and apoptosis. J. Biol. Chem. 278, 6495 – 6502.

Frederick, R.L., McCaffery, J.M., Cunningham, K.W., Okamoto, K., and Shaw, J.M. (2004). Yeast Miro GTPase, Gem1p, regulates mitochondrial morphology via a novel pathway. J. Cell Biol. 167, 87 – 98.Fu, C., Jain, D., Costa, J., Velve-Casquillas, G., and Tran, P.T. (2011). Mmb1p binds mitochondria to dynamic microtubules. Curr. Biol. *21*, 1431–1439.

Feng, J., Huang, H., and Yen, T.J. (2006). CENP-F is a novel microtubule-binding protein

that is essential for kinetochore attachments and affects the duration of the mitotic checkpoint delay. Chromosoma 115, 320 – 329.

Fission, M., Tumor, M., Kashatus, J. a, Nascimento, A., Counter, C.M., Kashatus, D.F., Kashatus, J. a, Nascimento, A., Myers, L.J., Sher, A., et al. (2015). Erk2 Phosphorylation of Drp1 Promotes Article Erk2 Phosphorylation of Drp1 Promotes Mitochondrial Fission and MAPK-Driven Tumor Growth. Mol. Cell 57, 537 – 551.

Glater, E.E., Megeath, L.J., Stowers, R.S., and Schwarz, T.L. (2006). Axonal transport of mitochondria requires milton to recruit kinesin heavy chain and is light chain independent. J. Cell Biol. *173*, 545–557.

Grigoriev, I., Gouveia, S.M., van der Vaart, B., Demmers, J., Smyth, J.T., Honnappa, S., Splinter, D., Steinmetz, M.O., Putney, J.W., Hoogenraad, C.C., et al. (2008). STIM1 Is a MT-Plus-End-Tracking Protein Involved in Remodeling of the ER. Curr. Biol. *18*, 177–182.

Kashatus, D.F., Lim, K.-H., Brady, D.C., Pershing, N.L.K., Cox, A.D., and Counter, C.M. (2011). RALA and RALBP1 regulate mitochondrial fission at mitosis. Nat. Cell Biol. 13, 1108 – 1115.

Hidalgo Carcedo, C., Bonazzi, M., Spanò, S., Turacchio, G., Colanzi, A., Luini, A., and Corda, D. (2004). Mitotic Golgi partitioning is driven by the membrane-fissioning protein CtBP3/BARS. Science *305*, 93–96.

Hilgendorf, K.I., Leshchiner, E.S., Nedelcu, S., Maynard, M. a, Calo, E., Ianari, A., Walensky, L.D., and Lees, J. a (2013). The retinoblastoma protein induces apoptosis directly at the mitochondria. Genes Dev. 27, 1003 – 1015.

Holt, S. V, Vergnolle, M. a S., Hussein, D., Wozniak, M.J., Allan, V.J., and Taylor, S.S. (2005). Silencing Cenp-F weakens centromeric cohesion, prevents chromosome alignment and activates the spindle checkpoint. J. Cell Sci. 118, 4889 – 4900.

Hussein, D., and Taylor, S.S. (2002). Farnesylation of Cenp-F is required for G2/M progression and degradation after mitosis. J. Cell Sci. 115, 3403 – 3414.

Horn, S.R., Thomenius, M.J., Johnson, E.S., Freel, C.D., Wu, J.Q., Coloff, J.L., Yang, C.-S., Tang, W., An, J., Ilkayeva, O.R., et al. (2011). Regulation of mitochondrial morphology by APC/CCdh1-mediated control of Drp1 stability. Mol. Biol. Cell *22*, 1207–1216.

Jiang, K., and Akhmanova, A. (2011). Microtubule tip-interacting proteins: a view from both ends. Curr. Opin. Cell Biol. *23*, 94–101.

Kashatus, D.F., Lim, K.-H., Brady, D.C., Pershing, N.L.K., Cox, A.D., and Counter, C.M. (2011). RALA and RALBP1 regulate mitochondrial fission at mitosis. Nat. Cell Biol. 13, 1108 – 1115.

Katajisto P, Dohla J, Chaffer C, Pentinmikko N, Marjanovic N, Iqbal S, et al. (2015) Asymmetric apportioning of aged mitochondria between daughter cells is required for

stemness. Science (80). , science.1260384.

Kornmann, B., Currie, E., Collins, S.R., Schuldiner, M., Nunnari, J., Weissman, J.S., and Walter, P. (2009). An ER-mitochondria tethering complex revealed by a synthetic biology screen. Science 325, 477 – 481.

Kornmann, B., Osman, C., and Walter, P. (2011). The conserved GTPase Gem1 regulates endoplasmic reticulum-mitochondria connections. Proc. Natl. Acad. Sci. 2 – 7.

Koshiba, T., Holman, H. a, Kubara, K., Yasukawa, K., Kawabata, S., Okamoto, K., MacFarlane, J., and Shaw, J.M. (2011). Structure-function analysis of the yeast mitochondrial Rho GTPase, Gem1p: implications for mitochondrial inheritance. J. Biol. Chem. 286, 354 – 362.

Lackner, L.L. (2013). Determining the shape and cellular distribution of mitochondria: The integration of multiple activities. Curr. Opin. Cell Biol. *25*, 471–476.

Lackner, L.L., Ping, H., Graef, M., Murley, A., and Nunnari, J. (2013). Endoplasmic reticulum-associated mitochondria-cortex tether functions in the distribution and inheritance of mitochondria. Proc. Natl. Acad. Sci. U. S. A. *110*, E458–E467.

Lawrence, E.J., and Mandato, C. a (2013). Mitochondria localize to the cleavage furrow in Mammalian cytokinesis. PLoS One 8, e72886.

Liao, H., Winkfein, R.J., Mack, G., Rattner, J.B., and Yen, T.J. (1995). CENP-F is a protein of the nuclear matrix that assembles onto kinetochores at late G2 and is rapidly degraded after mitosis. J. Cell Biol. 130, 507 – 518.

Li, T., Zheng, F., Cheung, M., Wang, F., and Fu, C. (2015). Fission yeast mitochondria are distributed by dynamic microtubules in a motor-independent manner. Sci. Rep. *5*, 11023.

Lu, L., Ladinsky, M.S., and Kirchhausen, T. (2009). Cisternal organization of the endoplasmic reticulum during mitosis. Mol. Biol. Cell *20*, 3471–3480.

Ma, L., Zhao, X., and Zhu, X. (2006). Mitosin/CENP-F in mitosis, transcriptional control, and differentiation. J. Biomed. Sci. 13, 205 – 213.

Maton, G., Edwards, F., Lacroix, B., Stefanutti, M., Laband, K., Lieury, T., Kim, T., Espeut, J., Canman, J.C., and Dumont, J. (2015). Kinetochore components are required for central spindle assembly. Nat. Cell Biol. 17, 697 – 705.

McKenney, R.J., Huynh, W., Tanenbaum, M.E., Bhabha, G., and Vale, R.D. (2014). Activation of cytoplasmic dynein motility by dynactin-cargo adapter complexes. Science (80-.). 345, 337 – 341.

Mitra, K., Rikhy, R., Lilly, M., and Lippincott-Schwartz, J. (2012). DRP1-dependent mitochondrial fission initiates follicle cell differentiation during Drosophila oogenesis. J. Cell Biol. 197, 487 – 497.

Moynihan, K.L., Pooley, R., Miller, P.M., Kaverina, I., and Bader, D.M. (2009). Murine

CENP-F Regulates Centrosomal Microtubule Nucleation and Interacts with Hook2 at the Centrosome. 20, 4790 – 4803.

Musinipally, V., Howes, S., Alushin, G.M., and Nogales, E. (2013). The microtubule binding properties of CENP-E's C-terminus and CENP-F. J. Mol. Biol. 425, 4427 – 4441.

Macaskill, A.F., Rinholm, J.E., Twelvetrees, A.E., Arancibia-Carcamo, I.L., Muir, J., Fransson, A., Aspenstrom, P., Attwell, D., and Kittler, J.T. (2009). Miro1 is a calcium sensor for glutamate receptor-dependent localization of mitochondria at synapses. Neuron 61, 541 – 555.

Mishra, P., and Chan, D.C. (2014). Mitochondrial dynamics and inheritance during cell division, development and disease. Nat. Publ. Gr. *15*, 634–646.

Mitra, K., Rikhy, R., Lilly, M., and Lippincott-Schwartz, J. (2012). DRP1-dependent mitochondrial fission initiates follicle cell differentiation during Drosophila oogenesis. J. Cell Biol. *197*, 487–497.

Nangaku, M., Sato-Yoshitake, R., Okada, Y., Noda, Y., Takemura, R., Yamazaki, H., and Hirokawa, N. (1994). KIF1B, a novel microtubule plus end-directed monomeric motor protein for transport of mitochondria. Cell *79*, 1209–1220.

Osman, C., Noriega, T.R., Okreglak, V., Fung, J.C., and Walter, P. (2015). Integrity of the yeast mitochondrial genome, but not its distribution and inheritance, relies on mitochondrial fission and fusion. Proc. Natl. Acad. Sci. 201501737.

Park, Y.-Y., and Cho, H. (2012). Mitofusin 1 is degraded at G2/M phase through ubiquitylation by MARCH5. Cell Div. *7*, 25.

Papadimou, E., Ménard, C., Grey, C., and Pucéat, M. (2005). Interplay between the retinoblastoma protein and LEK1 specifies stem cells toward the cardiac lineage. EMBO J. 24, 1750 – 1761.

Rattner, J.B., Rao, A., Fritzler, M.J., Valencia, D.W., and Yen, T.J. (1993). CENP-F is a .ca 400 kDa kinetochore protein that exhibits a cell-cycle dependent localization. Cell Motil. Cytoskeleton 26, 214 – 226.

Robertson, J.B., Zhu, T., Nasreen, S., Kilkenny, D., Bader, D., and Dees, E. (2008). CMF1-Rb interaction promotes myogenesis in avian skeletal myoblasts. Dev. Dyn. 237, 1424 – 1433.

Pon, L. a. (2011). Organelle transport: Mitochondria hitch a ride on dynamic microtubules. Curr. Biol. *21*, R654–R656.

Puhka, M., Vihinen, H., Joensuu, M., and Jokitalo, E. (2007). Endoplasmic reticulum remains continuous and undergoes sheet-to-tubule transformation during cell division in mammalian cells. J. Cell Biol. *179*, 895–909.

Quintero, O. a, Divito, M.M., Adikes, R.C., Kortan, M.B., Case, B., Lier, A.J., Panaretos,

N.S., Slater, S.Q., Rengarajan, M., Feliu, M., et al. (2009). Human Myo19 is a novel myosin that associates with mitochondria. *19*, 2008–2013.

Rafelski, S.M., Viana, M.P., Zhang, Y., Chan, Y.-H.M., Thorn, K.S., Yam, P., Fung, J.C., Li, H., Costa, L.D.F., Marshall, W.F., et al. (2012). Mitochondrial Network Size Scaling in Budding Yeast. Science (80-.). *338*, 822–824.

Reis, K., Fransson, A., and Aspenström, P. (2009). The Miro GTPases: at the heart of the mitochondrial transport machinery. FEBS Lett. 583, 1391 – 1398.

Rohn, J.L., 1, Patel, J. V., Neumann, B., Bulkescher, J., Mchedlishvili, N., McMullan, R.C., Quintero, O.A., Ellenberg, J., and Baum, and B. (2014). Myo19 Ensures Symmetric Partitioning of Mitochondria and Coupling of Mitochondrial Segregation to Cell Division.

Saotome, M., Safiulina, D., Szabadkai, G., Das, S., Fransson, A., Aspenstrom, P., Rizzuto, R., and Hajnóczky, G. (2008). Bidirectional Ca2+-dependent control of mitochondrial dynamics by the Miro GTPase. Proc. Natl. Acad. Sci. U. S. A. 105, 20728 – 20733.

Schwarz, T.L. (2013). Mitochondrial trafficking in neurons. Cold Spring Harb. Perspect. Med. 3, 1 – 15.

Shao, C.-Y., Zhu, J., Xie, Y.-J., Wang, Z., Wang, Y.-N., Wang, Y., Su, L.-D., Zhou, L., Zhou, T.-H., and Shen, Y. (2013). Distinct functions of nuclear distribution proteins LIS1, Ndel1 and NudCL in regulating axonal mitochondrial transport. Traffic 14, 785 – 797.

Suzuki, M., Danilchanka, O., and Mekalanos, J.J. (2014). Vibrio cholerae T3SS Effector VopE Modulates Mitochondrial Dynamics and Innate Immune Signaling by Targeting Miro GTPases. Cell Host Microbe 16, 581 – 591.

Senning, E.N., and Marcus, A.H. (2010). Actin polymerization driven mitochondrial transport in mating S. cerevisiae. Proc. Natl. Acad. Sci. U. S. A. *107*, 721–725.

Smyth, J.T., DeHaven, W.I., Bird, G.S., and Putney, J.W. (2007). Role of the microtubule cytoskeleton in the function of the store-operated Ca2+ channel activator STIM1. J. Cell Sci. *120*, 3762–3771.

Smyth, J.T., Beg, A.M., Wu, S., Putney, J.W., and Rusan, N.M. (2012). Phosphoregulation of STIM1 leads to exclusion of the endoplasmic reticulum from the mitotic spindle. Curr. Biol. *22*, 1487–1493.

Stowers, R.S., Megeath, L.J., Górska-Andrzejak, J., Meinertzhagen, I. a., and Schwarz, T.L. (2002). Axonal transport of mitochondria to synapses depends on Milton, a novel Drosophila protein. Neuron *36*, 1063–1077.

Sütterlin, C., Lin, C.Y., Feng, Y., Ferris, D.K., Erikson, R.L., and Malhotra, V. (2001). Polo-like kinase is required for the fragmentation of pericentriolar Golgi stacks during mitosis. Proc. Natl. Acad. Sci. U. S. A. *98*, 9128–9132.

Taguchi, N., Ishihara, N., Jofuku, A., Oka, T., and Mihara, K. (2007). Mitotic phosphorylation of dynamin-related GTPase Drp1 participates in mitochondrial fission.

J. Biol. Chem. 282, 11521 – 11529.

Toralová, T., Šušor, A., Němcová, L., Kepková, K., and Kaňka, J. (2009). Silencing CENPF in bovine preimplantation embryo induces arrest at 8-cell stage. Reproduction 138, 783 – 791.

Trushko, A., Schäffer, E., and Howard, J. (2013). The growth speed of microtubules with XMAP215-coated beads coupled to their ends is increased by tensile force. Proc. Natl. Acad. Sci. U. S. A. 110, 14670 – 14675.

Varadi, A., Johnson-Cadwell, L.I., Cirulli, V., Yoon, Y., Allan, V.J., and Rutter, G. a (2004). Cytoplasmic dynein regulates the subcellular distribution of mitochondria by controlling the recruitment of the fission factor dynamin-related protein-1. J. Cell Sci. *117*, 4389–4400.

van Spronsen, M., Mikhaylova, M., Lipka, J., Schlager, M. a, van den Heuvel, D.J., Kuijpers, M.,

Varis, A., Salmela, A.-L., and Kallio, M.J. (2006). Cenp-F (mitosin) is more than a mitotic marker. Chromosoma 115, 288 – 295.

Vergnolle, M.A.S., and Taylor, S.S. (2007). Cenp-F links kinetochores to Ndel1/Nde1/Lis1/dynein microtubule motor complexes. Curr. Biol. 17, 1173 – 1179.

Volkov, V. a, Grissom, P.M., Arzhanik, V.K., Zaytsev, A. V, Renganathan, K., McClure-Begley, T., Old, W.M., Ahn, N., and McIntosh, J.R. (2015). Centromere protein F includes two sites that couple efficiently to depolymerizing microtubules. J. Cell Biol. 209, 813 – 828.

Wallace, D.C. (2012). Mitochondria and cancer. Nat. Rev. Cancer 12, 685 – 698.

Waters, a. M., Asfahani, R., Carroll, P., Bicknell, L., Lescai, F., Bright, A., Chanudet, E., Brooks, A., Christou-Savina, S., Osman, G., et al. (2015). The kinetochore protein, CENPF, is mutated in human ciliopathy and microcephaly phenotypes. J Med Genet 52, 147 – 156.

Wulf, P.S., Keijzer, N., Demmers, J., Kapitein, L.C., et al. (2013). TRAK/Milton motor-adaptor proteins steer mitochondrial trafficking to axons and dendrites. Neuron 77, 485 – 502.

Wang, X., and Schwarz, T.L. (2009). The mechanism of Ca2+ -dependent regulation of kinesin-mediated mitochondrial motility. Cell 136, 163 – 174.

Wang, C., Du, W., Su, Q.P., Zhu, M., Feng, P., Li, Y., Zhou, Y., Mi, N., Zhu, Y., Jiang, D., et al. (2015). Dynamic tubulation of mitochondria drives mitochondrial network formation. Cell Res. 1–13.

Waterman-Storer, C.M., Gregory, J., Parsons, S.F., and Salmon, E.D. (1995). Membrane/microtubule tip attachment complexes (TACs) allow the assembly dynamics of plus ends to push and pull membranes into tubulovesicular networks in interphase

Xenopus egg extracts. J. Cell Biol. *130*, 1161–1169.

Yaffe, M.P., Stuurman, N., and Vale, R.D. (2003). Mitochondrial positioning in fission yeast is driven by association with dynamic microtubules and mitotic spindle poles. Proc. Natl. Acad. Sci. U. S. A. *100*, 11424–11428.

Zunino, R., Braschi, E., Xu, L., and McBride, H.M. (2009). Translocation of SenP5 from the nucleoli to the mitochondria modulates DRP1-dependent fission during mitosis. J. Biol. Chem. *284*, 17783–17795.

ACKNOWLEDGMENT

First I want to thank Benoît Kornmann for many reasons; for his scientific and intellectual support, for great discussions about the project, science in general and life in academia. Above all, I would like to thank Benoît for beeing a great mentor and for giving me the independence to follow my curiosity. Working in Benoit’s lab was a great opportunity and I believe that this experience will guide me along my academic career.

Special thanks goes to all of my current lab members, Martin Peterka, John Peter Arun Thomas, Qian Feng, Sebastian Helle, Alex Lang and Agnes Michel, for creating fun and enthusiastic working environment, for the scientific input and critical thinking, for supporting me during our shared time together. In addition, I would like to express deeply sincere gratitude to all of the lab members for proofreading the thesis. I appreciate it a lot. I got the pleasure to get to known and to teach to several highly motivated students during my PhD. Specifically, my highest gratitude goes to Sonja Meier, who helped me fractionate Cenp-F fusion protein, Can Akerman who helped with cloning of the CRISPR Miro1 plasmid and Florence Meier who helped analyzing and purifying human Miro1 and Miro2.

I also want to thank the members of my Thesis Committee, Benoît Kornmann, Paola Picotti, Patrick Meraldi and Anne Spang, for their helpful support and critical analysis of my work during our meetings.

Also I would like to thank our collaborators, who contributed to this project, namely to Vladimir Volkov (see Statement of contribution), Richard Macintosh for introducing Vladimir to us and sending cell-lines; Special thanks go to Thibault Courtheoux for his contribution to the Eb1 part. I would like also to thank Martin Soste and Andre Melnik for the mass spectrometry analysis. My sincere gratitude also goes to the ScopEM people for the microscopy support, and to the IBC staff.

Last but not least, I’m deeply indebted to my wife Talya, the active driving force for moving to Switzerland, for encouraging me to pursue my dreams and for great support.

I love you and I wish for us all the best the world can offer. Thank you for believing in me. I also would like to thank my parents, Isack and Sara – I wish you good health and long and happy life – my wife's parents Pnina and Eli, my brother and sister, Ofir and Iris and my friends at home.

GIL KANFER

Gil.kanfer.il@gmail.com
Telephone: +41 44 633 4114

Biology department
Institute of biochemistry
Otte-stern-weg 3
ETH Zurich
8046, Zurich
Switzerland

ACADEMIC QUALIFICATIONS

2011-Present	Swiss Federal Institute of Technology ETH Zurich, Switzerland, Institute of *Biochemistry.* **PhD track**, Molecular life science graduate program. Thesis: Mitochondria transport in dividing cells Thesis advisor: **Prof. Dr. Benoît Kornmann**
2008-2010	Tel Aviv University, Sackler Faculty of Medicine, Israel, Department of Human Molecular Genetics and Biochemistry. **M.Sc.** degree, Medical Sciences Graduate Studies. Thesis: The effect of Erythropoietin on telomerase activity. Thesis advisors: **Prof. Y. Nordenberg, Prof. MD. M.Lahav** Lab instructor: **Dr. O. Uziel**
2006-2008	Bar Ian University, Faculty of Life Sciences, Israel, **B.Sc**. degree, major in Cellular and molecular biology.
2004-2006	Tel Hai Gertrude and Morris Rodman College, Israel, **Practical Engineering** degree, major in Biotechnology.

PUBLICATION LIST

Kanfer, G., Courthéoux, T., Peterka, M., Meier, M., Soste, M., Melnik, A., Reis., Aspenström, P., Matthias Peter, M., Picotti, P., and Kornmann, B. (2015). Mitotic redistribution of the mitochondrial network by Miro and Cenp-F. Nat. Commun. 6, 8015.

Kanfer, G., and Kornmann, B. (Submitted). Dynamics of the mitochondrial network during mitosis.

Helle, S.C.J., **Kanfer, G**., Kolar, K., Lang, A., Michel, A.H., and Kornmann, B. (2013). Organization and function of membrane contact sites. Biochim. Biophys. Acta 1833, 2526–2541.

Uziel, O[1]., **Kanfer, G[1]**., Beery, E., Yelin, D., Shepshelovich, D., Bakhanashvili, M., Nordenberg, J., and Lahav, M. (2014). The effects of erythropoietin signaling on telomerase regulation in non-erythroid malignant and non-malignant cells. Biochem. Biophys. Res. Commun. 450, 274–282.

Weiss, C., Uziel, O., Wolach, O., Nordenberg, J., Beery, E., Bulvick, S., **Kanfer, G**., Cohen, O.,

Ram, R., Bakhanashvili, M., et al. (2012). Differential downregulation of telomerase activity by bortezomib in multiple myeloma cells-multiple regulatory pathways in vitro and ex vivo. Br. J. Cancer 107, 1844–1852.

PRESENTATIONS

- Cell Symposia: Multifaceted Mitochondria; Chicago, IL (2015)-Poster
- 1st Symposium held by the institute of Biochemistry, Switzerland (2015)- selected lecture
- 1st Mitochondria research meeting in Switzerland, 2014- Lecture
- The department of biology ETH symposium, Davos (2012)-Poster
- Selected worked present by undergraduate student from school of medicine Tel-Aviv university, 2010-Lucture

SELCTED AWARDS AND HONORS

-I-CORE Grant for excellent undergraduate students, 2008-2010 (40,000 INS)
-Molecular life science Zurich travel Grant, 2015 (1000 CHF)
-Selected talk held by undergraduate students, 2010
-Environmental biology presentation exhibition award, 2007 (500 INS)
-Practical engineering first year highest grades awards, 2006

SKILLS AND TECHNIQUES

Broad experience in microscopy, protein/organelle isolation and gene cloning techniques in the fields of organelle communication, membrane transport, cell cycle and cytoskeleton.

Microscopy: Live cell and fixed florescence microscopy, super resolution Microscopy (S.I.M.), Total internal reflection microscopy, transmission electron microscopy, large scale imaging performance using light microscopy scanners.

Molecular Biology: CRISPR/Cas system (design and perform knockout and knockin in cell culture), Gene cloning in bacteria yeast and mammalian cells, yeast genetics, qRT Real Time P.C.R., Cell Sorting and cell cycle analysis by Flow Cytometry, generation of stable cell lines.

Protein Isolation: Immunopreciptation, ion exchange chromatography, Size-exclusion chromatography, protein Tag Purification (His, Flag, Strep), organelle purification using "continuous centrifugation"

Mass spectrometry: Tandem affinity purification combined with mass spectrometry, peptide preparation, C18 Reversed Phase LC Columns, stable isotope labeling by amino acids in cell culture.

Imaging Data analysis: High level of skills in designing and analyzing large sets of microscopy data using verity of tools as Fiji, Matlab, CellProfiler

REFERENCES

- Prof. Benoît Kornmann (benoit.kornmann@bc.biol.ethz.ch, +41 44 633 6575)
- Prof. Picotti Paola (paola.picotti@bc.biol.ethz.ch, +41 44 633 25 58)
- Dr. Orit Uziel (Oritu@clalit.org.il, +972-3-9376796)